Spectral Element Analysis of Bars, Beams, and Levy Plates

by

Thomas Black

Thesis submitted to the faculty of
Virginia Polytechnic Institute and State University
in partial fulfillment of the requirements of the degree of

Master of Science

in

Mechanical Engineering

Dr. Robert West Committee Chair

Dr. Donald Leo

Dr. Rakesh Kapania

May 18, 2005
Blacksburg, Virginia

Keywords: Spectral Elements, Dynamic Stiffness, Bar, Beam, Plate, Continuum

Spectral Element Analysis of Bars, Beams, and Levy Plates

Thomas Black

Abstract

This thesis is primarily concerned with the development and coding of a Levy-type spectral plate element to analyze the harmonic response of simply supported plates in the mid to high frequency range. The development includes the governing PDE, displacement field, shape function, and dynamic stiffness matrix. A two DOF spectral Love bar element and both a four DOF spectral Euler-Bernoulli and a four DOF spectral Timoshenko beam element are also developed to gain insight into the performance of spectral elements.

A cantilever beam example is used to show how incorporating eigenfunctions for the dynamic governing PDE into the displacement field enables spectral beam elements to represent the structural dynamics exactly. A simply supported curved beam example is used to show that spectral beam elements can converge the effects of curved geometry with up to a 50% reduction in the number of elements when compared to conventional FE. The curved beam example is also used to show that the rotatory inertia and shear deformation, from Timoshenko's beam theory, can result in up to a 28% shift in natural frequency over the first three bending modes.

Finally, a simply supported Levy-plate model is used to show that the spectral Levy-type plate element converges the dynamic solution with up to three orders of magnitude fewer DOF then the conventional FE plate formulation. A simply-supported plate example problem is used to illustrate how the coefficients of the Fourier series expansion can be used as edge DOF for the spectral Levy-plate element. The Levy-plate element development gives insight to future research developing a general spectral plate element.

Table of Contents

Abstract ii

Table of Contents iii

List of Figures vi

List of Tables viii

List of Symbols ix

Greek Symbols x
Special Notation xi
Superscripts xi

1. Introduction 1

1.1. Problem Statement 1
1.2. Hypothesis 2
1.3. Background of Spectral Elements 2
1.4. Objectives 3
1.4.1. Develop a Love Spectral Bar Element 3
1.4.2. Develop an Euler-Bernoulli and Timoshenko Spectral Beam Element 4
1.4.3. Develop a Spectral Beam Element of Arbitrary Orientation 4
1.4.4. Develop a Spectral Levy-type Plate Element 4
1.5. Scope 5
1.5.1. Linear Elastic Isotropic Material 5
1.5.2. Harmonic Analysis 5
1.5.3. Relatively Simple Geometry and Meshing 5
1.6. Thesis Overview 5
1.6.1. Literature Review 5
1.6.2. Bar Elements 6
1.6.3. Beam Elements 6
1.6.4. Levy-type Plate Elements 6
1.6.5. Conclusion 7

2. Literature Review 8

2.1. Develop a Love Spectral Bar Element 8
2.1.1. Literature on Conventional Bar Elements 8
2.1.2. Literature on Spectral Bar Elements 8

2.2. Develop an Euler-Bernoulli and Timoshenko Spectral Beam Element 9
2.2.1. Literature on Conventional Beam Elements 9
2.2.2. Literature on Spectral Beam Elements 10
2.3. Develop a Spectral Beam Element of Arbitrary Orientation 11
2.4. Develop a Spectral Levy-type Plate Element 11
2.4.1. Literature on the Development of Conventional Plate Elements 11
2.4.2. Literature on the Development of Levy-type Spectral Elements 12
3. Bar Elements 14
3.1. Conventional Bar Elements 14
3.1.1. Development of the Governing Equation 14
3.1.2. Representation of Displacement Field 17
3.1.3. Dynamic Stiffness Formulation 20
3.2. Spectral Bar Elements 22
3.2.1. Development of Governing Equation 22
3.2.2. Representation of Displacement Field 24
3.2.3. Dynamic Stiffness Formulation 27
3.3. Chapter Summary 30
4. Beam Elements 32
4.1. Conventional Beam Element 32
4.1.1. Development of Governing Equation 32
4.1.2. Representation of the Displacement Field 34
4.1.3. Dynamic Stiffness 37
4.2. Spectral Elements 39
4.2.1. Development of Governing Equation 39
4.2.2. Representation of the Displacement Field 41
4.2.3. Dynamic Stiffness 44
4.3. Straight Geometry Example Problem 48
4.4. Curved Geometry Example Problem 56
4.5. Timoshenko Beam Spectral Element 61
4.5.1. Development of Governing Equations 61
4.5.2. Representation of Displacement Field for Timoshenko Element 65
4.5.3. Dynamic Stiffness for Timoshenko Element 69
4.5.4. Curved Geometry Example Revisited 73
4.6. Chapter Summary 76
5. Levy-Type Kirchhoff Plate Element 79
5.1. Conventional Plate Elements 79
5.1.1. Development of Governing Equation 79
5.1.2. Representation of the Displacement Field 81

5.1.3. Dynamic Stiffness 84
5.2. Levy-Type Spectral Plate Elements 86
5.2.1. Governing Equation 86
5.2.2. Representation of the Displacement Field 91
5.2.3. Dynamic Stiffness 96
5.3. Straight Example Problem 105
5.3.1. Single Point Response Comparison 106
5.3.2. Multiple Point Response Comparison 115
5.4. Chapter Summary 119
6. Summary, Conclusions, and Recommendations 124
6.1. Review of Objectives 124
6.1.1. Develop a Love Spectral Bar Element 124
6.1.2. Develop Euler-Bernoulli and Timoshenko Spectral Beam Element 124
6.1.3. Develop a Spectral Beam Element of Arbitrary Orientation 125
6.1.4. Develop a Spectral Levy-type Plate Element 125
6.2. Conclusions 126
6.2.1. Incorporating Eigenfunctions into Element Shape Functions 126
6.2.2. Performance of Spectral Elements 126
6.3. Future Work 127
6.3.1. General Spectral Plate Element 127
6.3.2. Spectral Element User Interface 128
7. References 130
Appendix A Euler-Bernoulli Spectral Beam Dynamic Stiffness Matrix 133
Appendix B Spectral Plate Element Code 134
Appendix C Spectral and Conventional Plate Convergence 136

List of Figures

Figure 1. Schematic of Standard Bar Element with Nodal DOF 17
Figure 2. Free Body Diagram of an Infinitesimal Bar Element 22
Figure 3. Schematic of Spectral Bar Element with Nodes and DOF 27
Figure 4. Conventional Beam Element Degrees of Freedom 33
Figure 5. Free Body Diagram of Differential Beam Element with Positive Shear and Moment 39
Figure 6. Schematic of Nodal DOF of Spectral Euler-Bernoulli Beam Element 45
Figure 7. Schematic of Cantilever Beam Example Problem 49
Figure 8. Comparison of End Node Deflection for 5 Conventional Elements and 1 Spectral Element 51
Figure 9. Deformed Shapes for Forcing Frequencies of 1000, 3000, and 5000 *Hz*... 52
Figure 10. Comparison of End Node Deflection for 34 Conventional Elements and 1 Spectral Element 53
Figure 11. Deformed Shape Comparison for 1000, 3000, and 5000 *Hz* with 1 Spectral and 34 Conventional FE Elements..... 54
Figure 12. Percent Difference Using 1 Spectral and 34 Conventional Elements 55
Figure 13. Schematic of Curved Mirror Profile and Beam Cross Section..... 56
Figure 14. Comparison of Deformed Shape for FRF Peaks 2 and 3 of the Curved Problem 59
Figure 15. Receptance for Curved Example Using 10 Spectral and 16 Conventional Elements..... 60
Figure 16. Free Body Diagram of a Differential Element of a Timoshenko Beam... 62
Figure 17. Definitions of Bending, Shear, and Total Slope. 64
Figure 18. Nodal DOF of Spectral Timoshenko Beam Element 70
Figure 19. Schematic of Curved Mirror Cross-Section 74
Figure 20. Euler-Bernoulli, Timoshenko Receptance Comparison 75
Figure 21. Positive Orientation of Nodal DOF for Kirchhoff Plate Element 80
Figure 22. Free Body Diagram of Differential Kirchhoff Plate with Positive Shear and Moment Orientation 87
Figure 23. Stress Components for the Visible Faces of a Differential Plate Element 89
Figure 24. Schematic of Boundary Conditions for Levy-type Plate..... 92
Figure 25. Edge DOF of Levy-type Spectral Plate Element..... 97
Figure 26. Schematic of Simply Supported Plate 106
Figure 27. 24X24 Element ANSYS Model with Single Comparison Point 107
Figure 28. Convergence of the Displacement of the Center of Free Edge Using ANSYS Shell63 Mesh for Various Frequencies..... 109
Figure 29. Convergence of the Displacement of the Center of Free Edge Using Single Levy-type Spectral Element 110
Figure 30. Response of Center of Free Edge vs. Frequency *m=1* Spectral and 24X24 SHELL63 111
Figure 31. Response of Center of Free Edge vs. Frequency *m=11* Spectral and 24X24 SHELL63 112
Figure 32. Deformed Shapes of Single Levy-type Spectral Model at 10, 100, 300, 600 *Hz, m=11* 113

Figure 33. Deformed Shapes of Single Levy-type Spectral Model at 1500, 2000, 3000, 4500 *Hz, m=11* 114
Figure 34. Layout of Nodes Used in the Multi-point Convergence Study 116
Figure 35. Conventional Element Convergence by Doubling Number of Elements per Edge 117
Figure 36. Levy-Type Spectral Element Convergence by Increasing Number of Fourier Terms..... 118
Figure 37. Relative Error of 25 Point Response Between Spectral *m=11* and FEA 119

List of Tables

Table 1. Summary of the Differences Between Conventional and Spectral Bar Elements 31
Table 2. Summary of Number of Elements Required to Converge the Peaks of the Response 50
Table 3. Summary of Number of Elements Required to Converge Receptance Peaks 59
Table 4. Percent Change Due to Rotatory Inertia and Shear Deformation in FRF Peaks 75
Table 5. Summary of Formulation Differences Between Conventional and Spectral Euler-Bernoulli Beams 77
Table 6. ANSYS Models Used in Comparison of Conventional and Spectral Response 108
Table 7. Comparison of Displacement of the Center of the Free Edge for 24X24 FEA Mesh and *m=1* Spectral Models 111
Table 8. Comparison of Displacement of the Center of the Free Edge for 96X96 FEA Mesh and *m=11* Spectral Models 115
Table 9. Formulation Differences Between Conventional and Spectral Levy-type Plate Elements 120

List of Symbols

A	Cross Sectional Area
$\overline{A}, \overline{B}, \overline{C}, ...$	Unknown Coefficients
B	Strain Displacement Matrix
D	Fourier Transformed Displacement Coefficient Matrix
D	Flexural Rigidity of Kirchhoff Plate
d	Temporal Vector of Element Degrees of Freedom
E	Modulus of Elasticity
F	Fourier Transformed Force Coefficient Matrix
F	Axial Rod Force
f	Vector of Element Forces
f	External Load
G	Shear Modulus
h_y	Beam Height y-Direction
h_z	Beam Height z-Direction
I	Area Moment of Inertia
i	Imaginary Number $\sqrt{-1}$
K_1	Timoshenko Transverse Shear Coefficient
K_2	Timoshenko Rotatory Inertia Coefficient
$\mathbf{K}_{dyn}$	Dynamic Stiffness Matrix
k	Elemental Stiffness Matrix
k	Axial Wave Number for Bar Element
L	Beam Length
M	Bending Moment in Beam or Bending Moment Resultant for Plate
m	Elemental Mass Matrix
m	Summation Index
N	Elemental Shape Function

$p_{1,2,3,4}$	Flexural Spatial Wave Number in Plate
Q	Shear Resultant per length for Kirchhoff Plate
$R_{1,2,3,4}$	Timoshenko Coefficient Amplitude Ratio
$\mathbf{r}_{ext}$	External Nodal Loads
$T(t)$	Assumed Temporal Component of Separable Solution
t	Time Variable
u	Axial Displacement in Rod
$\mathbf{u}$	Vector of Nodal DOF
V	Transverse Shear
w	Transverse Displacement
$X(x)$	Assumed Spatial Component of Separable
x	Space Variable
y	Space Variable

Greek Symbols

α	Flexural Wave Number for Beam Element
β	Beam Slope Due to Shear in Timoshenko Theory
σ	Normal Stress
τ	Shear Stress
μ	Mass Density
θ	Beam Nodal Rotation DOF
ω	Circular Forcing Frequency
ψ	Beam Slope Due to Bending in Timoshenko Theory

Special Notation

$[\ ]$	Matrix
$\{\ \}$	Vector
$\mathcal{F}$	Fourier Series Expansion

Superscripts

w'	Space Derivative
$\dot{w}$	Time Derivative
$\overline{A}$	Unknown Coefficient
$\widetilde{A}$	Unknown Coefficient
θ_x	Rotation About y-direction, Partial Derivative of w with Respect to x
σ_{xx}	Plate Stress Tensor Notation, First Subscript is Surface Normal Direction, Second Subscript is Stress component Direction

1. Introduction

1.1. Problem Statement

A design of a new light-weight deployable satellite telescope requires a thinner mirror than is commonly used in order to decrease the overall weight of the satellite. Decreasing the mirror thickness makes the mirror prone to vibration that causes the image to become distorted. The use of an active control system to control the mirror surface and eliminate the image distortion is currently under investigation. The design of the active control system requires an accurate model of the mirror vibration. Conventional finite element models of the mirror are large and are not well suited to represent the deformed shape of the mirror surface in the low to mid frequency range.

The telescope designers wish to develop a technique to analyze the dynamics of the mirror with more fidelity, higher frequency capability, and a reduced model size as compared to conventional finite elements. The technique and resulting code need to be compatible with SIMULINK to aid in the active control of the mirror.

The main focus of this study is to develop, code, and characterize a spectral Levy-type plate element that with further development has the potential of modeling the dynamics of a parabolic mirror. The development of the element includes defining the formulation of the elements shape functions and dynamic stiffness matrix. Coding the element includes writing a MATLAB-based code that uses the spectral element to analyze the vibration of the parabolic mirror. The characterization of the spectral element includes a comparison of the performance to that of a conventional plate element in terms of computational resources and solution convergence.

1.2. Hypothesis

The general hypothesis of this research is that the spectral element will produce a more precise dynamic solution with fewer elements than conventional finite element analysis. Furthermore, it is hypothesized that it is possible to incorporate a form of the eigenfunctions of the dynamics problem into the shape function and dynamic stiffness matrix of the spectral element.

1.3. Background of Spectral Elements

Conventional finite element analysis has been around for almost 45 years and has become a highly accepted form of structural analysis. Conventional finite elements are typically based on static solutions and work very well to solve static problems. In typical static structural problems the structure is meshed to represent the geometry, loads, and boundary conditions. The element mesh is then refined to capture the deformation of the structure until the deformed solution converges to an accepted value. The mesh refinement is required because conventional elements use a simple polynomial representation of the displacement field. The polynomial representation is only capable of representing simple loads and boundary conditions. Typically, the geometry, loads, and boundary conditions of the problem are beyond the solution capability of a single element. Increasing the number of elements in the mesh results in geometry, loading, and boundary conditions that allow the capability of the elements to approach the true solution.

As the problem type advances from static to dynamic, the geometry, loads, boundary conditions, and the mechanics must be converged to an acceptable solution. Typically, more finite elements are required to converge a dynamic finite element model than the same static model. Furthermore, the number of elements required to converge the dynamic finite element model tend to increases with increased frequency. The number of elements required to model a structure at high frequency may easily exceed a practical number to solve in a timely manner.

A logical alternative to increasing the number of elements is to increase the polynomial order of the interpolation functions that the elements are based on. This approach is called p-type convergence. Typically, the order of the polynomial interpolation function is increased, while the spatial mesh is held constant, until more accurate results are obtained.

Spectral elements use a variation of p-type convergence. Spectral elements base the element interpolation functions on the eigenfunctions of the differential equation used to represent the dominant mechanics in the problem. This results in the "exact" form of the displacement field for the interpolation function. The interpolation functions of spectral elements are based on trigonometric functions, opposed to polynomial functions of conventional elements. The trigonometric functions incorporate the frequency of the response into the interpolation function. Having the interpolation function based on the eigenfunction means that a single spectral element will give the "exact" dynamic solution across the element for simple loading and boundary conditions. Even for dynamic analysis, it is only necessary to converge the geometry, loads, and boundary conditions. It is not necessary to converge the dynamics, as it is for the case with traditional finite elements. This results in a reduced number of elements, and thus a reduced model size for a spectral element model as compared to the conventional finite element model.

1.4. Objectives

1.4.1. Develop a Love Spectral Bar Element

The first step in the development of the spectral bar element is to determine the eigenfunctions of the governing bar differential equation based on Love's theory. The eigenfunctions must then be incorporated into the displacement field of the element. Then, the dynamic stiffness matrix and element shape functions can be formulated from the representation of the displacement field.

1.4.2. Develop an Euler-Bernoulli and Timoshenko Spectral Beam Element

Similar to the objective of the bar element, the steps to formulate the spectral beam element are: determine the eigenfunctions of the governing beam equation, incorporate the eigenfunctions into the displacement field, and then formulate a dynamic stiffness matrix and the spectral shape function from the displacement field. This objective applies to both Euler-Bernoulli theory and Timoshenko beam theory, so the performance of the two beam elements can be compared. The element will then be coded into MATLAB and its results compared to conventional FEA results.

1.4.3. Develop a Spectral Beam Element of Arbitrary Orientation

The third main objective will be to modify the spectral beam elements to handle arbitrary orientation in the plane. This will require the axial degrees of freedom of the spectral bar element to be included in the beam element. A MATLAB code will then be written to compare the spectral element to conventional FEA results.

1.4.4. Develop a Spectral Levy-type Plate Element

The fourth main objective is to extend the spectral beam element method to a two-dimensional Kirchhoff Levy-type plate element. This will require solving the governing plate equation and obtaining the eigenfunctions for the Levy-type plate. The eigenfunctions will need to satisfy arbitrary boundary conditions on two opposing edges while satisfying the simply supported boundaries on the two remaining edges. Once a representation of the displacement field is found, a dynamic stiffness matrix can be formed. Finally, the element can be coded in MATLAB and the spectral results can be compared to conventional FEA.

1.5. Scope

1.5.1. Linear Elastic Isotropic Material

Only linear elastic materials are considered in this study. The study will investigate the dynamics of continuous beams and plates of isotropic homogeneous materials that undergo deflections that can be classified as small deflections.

1.5.2. Harmonic Analysis

Static analysis is not covered by this study. Static analysis must be treated as a special case of zero frequency. Only harmonic forcing dynamic analysis will be analyzed. The study will compare the spectral element analysis results to the finite element results for harmonic excitation.

1.5.3. Relatively Simple Geometry and Meshing

The application of the elements developed will be restricted to flat and simply curved geometry. It is not the goal of this study to develop the techniques to analyze and mesh complicated geometry.

1.6. Thesis Overview

1.6.1. Literature Review

The literature review given in chapter 2 discusses relevant references that pertain to each of the objectives listed in section 1.3. Contained in the discussion are descriptions of the work done by the authors and its application to the work undertaken within the thesis.

The literature review contains sources for the development of both conventional and spectral bar, beam, and plate elements. References are given for Euler-Bernoulli and Timoshenko beam elements as well as beam elements of arbitrary orientation. The

plate references are limited to Kirchhoff theory and elements aligned with rectangular coordinates.

1.6.2. Bar Elements

Chapter 3 contains a comparison of the development of conventional and spectral bar elements. No example problems are considered, only a discussion of the fundamental differences between conventional FEA and spectral analysis. The fundamental differences discussed include the development of the shape functions and formulation of the dynamic stiffness matrix.

1.6.3. Beam Elements

Chapter 4 contains a comparison of the development of Euler-Bernoulli conventional and spectral beam elements. The comparisons include the development of the shape functions and formulation of the dynamic stiffness matrix. A cantilever beam example is used to illustrate the ability of the spectral element to capture the mechanics of the dynamic problem.

In addition to the Euler-Bernoulli formulation, a Timoshenko spectral beam development is given in section 4.5. A curved simply supported beam example is used to show the effects of shear deformation and rotatory inertia on the solution.

1.6.4. Levy-type Plate Elements

Chapter 5 contains a comparison of the development of the conventional and Levy-type spectral Kirchhoff plate elements. The comparisons include the development of the shape functions and formulation of the dynamic stiffness matrix. A simply supported plate with uniform loads is used to compare the results of the conventional and spectral models. The solutions are compared on single and multi-point levels.

1.6.5. Conclusion

Chapter 6 contains a summary of the objectives set forth in section 1.3. A summary of the results found in the thesis including; incorporating eigenfunctions into the shape function of spectral elements and evaluating the performance of spectral elements. Recommendations on the coding, utilization, and future of spectral elements are also given.

2. Literature Review

2.1. Develop a Love Spectral Bar Element

2.1.1. Literature on Conventional Bar Elements

The conventional bar element will need to be formulated as a baseline for comparison with the spectral bar element. The major issues in the conventional development are: forming the governing structural dynamics equation, understanding the assumptions made in obtaining a solution to the governing equation, determining the representation of the displacement field based on the assumptions, and formulation of the mass and stiffness matrices.

The most popular discrete method for dynamic bar analysis is the Finite Element Method (FEM). Cook [3] is a good introductory text covering the basics of the FEM. Cook gives a complete development of the bar element shape function and stiffness matrix.

2.1.2. Literature on Spectral Bar Elements

The major issues in the spectral bar development are: determining the governing differential equation, obtaining the eigenfunctions from the governing equation, and forming the shape functions and the dynamic stiffness matrix from the eigenfunctions. The following are relevant references that give insight into solutions to theses major issues.

Standard vibration texts such as Thompson [22] and Inman [11] have detailed explanations of traditional continuous methods for Love's bar theory. These explanations include development of the governing equations and the solutions to the equations. Inman's [11] development of the governing equation seems more useful in determining the dynamic eigenfunctions for the bar.

Doyle [5] gives a derivation of a spectral bar element with explanation of shape functions and dynamic stiffness matrices. Two of the key ideas found in Doyle's work are a Fourier transform solution to the governing bar equation and a formulation of spatial wave numbers. Both of these ideas are important to the development and implementation of the spectral bar element. Doyle also gives background on bar dynamics including wave reflection and thermoelastic waves.

2.2. Develop an Euler-Bernoulli and Timoshenko Spectral Beam Element

2.2.1. Literature on Conventional Beam Elements

Similar to the major issues of the conventional bar element, the major issues in developing the beam element are: understanding the assumptions made in obtaining a solution to the governing equation, determining the representation of the displacement field based on the assumptions, and formulation of the mass and stiffness matrices. In addition, these issues will have to be resolved for both Euler-Bernoulli and Timoshenko beam theories.

The main techniques of dynamic beam analysis can be divided into continuous and discrete methods. Standard vibration texts such as Thompson [22] and Inman [11] have detailed explanations of traditional continuous methods for Euler-Bernoulli beam theory. Higher order continuous beam theories that include shear and rotatory inertia effects are well explained by Timoshenko [20].

The most popular discrete method for dynamic beam analysis is the finite element method (FEM). Cook [3] is a good introductory text covering the basics of the FEM. Dym and Shames [6] and Haug, Choi, and Komkov [9] both give detailed derivations of the finite element method for beams as well as more complicated elements. Cook even gives the stiffness matrix of a beam that includes the effects of shear deformation and is most appropriate for the information needed in this study.

2.2.2. Literature on Spectral Beam Elements

The major issues in the spectral beam development are: determining the governing differential equation, obtaining the eigenfunctions from the governing equation, and forming shape functions and the dynamic stiffness matrix from the eigenfunctions. These issues apply to both Euler-Bernoulli and Timoshenko beam theories. The following are relevant references that give insight to solutions of theses major issues.

Kulla [14 and 15] gives an explanation of the formulation for an Euler-Bernoulli spectral beam element. Kulla takes a classical separation of variables approach to the solution of the governing differential equation. The formulation of the element includes the development of eignefunctions, spatial wave numbers, and a dynamic stiffness based on the eigenfunctions. Kulla [14 and 15] explicitly gives the dynamic stiffness matrix for the Euler-Bernoulli beam.

Doyle [5] gives a derivation of a Timoshenko spectral beam element. Doyle takes a Fourier transform approach to the solution to the governing differential equation. The approach uses eigenfunctions and spatial wave numbers similar to Kulla's approach. Doyle explicitly gives the dynamic stiffness and shape functions for the Timoshenko beam element. Doyle also gives background on beam dynamics including the reflection of waves, curved beams, and rings.

Kulla [14 and 15] and Doyle [5] are the best references for Euler-Bernoulli and Timoshenko spectral beam element formulations respectively. The development of the governing equations for Euler-Bernoulli and Timoshenko are best given by Inman [11] and Timoshenko [20] respectively.

2.3. Develop a Spectral Beam Element of Arbitrary Orientation

The major issue in developing a spectral beam element of arbitrary orientation in the plane is determining the required spatial transformation matrix. The transformation matrix will have to transform the nodal degrees of freedom (DOF) of the spectral element from the local elemental coordinate system to a global coordinate system. This will allow for the representation of curved structures with straight element sections. Because the arbitrary beam element will be composed of a bar superimposed onto a beam, the transformation of both bar and beam nodal DOF will be required.

The transformation matrices for arbitrary orientation of conventional bar and beam elements are covered by Cook [4]. A similar explanation is give by Doyle [5] concerning general frame structures for spectral elements. Doyle's explanation contains all of the DOF to transform in general 3D space. The unused DOF would need to be removed before the transformation matrix could be used on the in-plane elements considered in this study. Cook's discussion is better for this study because it is easier to specialize and apply the transformation matrix for in-plane elements.

2.4. Develop a Spectral Levy-type Plate Element

2.4.1. Literature on the Development of Conventional Plate Elements

The major issues in formulating a conventional plate element include: understanding the assumptions in forming a solution to the governing equation, forming a representation of the displacement field from the solution, and generating mass and stiffness matrices from the displacement field. The remainder of the section gives references related to solving the major issues.

Ventsel and Krauthammer [23] give a good introduction to conventional plate elements. This includes basic formulation of rectangular and triangular elements. Cook [3] also discusses plate elements for both Kirchhoff and Mindlin theories. Dym and Shames [6] also give a well-organized discussion of plate elements and choice of interpolation functions. Finally, Haug, Choi, and Komkov [9] devote a section to finite element formulation including plates and complete mass and stiffness matrices for a Kirchhoff element.

Ventsel and Krauthammer [23] and Cook [3] are the works best related to the work undertaken in this study. Ventsel's and Krauthammer's development of classical plate theory is very much on the same level as the development of the governing equations in this study. Cook's development of conventional plate elements is well suited for developing a baseline element for comparison of the spectral element.

2.4.2. Literature on the Development of Levy-type Spectral Elements

The major issues in developing a Levy-type spectral plate element are: forming the governing partial differential equation, understanding the assumptions required to generate a representation of the displacement field that will be capable of modeling the dynamics of a simply supported plate, and incorporating the displacement field into a dynamic stiffness matrix. It is especially important to understand the process of obtaining a solution to the dynamic governing differential equation. A simple closed form solution to the general dynamic governing differential plate equation is not commonly known. The remainder of the section gives references that aid in the solution to these issues.

Similarly to beams, the main techniques of dynamic plate analysis can be divided into continuous and discrete methods. Ventsel and Krauthammer [23] give a good explanation of continuous plate vibration starting from basic statics and progressing to vibration and then FEM. Ventsel and Krauthammer only handle simply supported and Levy-type plates in their continuous vibration theory. Gorman [7 and 8]

introduces the method of superposition to analyze the vibration of plates with arbitrary boundary conditions. It is Gorman's method that forms the basis for the formulation of the general spectral plate element with arbitrary boundary conditions on all edges.

Doyle [5] gives a development of a Levy-type spectral element. Danial, Doyle, and Rizzi [19] apply the Levy-type element to the analysis of folded plate structures. Lee and Lee [17] also give a development of a Levy-type plate element. Kulla [14 and 15] and Kevorkian and Pascal [12] both report methods to formulate a general spectral plate element that is capable of handling arbitrary boundary conditions. Kulla suggests a spatial Fourier expansion of the boundary conditions along each edge. Kevorkian and Pascal [12] offer a similar idea of projecting the boundary conditions onto *sin* and *cos* functions. Kevorkian and Pascal also give an energy method to determine a dynamic stiffness for the spectral plate element.

Doyle [5], Kulla [14 and 15], and Kevorkian [12] are the most relevant works to the major issues in this study. Doyle's work is a good guide to developing a Levy-type spectral plate element. Kulla's and Kevorkian's work offers insight into a general spectral plate element. It will be good to keep Kulla's and Kevorkian's work in mind in order to make the Levy-type element extendable to a general spectral plate element in the future.

Based on the literature surveyed in this chapter the current state-of-the-art in spectral elements is one-dimensional elements, such as bar and beam elements, and special case two-dimensional plate elements, such as Navier's solution and Levy's solution. The general two-dimensional element formulation is only documented in a few sources and the reproduction of the work is difficult due to the brevity of the papers. The most challenging issue with the general plate element is the dynamic solution of arbitrary boundary condition. The sources discussed here are used to develop the Levy-type plate element and investigate the extension of the element to a general plate element as reported by Kulla and Kevorkian.

3. Bar Elements

The development of both conventional and spectral bar elements are discussed in sections 3.1 and 3.2 respectively. Each development section consists of subsections that cover the development of the governing equation, the interpolation function, and the dynamic stiffness matrix. The subsections provide definitions and conventions that lead to the development of both the conventional and spectral elements. Finally, the major differences between the conventional and spectral element formulations are summarized in section 3.3.

3.1. Conventional Bar Elements

3.1.1. Development of the Governing Equation

The general governing equation for structural dynamics is formed by requiring that the work done by external loads be equal to the sum of work absorbed by inertial and internal forces. Virtual Work Methods are applied to the structure to analyze the energy of the system. The Virtual Work Method yields integral expressions for mass and stiffness matrices that minimize the kinetic and potential energies in the system. Separable forms of the displacement fields are assumed in the solutions to the energy minimization. The resulting mass and stiffness matrices are based on the assumed forms of the displacement fields. The remainder of the subsection describes the development of the governing structural dynamics equation.

For a single linear elastic element of volume (V), loaded with only concentrated forces $(\mathbf{p}_i)$, the matrix form of the virtual work energy balance can be written as

$$\sum_{i=1}^{n} \{\delta \mathbf{u}\}_i^T \{\mathbf{p}\}_i = \int \left(\{\delta \mathbf{u}\}^T \mu \{\ddot{\mathbf{u}}\} + \{\delta \boldsymbol{\varepsilon}\}^T \{\boldsymbol{\sigma}\} \right) dV \tag{1}$$

$\{\delta\mathbf{u}\}_i$ are the virtual displacements which correspond to the concentrated forces at a total of n points, μ is the mass density, and $\{\delta\mathbf{u}\}$ and $\{\delta\boldsymbol{\varepsilon}\}$ are the virtual displacements and corresponding virtual strains, Cook [3]. Structural damping, surface tractions, and body forces are not of concern in this study and have been left out of the energy balance. Next, traditional finite element discretization and a separable solution are assumed. The assumed separable form of the displacement fields, $\{\mathbf{u}\}$, is

$$\{\mathbf{u}\} = [\mathbf{N}]\{\mathbf{d}\} \tag{2}$$

where, $[\mathbf{N}]$ is the shape function and represents the spatial component of the solution, and $\{\mathbf{d}\}$ is a vector of nodal DOF and represents the temporal component of the separable solution. The strain matrix, $\{\boldsymbol{\varepsilon}\}$, can be defined in terms of the strain-displacement matrix, $[\mathbf{B}]$, and the vector of nodal DOF as

$$\{\boldsymbol{\varepsilon}\} = [\mathbf{B}]\{\mathbf{d}\} \tag{3}$$

Similarly for linear elastic materials, the stresses, $\{\boldsymbol{\sigma}\}$ can be defined as

$$\{\boldsymbol{\sigma}\} = [\mathbf{E}][\mathbf{B}]\{\mathbf{d}\} \tag{4}$$

Substituting Equations (2), (3), and (4) into Equation (1) and factoring gives

$$\{\delta\mathbf{d}\}^T\left[\int \mu[\mathbf{N}]^T[\mathbf{N}]dV\{\ddot{\mathbf{d}}\} + \int [\mathbf{B}]^T[\mathbf{E}][\mathbf{B}]dV\{\mathbf{d}\} - \sum_{i=1}^{n}\{\mathbf{p}\}_i\right] = 0 \tag{5}$$

The bracketed term in Equation (5) must equal zero for the equation to give a nontrivial solution. Setting the bracketed term equal to zero and renaming the nodal loads as $\{\mathbf{r}_{ext}\}$ gives

$$\int \mu[\mathbf{N}]^T[\mathbf{N}]dV\{\ddot{\mathbf{d}}\} + \int [\mathbf{B}]^T[\mathbf{E}][\mathbf{B}]dV\{\mathbf{d}\} = \{\mathbf{r}_{ext}\} \tag{6}$$

Defining the integral in front of $\{\ddot{\mathbf{d}}\}$ as the mass matrix, $[\mathbf{m}]$, gives

$$[\mathbf{m}] = \int \mu[\mathbf{N}]^T[\mathbf{N}]dV \tag{7}$$

Similarly, defining the integral in front of $\{\mathbf{d}\}$ as the stiffness matrix, $[\mathbf{k}]$, gives

$$[\mathbf{k}] = \int [\mathbf{B}]^T[\mathbf{E}][\mathbf{B}]dV \tag{8}$$

Finally, substituting Equations (7) and (8) into Equation (6) gives the common form of the governing Finite Element structural dynamics equation for undamped structures with nodal loading to be

$$[\mathbf{m}]\{\ddot{\mathbf{d}}\} + [\mathbf{k}]\{\mathbf{d}\} = \{\mathbf{r}_{ext}\} \tag{9}$$

The governing structural dynamics Equation (9) was formed using virtual work techniques to analyze the energy of the system. A separable form of the displacement field was assumed in the solution of the energy functional. Mass and stiffness matrices were formulated, based on the assumed form of the displacement field, that minimize the kinetic and potential energies respectively. The following section describes the choices for the spatial and temporal components of the separable solution.

3.1.2. Representation of Displacement Field

The development of Equation (9) assumed separable forms of the displacement fields. Applying Equation (9) to the bar element, shown in Figure 1, requires choosing a basis function to represent the spatial and temporal components of the separable solution, given in Equation (2). The basis function can then be used to form the shape function, $[\mathbf{N}]$, that will satisfy arbitrary nodal boundary conditions. The shape function is then used in the formulation of the mass and stiffness matrices, as shown in Equations (7) and (8) respectively.

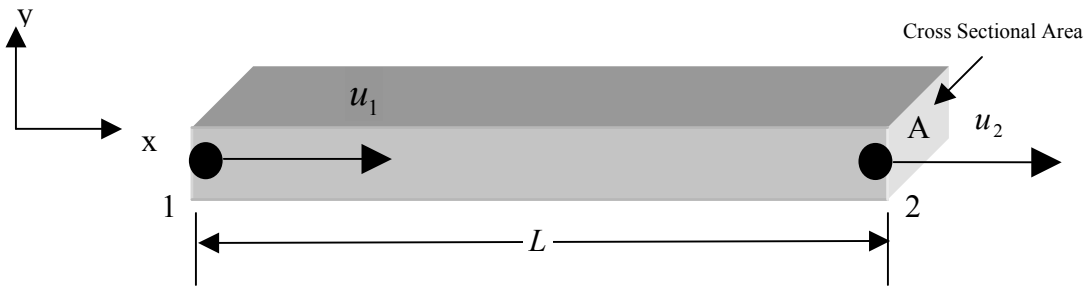

Figure 1. Schematic of Standard Bar Element with Nodal DOF

In conventional finite element analysis the spatial form of the displacement field of the bar,

$$X(x) = \overline{A}x + \overline{B} \tag{10}$$

is chosen to be the basis function for the shape function formulation. $\overline{A}$ and $\overline{B}$ are unknown constants to be determined through the application of boundary conditions. For the case of harmonic excitation, the basis function chosen for the temporal component of the separable solution is assumed to have the form

$$T(t) = e^{\mathrm{i}\omega t} \tag{11}$$

where, ω is the circular forcing frequency. The total assumed representation of the basis function for the displacement field then becomes the spatial solution multiplied by the temporal solution

$$u(x,t) = X(x)T(t) \tag{12}$$

Substituting the expressions for the spatial and temporal solutions from Equations (10) and (11) yields the following form of the total assumed basis function.

$$u(x,t) = \left(\overline{A}x + \overline{B}\right)e^{\mathrm{i}\omega t} \tag{13}$$

The basis function in Equation (13) can now be used to formulate the shape function. Writing the total basis function, Equation (13), in matrix form gives

$$u(x,t) = [\mathbf{X}]\{\mathbf{a}\}e^{\mathrm{i}\omega t} \tag{14}$$

such that the spatial solution is given by

$$X(x) = [\mathbf{X}]\{\mathbf{a}\} \tag{15}$$

where, $[\mathbf{X}]$ is a row vector formed from the spatial solution, $X(x)$, and is written as

$$[\mathbf{X}] = [x \quad 1] \tag{16}$$

The column vector $\{\mathbf{a}\}$ is a column vector of the unknown coefficients

$$\{\mathbf{a}\} = \begin{Bmatrix} \overline{A} \\ \overline{B} \end{Bmatrix} \tag{17}$$

The axial displacements of the two ends of the bar, shown as u_1 and u_2 in Figure 1, are chosen to be the nodal DOF. The vector $\{\mathbf{d}\}$ from Equation (2) is defined as the temporal solution of the nodal DOF.

$$\{\mathbf{d}\} = \begin{Bmatrix} u_1 \\ u_2 \end{Bmatrix} e^{\mathbf{i}\omega t} \tag{18}$$

Evaluating Equation (13) at the two nodes and writing in matrix form gives

$$\begin{Bmatrix} u_1 \\ u_2 \end{Bmatrix} e^{i\omega t} = [\mathbf{A}]\{\mathbf{a}\} e^{\mathbf{i}\omega t} \tag{19}$$

where, $[\mathbf{A}]$ is a matrix of row vectors, $[\mathbf{X}]$ evaluated at the nodal locations. For the case of the bar element $[\mathbf{A}]$ is given by

$$[\mathbf{A}] = \begin{bmatrix} 0 & 1 \\ L & 1 \end{bmatrix} \tag{20}$$

The vector $\{\mathbf{a}\}$ is as given before in Equation (17), a column vector of the unknown coefficients. Substituting Equation (14) into the left side of Equation (2) for $\{\mathbf{u}\}$ and substituting Equation (19) into the right side of Equation (2) for $\{\mathbf{d}\}$ gives

$$[\mathbf{X}]\{\mathbf{a}\} e^{i\omega t} = [\mathbf{N}][\mathbf{A}]\{\mathbf{a}\} e^{i\omega t} \tag{21}$$

The shape function can now be solved from Equation (21) to be

$$[\mathbf{N}] = [\mathbf{X}][\mathbf{A}]^{-1} \tag{22}$$

Substituting the expressions for $[\mathbf{X}]$ from Equation (16) and $[\mathbf{A}]$ from Equation (20), the shape function of the bar can then be written as

$$[\mathbf{N}] = \begin{bmatrix} \left(1 - \frac{x}{L}\right) & \frac{x}{L} \end{bmatrix} \tag{23}$$

The conventional bar element shape function, shown in Equation (23), was formed from the assumed separable form of the displacement field. The polynomial function that represents the static axial displacement field was used as basis function for the spatial solution. A complex exponential was used as the temporal solution because of the interest in only harmonic excitation. The basis function was then incorporated into the shape function such that the displacement field could be calculated from the nodal displacements. The following section describes the details in forming the dynamic stiffness matrix from the assumed shape function and temporal solution.

3.1.3. Dynamic Stiffness Formulation

The dynamic stiffness of the bar element that is harmonically forced can be found by substituting the assumed form of the temporal solution into the governing structural dynamics equation and regrouping terms. The resulting dynamic stiffness is a single matrix that can be used to calculate the harmonic response of the nodal displacements and loads. The mass and stiffness matrices that makeup the dynamic stiffness are completely defined by the shape functions determined in section 3.1.2.

The general definitions of the mass matrix, $[\mathbf{m}]$, and the stiffness matrix, $[\mathbf{k}]$, are given in Equations (7) and (8) respectively. The mass and stiffness matrices for the bar element, shown in Figure 1, and the shape function, given in Equation (23), are

$$[\mathbf{m}] = \int_0^L \mu A [\mathbf{N}]^T [\mathbf{N}] dx \tag{24}$$

$$[\mathbf{k}] = \int_0^L EA [\mathbf{B}]^T [\mathbf{B}] dx \tag{25}$$

where, μ is the mass density of the material, A is the constant cross-sectional area of the bar element, E is the modulus of elasticity of the material. The strain displacement matrix for the bar, $[\mathbf{B}]$, is defined as

$$[\mathbf{B}] = \frac{d}{dx}[\mathbf{N}] \tag{26}$$

Substituting the assumed form of the temporal solution, $\{\mathbf{d}\}$ given in Equation (18), into the governing structural dynamics equation, Equation (9), gives

$$-\omega^2 [\mathbf{m}]\{\mathbf{d}\} + [\mathbf{k}]\{\mathbf{d}\} = \{\mathbf{r}_{ext}\} \tag{27}$$

where, the harmonic term, $e^{i\omega t}$, has been canceled from both sides of the equation. The dynamic stiffness for the conventional bar element can then be written as

$$[\mathbf{K}_{Dyn}] = -\omega^2 [\mathbf{m}] + [\mathbf{k}] \tag{28}$$

Such that

$$[\mathbf{K}_{Dyn}]\{\mathbf{d}\} = \{\mathbf{r}_{ext}\} \tag{29}$$

The dynamic stiffness matrix, given in Equation (28), was formed by incorporating the assumed temporal solution into the governing structural dynamics equation. Notice that the mass and stiffness matrices are computed separately and then added together. The inertia effects are incorporated through scaling the mass matrix by the forcing frequency squared. The following section discusses the development of the spectral bar element.

3.2. Spectral Bar Elements

3.2.1. Development of Governing Equation

The development of the governing equation for the spectral bar element begins with the free body diagram of an infinitesimal bar element shown in Figure 2. The bar is assumed to have a constant cross-sectional area and isotropic material properties. A force balance in the axial direction on the bar element yields a separable partial differential equation (PDE) that is second order in both time and space. The remainder of the subsection describes the process of developing the governing equation for the spectral bar element.

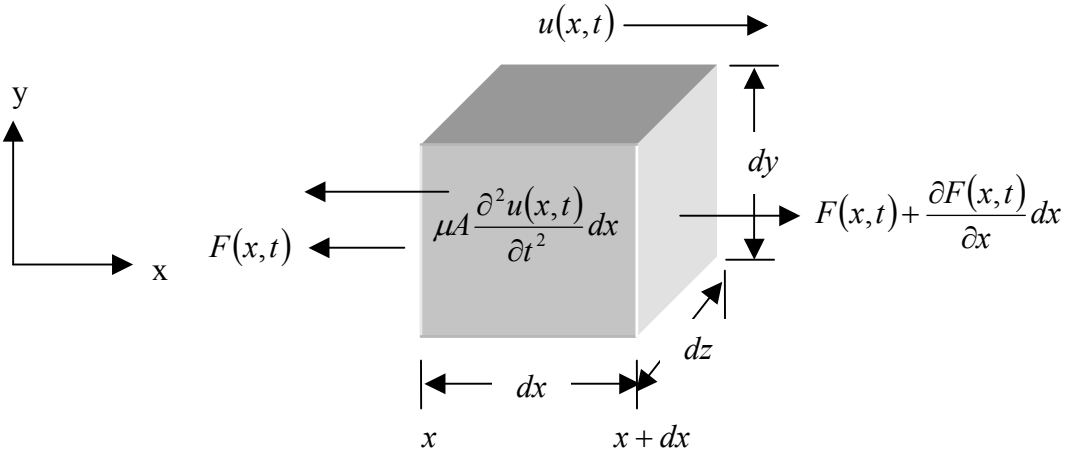

Figure 2. Free Body Diagram of an Infinitesimal Bar Element

The free body diagram of an infinitesimal bar element is shown in Figure 2. $F(x,t)$ is the axial force in the bar and $u(x,t)$ is the axial displacement of the bar. Writing the sum of forces in the x-direction yields

$$-F(x,t)+F(x,t)+\frac{\partial F(x,t)}{\partial x}-\mu A\frac{\partial^2 u(x,t)}{\partial t^2}=0 \tag{30}$$

where, A is the constant cross sectional area. The axial force is given by

$$F(x,t)=\sigma(x,t)A \tag{31}$$

and the axial stress, $\sigma(x,t)$, can be written in terms of the elastic modulus, E, and the axial strain, $\frac{\partial u(x,t)}{\partial x}$, as

$$\sigma(x,t)=E\frac{\partial u(x,t)}{\partial x} \tag{32}$$

Substituting Equations (31) and (32) into (30) results in the governing partial differential equation for the dynamic elastic bar as

$$\frac{E}{\mu}\frac{\partial^2 u(x,t)}{\partial x^2}=\frac{\partial^2 u(x,t)}{\partial t^2} \tag{33}$$

The governing PDE for the dynamic elastic bar was determined through the balancing of forces on an infinitesimal bar element in the axial direction. The resulting separable PDE is second order in both time and space. The following section describes the development of the solution to the governing PDE.

3.2.2. Representation of Displacement Field

The governing bar PDE, Equation (33), is a separable partial differential equation. The solution can be found using a separation of variables technique. Separating the variables yields two constant coefficient second order ordinary differential equations (ODE). One ODE governs space and one governs time. A general exponential solution is assumed for each of the two ODEs. The remainder of the subsection describes the development of the solution to the governing bar PDE.

Assuming a separable form of the solution to Equation (33) as

$$u(x,t) = X(x)T(t) \tag{34}$$

and substituting the assumed solution into the governing partial differential Equation (33) gives,

$$\frac{E}{\mu}\frac{X''}{X} = \frac{\ddot{T}}{T} \tag{35}$$

Now, setting each side of Equation (35) equal to an unknown constant gives two constant coefficient ordinary differential equations, Boyce and DiPrima [2].

$$\frac{E}{\mu}\frac{X''}{X} = \overline{C} \tag{36}$$

$$\frac{\ddot{T}}{T} = \overline{C} \tag{37}$$

The assumed temporal solution for the case of harmonic forcing is the same used in the conventional element

$$T(t) = \overline{D} e^{\mathbf{i}\omega t} \tag{38}$$

Substituting the assumed temporal solution, Equation (38), into Equation (37) gives

$$\left(-\omega^2\right)\overline{D} e^{\mathbf{i}\omega t} - \overline{C}\,\overline{D} e^{\mathbf{i}\omega t} = 0 \tag{39}$$

Simplifying and solving for the unknown coefficient $\overline{C}$ gives

$$\overline{C} = -\omega^2 \tag{40}$$

The assumed form of the solution to the spatial ordinary differential Equation (36) is

$$X(x) = \overline{A} e^{\mathbf{i}kx} \tag{41}$$

Substituting the assumed form into Equation (36) gives

$$\frac{E}{\mu}\left(-k^2\right)\overline{A} e^{\mathbf{i}kx} - \overline{C}\,\overline{A} e^{\mathbf{i}kx} = 0 \tag{42}$$

Substituting the value of $\overline{C}$ found from the temporal ODE in Equation (40) into Equation (42) and simplifying gives a characteristic relation between the temporal frequency and the spatial wave number

$$-\frac{E}{\mu}k^2 + \omega^2 = 0 \tag{43}$$

Solving for the spatial wave number (k) gives two possible values

$$k_1 = \sqrt{\frac{\mu}{E}\omega^2}$$
$$k_2 = -\sqrt{\frac{\mu}{E}\omega^2} \tag{44}$$

Using one exponential function for each possible value of spatial wave number results in a spatial solution of the form

$$X(x) = \overline{A}e^{\mathbf{i}k_1 x} + \overline{B}e^{\mathbf{i}k_2 x} \tag{45}$$

where, k_1 and k_2 are the two possible values of wave number from the spectral relation, Equation (44). Equation (45) is the eigenfunction of the governing PDE. Combining the complete spatial solution, Equation (45), and temporal solution, Equation (38), and combining coefficients, gives a total solution for the displacement field to be

$$u(x,t) = \left(\overline{A}e^{\mathbf{i}k_1 x} + \overline{B}e^{\mathbf{i}k_2 x}\right)e^{\mathbf{i}\omega t} \tag{46}$$

The solution to the governing bar PDE was found through a separation of variables technique. The resulting constant coefficient ODEs were assumed to have exponential solutions. Substituting the exponential solutions into the spatial ODE resulted in a second order characteristic equation. The characteristic equation had two possible roots, or values of spatial wave number. The two possible spatial wave numbers were incorporated into the complete spatial to form the eigenfunction of the governing PDE. The following section describes the development of dynamic stiffness matrix based on the complete form of the displacement field including the eigenfunction.

3.2.3. Dynamic Stiffness Formulation

The total representation of the displacement field, Equation (46), has been established from the governing differential equation, Equation (33). The dynamic stiffness matrix for harmonic forcing can now be formulated based on the representation of the displacement field. The dynamic stiffness is formulated by a direct method using the nodal displacements and forces to eliminate the unknown coefficients in the representation of the displacement field. The spectral bar element uses the axial displacement at two nodes for DOF. The nodal layout and DOF of the spectral rod element is shown in Figure 3.

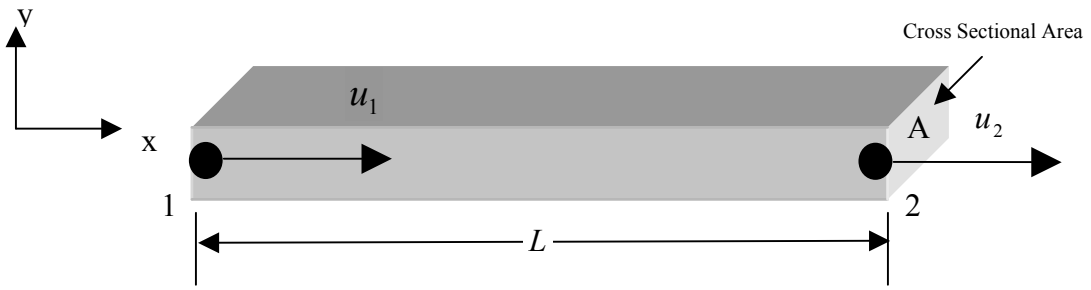

Figure 3. Schematic of Spectral Bar Element with Nodes and DOF

The nodal displacements and nodal forces can be written in terms of the unknown coefficients $\overline{A}$ and $\overline{B}$. The spatial component of the nodal displacements, u_1 and u_2, are found by evaluating Equation (45) at the nodes.

$$\begin{aligned} u_1 &= X(0) = \overline{A} + \overline{B} \\ u_2 &= X(L) = \overline{A}e^{\mathrm{i}k_1 L} + \overline{B}e^{\mathrm{i}k_2 L} \end{aligned} \tag{47}$$

Writing Equation (47) in matrix form and incorporating the temporal component of the solution, $e^{\mathrm{i}\omega t}$, gives

$$\{\mathbf{d}\} = \begin{Bmatrix} u_1 \\ u_2 \end{Bmatrix} e^{\mathbf{i}\omega t} = [\mathbf{D}] \begin{Bmatrix} \overline{A} \\ \overline{B} \end{Bmatrix} e^{\mathbf{i}\omega t} \tag{48}$$

In this case the matrix $[\mathbf{D}]$ has the form

$$[\mathbf{D}] = \begin{bmatrix} 1 & 1 \\ e^{\mathbf{i}k_1 L} & e^{\mathbf{i}k_2 L} \end{bmatrix} \tag{49}$$

Similarly, evaluating the spatial axial force,

$$f(x) = EA \frac{\partial X(x)}{\partial x} \tag{50}$$

at the nodes and writing in matrix form and including the temporal component gives

$$\{\mathbf{f}\} = \begin{Bmatrix} f_1 \\ f_2 \end{Bmatrix} e^{\mathbf{i}\omega t} = [\mathbf{F}] \begin{Bmatrix} \overline{A} \\ \overline{B} \end{Bmatrix} e^{\mathbf{i}\omega t} \tag{51}$$

In this case $[\mathbf{F}]$ has the form

$$[\mathbf{F}] = EA \begin{bmatrix} \mathbf{i}k_1 & \mathbf{i}k_2 \\ \mathbf{i}k_1 e^{\mathbf{i}k_1 L} & \mathbf{i}k_2 e^{\mathbf{i}k_2 L} \end{bmatrix} \tag{52}$$

The dynamic stiffness matrix, $[\mathbf{K}_{Dyn}]$, by definition relates the nodal displacements, $\{\mathbf{d}\}$, to the nodal loads, $\{\mathbf{f}\}$,

$$\{\mathbf{f}\} = [\mathbf{K}_{Dyn}]\{\mathbf{d}\} \tag{53}$$

The dynamic stiffness matrix can be found by eliminating the vector of unknown coefficients, $\left\{\begin{matrix}\overline{A}\\ \overline{B}\end{matrix}\right\}$, from Equations (48) and (51). Solving for $\left\{\begin{matrix}\overline{A}\\ \overline{B}\end{matrix}\right\}e^{\mathbf{i}\omega t}$ in Equation (48) gives

$$\left\{\begin{matrix}\overline{A}\\ \overline{B}\end{matrix}\right\}e^{\mathbf{i}\omega t} = \left[\mathbf{D}\right]^{-1}\left\{\mathbf{d}\right\} \tag{54}$$

Substituting the expression for the vector of unknowns from Equation (54) into Equation (51) gives

$$\left\{\mathbf{f}\right\} = \left[\mathbf{F}\right]\left[\mathbf{D}\right]^{-1}\left\{\mathbf{d}\right\} \tag{55}$$

The dynamic stiffness matrix that relates the nodal displacements to the nodal forces is then

$$\left[\mathbf{K}_{Dyn}\right] = \left[\mathbf{F}\right]\left[\mathbf{D}\right]^{-1} \tag{56}$$

The explicit form of the dynamic stiffness for the spectral bar element is

$$\left[\mathbf{K}_{Dyn}\right] = EA\begin{bmatrix} \dfrac{\mathbf{i}k_1 e^{\mathbf{i}k_2 L} - \mathbf{i}k_2 e^{\mathbf{i}k_1 L}}{e^{\mathbf{i}k_2 L} - e^{\mathbf{i}k_1 L}} & \dfrac{\mathbf{i}k_2 - \mathbf{i}k_1}{e^{\mathbf{i}k_2 L} - e^{\mathbf{i}k_1 L}} \\ \dfrac{(k_1 - k_2)\mathbf{i}e^{\mathbf{i}k_1 L}e^{\mathbf{i}k_2 L}}{e^{\mathbf{i}k_2 L} - e^{\mathbf{i}k_1 L}} & \dfrac{\mathbf{i}k_2 e^{\mathbf{i}k_2 L} - \mathbf{i}k_1 e^{\mathbf{i}k_1 L}}{e^{\mathbf{i}k_2 L} - e^{\mathbf{i}k_1 L}} \end{bmatrix} \tag{57}$$

The shape function for the spectral bar element can be formulated as the matrix that relates the displacement field to the nodal DOF as given earlier in Equation (2).

$$\left\{\mathbf{u}\right\} = \left[\mathbf{N}\right]\left\{\mathbf{d}\right\} \tag{2}$$

In the case of the spectral bar element the shape function matrix can be written as

$$[\mathbf{N}] = \begin{bmatrix} e^{\mathbf{i}k_1 x} & e^{\mathbf{i}k_2 x} \end{bmatrix} [\mathbf{D}]^{-1} \tag{58}$$

The shape function matrix of the spectral bar element in explicit form is

$$[\mathbf{N}] = \begin{bmatrix} \dfrac{-e^{\mathbf{i}k_1 x} e^{\mathbf{i}k_2 L} + e^{\mathbf{i}k_2 x} e^{\mathbf{i}k_1 L}}{-e^{\mathbf{i}k_2 L} + e^{\mathbf{i}k_1 L}} & \dfrac{e^{\mathbf{i}k_1 x} - e^{\mathbf{i}k_2 x}}{-e^{\mathbf{i}k_2 L} + e^{\mathbf{i}k_1 L}} \end{bmatrix} \tag{59}$$

In review, the dynamic stiffness matrix was developed through a direct method using the nodal displacements and forces to eliminate the unknown coefficients in the displacement field. The displacement field that the nodal displacements and forces were based on was the solution to the governing PDE developed in section 3.2.2, Equation (46). Because the dynamic stiffness is based on the exact solution to the governing PDE, the nodal displacements and forces obtained through the use of the dynamic stiffness will also be exact, provided that the problem is consistent with the simple boundary and loading conditions used to formulate the element. The exact form of the displacement field was also incorporated into a shape function for the spectral bar element.

3.3. Chapter Summary

The conventional element governing equation was based on energy methods. The conventional approach resulted in integral expressions for mass and stiffness matrices that minimize the kinetic and potential energies in the system. The spectral element governing equation was based on the summation of forces on a differential element. The force balance resulted in a second order, separable, partial differential equation.

The representation of the displacement field was the major difference between the conventional and spectral formulations. Conventional elements used a polynomial function, equivalent to the solution for a static displacement field, as a basis function for the element shape functions. Spectral elements used the spatial solution to the separable governing PDE, equivalent to the eigenfunction, as the basis function for the element.

The dynamic stiffness matrix formulation was the second major difference between the conventional element formulation and the spectral element formulation. The conventional formulation combined mass and stiffness matrices based on the polynomials basis functions to form a dynamic stiffness matrix. The dynamic stiffness matrix incorporates inertial effects through scaling the mass matrix by the forcing frequency squared. The scaled mass matrix is then added to the static stiffness matrix to result in a dynamic stiffness matrix.

The spectral formulation used a direct method to form the dynamic stiffness matrix. The nodal displacements and forces were calculated using the basis eigenfunction. The relation between the nodal displacements and forces resulted in a dynamic stiffness matrix that included the effects of frequency, inertia, and stiffness. Table 1 shows a side-by-side comparison of the major differences between conventional and spectral bar element formulation.

Table 1. Summary of the Differences Between Conventional and Spectral Bar Elements

	Conventional Bar	Spectral Bar
Governing Equation	$[\mathbf{m}]\{\ddot{\mathbf{d}}\}+[\mathbf{k}]\{\mathbf{d}\}=\{\mathbf{r}_{ext}\}$	$\frac{E}{\mu}\frac{\partial^2 u(x,t)}{\partial x^2}=\frac{\partial^2 u(x,t)}{\partial t^2}$
Basis Function	$u(x,t)=\left(\overline{A}x+\overline{B}\right)e^{i\omega t}$	$u(x,t)=\left(\overline{A}e^{ik_1x}+\overline{B}e^{ik_2x}\right)e^{i\omega t}$
Dynamic Stiffness Formulation	$[\mathbf{K}_{Dyn}]=-\omega^2[\mathbf{m}]+[\mathbf{k}]$	$[\mathbf{K}_{Dyn}]=[\mathbf{F}][\mathbf{D}]^{-1}$
Shape Function	$[\mathbf{N}]=\left[\left(1-\frac{x}{L}\right)\quad\frac{x}{L}\right]$	$[\mathbf{N}]=\left[\frac{-e^{ik_1x}e^{ik_2L}+e^{ik_2x}e^{ik_1L}}{-e^{ik_2L}+e^{ik_1L}}\quad\frac{e^{ik_1x}-e^{ik_2x}}{-e^{ik_2L}+e^{ik_1L}}\right]$

4. Beam Elements

The development of both conventional and spectral Euler-Bernoulli beam elements is discussed in sections 4.1 and 4.2 respectively. Each development section consists of subsections that cover the governing equations, displacement field, and dynamic stiffness matrices. After the differences in the developments of the conventional and spectral elements are discussed, three example problems are used to demonstrate the performance differences between the two elements. The first example, a straight cantilever beam with an end load, demonstrates the ability of the spectral beam element to model the dynamic response. The second example, a curved simply supported beam with load at center span, shows the ability of the spectral beam element to capture effects of geometry. The third example shows how higher order beam theory can be incorporated into the spectral element and the effects the higher order theory has on the solution. Finally, a summary of the major differences between the conventional and spectral element formulations are summarized in section 4.6.

4.1. Conventional Beam Element

4.1.1. Development of Governing Equation

The conventional beam element has 2 nodes with 2 degrees of freedom (DOF) at each node. Figure 4 shows the degrees of freedom of a single beam element with the positive orientation of the displacements. The 2 degrees of freedom used at each node were transverse displacement (w) and in plane rotation (θ).

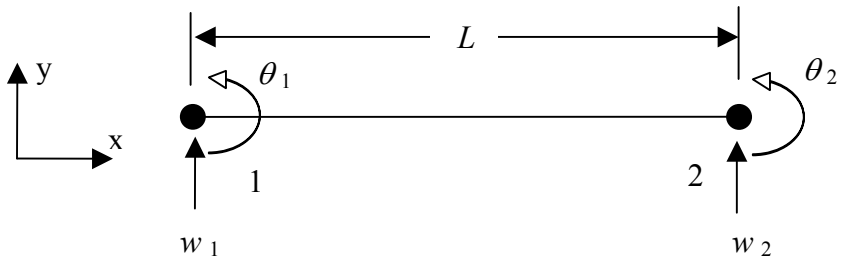

Figure 4. Conventional Beam Element Degrees of Freedom

The development of the governing equation for a conventional beam element follows the same concept as the conventional bar element. The beam element will use bending and shearing DOF instead of the axial DOF used in the bar element. The governing equation is obtained by minimizing the sum of the kinetic and potential energies in the system. Section 3.1.1 gives the development of the governing structural dynamics equation for conventional elements. The governing structural dynamics equation for the beam element is repeated here for convenience

$$[\mathbf{m}]\{\ddot{\mathbf{d}}\}+[\mathbf{k}]\{\mathbf{d}\}=\{\mathbf{r}_{ext}\} \tag{9}$$

where, $[\mathbf{m}]$ is the mass matrix, $[\mathbf{k}]$ is the stiffness matrix, $\{\mathbf{r}_{ext}\}$ is a vector of external loads, and $\{\mathbf{d}\}$ is the temporal solution DOF vector of the beam element. The following section describes the choice of basis function and development of the shape functions from the basis function.

4.1.2. Representation of the Displacement Field

Applying Equation (9) to the beam element shown in Figure 4, requires choosing a representation of the shape function, $[\mathbf{N}]$, for the spatial component of the separable solution assumed in Equation (2). A polynomial basis function that represents the static transverse displacement field is used to formulate the shape function. The shape function can then be used to form the mass and stiffness matrices.

In conventional finite element analysis the static approximation for the transverse displacement field of the beam is a cubic polynomial given as

$$X(x) = \overline{A}x^3 + \overline{B}x^2 + \overline{C}x + \overline{D} \tag{60}$$

The cubic polynomial is chosen to be the basis for the shape function formulation. $\overline{A}, \overline{B}, \overline{C}$, and $\overline{D}$ are unknown coefficients to be determined by application of boundary conditions. For the case of harmonic excitation, the basis of the temporal component of the separable solution is assumed to have the form

$$T(t) = \overline{E}e^{\mathrm{i}\omega t} \tag{61}$$

where ω is the circular forcing frequency. The total assumed representation of the basis function for the transverse displacement field is then given by multiplying the spatial solution, Equation (60), by the temporal solution, Equation (61), and combining coefficients

$$w(x,t) = \left(\overline{A}x^3 + \overline{B}x^2 + \overline{C}x + \overline{D}\right)e^{\mathrm{i}\omega t} \tag{62}$$

The out-of-plane rotation, $\theta(x,t)$, is then given by the derivative of the transverse displacement, $w(x,t)$, with respect to the x-direction as

$$\theta(x,t) = \frac{\partial w(x,t)}{\partial x} = \left(3\overline{A}x^2 + 2\overline{B}x + \overline{C}\right)e^{i\omega t} \tag{63}$$

The shape functions for the transverse displacement and rotation of the beam element can now be formulated following the same procedure as the conventional bar element. Writing the assumed form of the solution, Equations (62) and (63), in matrix form gives

$$\begin{Bmatrix} w(x,t) \\ \theta(x,t) \end{Bmatrix} = [\mathbf{X}]\{\mathbf{a}\}e^{i\omega t} \tag{64}$$

The matrix $[\mathbf{X}]$ is a 2X4 matrix formed from the spatial solution and its derivative with respect to x and is written as

$$[\mathbf{X}] = \begin{bmatrix} x^3 & x^2 & x & 1 \\ 3x^2 & 2x & 1 & 0 \end{bmatrix} \tag{65}$$

The vector $\{\mathbf{a}\}$ is a column vector of the unknown coefficients

$$\{\mathbf{a}\} = \begin{Bmatrix} \overline{A} \\ \overline{B} \\ \overline{C} \\ \overline{D} \end{Bmatrix} \tag{66}$$

The transverse displacement and out-of-plane rotation due to bending at each end of the beam, shown as $w_1, w_2, \theta_1, \theta_2,$ in Figure 4, were chosen as the nodal DOF. The vector $\{\mathbf{d}\}$, from Equation (2), is then defined as the temporal solution of the nodal DOF.

$$\{\mathbf{d}\} = \begin{Bmatrix} w_1 \\ \theta_1 \\ w_2 \\ \theta_2 \end{Bmatrix} e^{\mathrm{i}\omega t} \tag{67}$$

Evaluating Equations (62) and (63) at the nodes and writing in matrix form gives

$$\begin{Bmatrix} w_1 \\ \theta_1 \\ w_2 \\ \theta_2 \end{Bmatrix} e^{i\omega t} = [\mathbf{A}]\{\mathbf{a}\} e^{\mathrm{i}\omega t} \tag{68}$$

where, $[\mathbf{A}]$ is a matrix of the row vectors of $[\mathbf{X}]$ evaluated at the nodes. For the case of the beam element, $[\mathbf{A}]$ is given by

$$[\mathbf{A}] = \begin{bmatrix} 0 & 0 & 0 & 1 \\ 0 & 0 & 1 & 0 \\ L^3 & L^2 & L & 1 \\ 3L^2 & 2L & 1 & 0 \end{bmatrix} \tag{69}$$

Again, $\{\mathbf{a}\}$ is the vector of unknown coefficients as given in Equation (66). Now, using the expression for the shape function from section 3.1.2

$$[\mathbf{N}] = [\mathbf{X}][\mathbf{A}]^{-1} \tag{22}$$

The shape functions for the beam element can be written as

$$[\mathbf{N}] = \begin{bmatrix} \mathbf{N}_w \\ \mathbf{N}_\theta \end{bmatrix} = \begin{bmatrix} 1 - \dfrac{3x^2}{L^2} + \dfrac{2x^3}{L^3}, & x - \dfrac{2x^2}{L} + \dfrac{x^3}{L^2}, & \dfrac{3x^2}{L^2} - \dfrac{2x^3}{L^3}, & -\dfrac{x^2}{L} + \dfrac{x^3}{L^2} \\ 6\left(\dfrac{x^2}{L^3} - \dfrac{x}{L^2}\right), & \dfrac{3x^2}{L^2} - \dfrac{4x}{L} + 1, & 6\left(\dfrac{x}{L^2} - \dfrac{x^2}{L^3}\right), & \dfrac{3x^2}{L^2} - \dfrac{2x}{L} \end{bmatrix} \tag{70}$$

where, the first row is the shape function for the transverse displacement, $w(x)$, and the second row is the shape function for the rotation due to bending, $\theta(x)$.

The conventional beam element shape functions, shown in Equation (70), were formed from the assumed separable form of the displacement field. The polynomial function that represents the static transverse displacement field was used as the basis function for the spatial component of the solution. A complex exponential was used as the temporal solution because of the interest in only harmonic excitation. The basis function was then incorporated into the shape functions such that the displacement field could be calculated from the nodal displacements. The following section describes the details in forming the dynamic stiffness matrix from the assumed shape function and temporal solution.

4.1.3. Dynamic Stiffness

The dynamic stiffness matrix for a harmonically forced beam element can be found by substituting the assumed form of the temporal solution into the governing structural dynamics equation and regrouping the terms. The resulting dynamic stiffness is a single matrix that can be used to calculate the harmonic response of the nodal displacements and loads. The mass and stiffness matrices that make up the dynamic stiffness matrix are defined by the shape function determined in section 4.1.2.

The mass matrix, $[\mathbf{m}]$, and the stiffness matrix, $[\mathbf{k}]$, from Equations (7) and (8) respectively, simplified for the beam element are

$$[\mathbf{m}] = \int_0^L \mu A [\mathbf{N}]^T [\mathbf{N}] dx \tag{71}$$

$$\left[\mathbf{k}\right] = \int_0^L E\,I\left[\mathbf{B}\right]^T\left[\mathbf{B}\right]dx \tag{72}$$

where, μ is the mass density, A is the cross sectional area, E is the elastic modulus, and I is the area moment of inertia. The strain-displacement matrix, $\left[\mathbf{B}\right]$, is given by

$$\left[\mathbf{B}\right] = \frac{d}{dx^2}\left[\mathbf{N}\right] \tag{73}$$

where, $\left[\mathbf{N}\right]$ is the shape function matrix given by Equation (70).

Substituting the assumed form of the temporal solution, $\left\{\mathbf{d}\right\}$, from Equation (67), into the governing structural dynamics equation, Equation (9), gives

$$-\omega^2\left[\mathbf{m}\right]\left\{\mathbf{d}\right\} + \left[\mathbf{k}\right]\left\{\mathbf{d}\right\} = \left\{\mathbf{r}_{ext}\right\} \tag{74}$$

where, the exponential term, $e^{i\omega t}$, has been cancelled from both sides of the equation. The dynamic stiffness, $\mathbf{K}_{Dyn}$, of the conventional beam element can then be written as

$$\left[\mathbf{K}_{Dyn}\right] = -\omega^2\left[\mathbf{m}\right] + \left[\mathbf{k}\right] \tag{75}$$

such that,

$$\left[\mathbf{K}_{dyn}\right]\left\{\mathbf{d}\right\} = \left\{\mathbf{r}_{ext}\right\} \tag{76}$$

The dynamic stiffness matrix, given in Equation (75) above, was formed by incorporating the assumed temporal solution into the governing structural dynamic equation. Notice that the mass and stiffness matrices are computed separately and then added together. The inertia effects are incorporated through scaling the mass matrix by the forcing frequency squared.

4.2. Spectral Elements

4.2.1. Development of Governing Equation

The formulation of the governing equation for the Euler-Bernoulli prismatic beam, with constant cross section, begins with the free body diagram of a differential element of the beam, shown in Figure 5. The inertial force associated with transverse acceleration has been included in the free body diagram in the form of a D'Alembert's Principle formulation. The shear-pair and moment-pair shown in Figure 5 establish the positive sign convention to be used in the formulation.

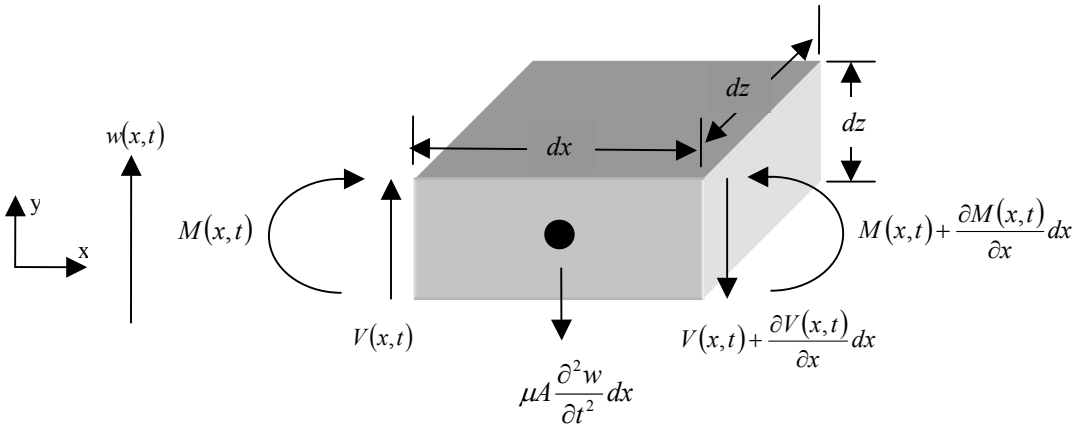

Figure 5. Free Body Diagram of Differential Beam Element with Positive Shear and Moment

The force balance in the y-direction can be written as

$$V(x,t)-V(x,t)-\frac{\partial V(x,t)}{\partial x}dx-\mu A\frac{\partial^2 w(x,t)}{\partial t^2}dx=0 \tag{77}$$

where, A is the constant cross sectional area, $dydz$. Simplifying the force balance gives

$$\frac{\partial V(x,t)}{\partial x}=-\mu A\frac{\partial^2 w(x,t)}{\partial t^2} \tag{78}$$

The moment balance about the center of the differential element can be written as

$$-M(x,t)+M(x,t)+\frac{\partial M(x,t)}{\partial x}dx-V(x,t)\frac{dx}{2}-\left(V(x,t)+\frac{\partial V(x,t)}{\partial x}dx\right)\frac{dx}{2}=0 \tag{79}$$

Simplifying the moment balance and disregarding terms with higher order smallness yields the following expression for the shear.

$$V(x,t)=\frac{\partial M(x,t)}{\partial x} \tag{80}$$

Substituting the expression for the shear from Equation (80) into the simplified force balance in Equation (78) gives

$$\frac{\partial^2 M(x,t)}{\partial x^2}=-\mu A\frac{\partial^2 w(x,t)}{\partial t^2} \tag{81}$$

The moment-curvature relationship from elementary flexure theory is known to be

$$M(x,t)=EI\frac{\partial^2 w(x,t)}{\partial x^2} \tag{82}$$

Substituting the elementary equation for the moment, Equation (82), into Equation (81) yields the common form of the unforced Euler-Bernoulli governing equation as

$$EI\frac{\partial^4 w(x,t)}{\partial x^4} = -\mu A\frac{\partial^2 w(x,t)}{\partial t^2} \tag{83}$$

The governing PDE for the prismatic Euler-Bernoulli beam element was determined through the balancing of forces and moments on an infinitesimal beam element. The resulting separable PDE is fourth order in space and second order in time. The following subsection described the development of the solution of the governing PDE.

4.2.2. Representation of the Displacement Field

Similar to the spectral bar element, a solution to the governing beam equation can be found using a separation of variables technique. Separating the variables yields one constant coefficient fourth order ODE in space and one constant coefficient second order ODE in time. A general exponential solution can be assumed for each of the two ODEs. The remainder of the subsection gives the details of the development of the solution to the governing PDE.

A separable solution of the form

$$w(x,t) = X(x)T(t) \tag{84}$$

is assumed for the transverse displacement. Substituting the assumed solution, Equation (84), into the governing PDE, Equation (83), and grouping $X(x)$ terms on one-side gives

$$EI\frac{X''''(x)}{X(x)} = -\mu A\frac{\ddot{T}(t)}{T(t)} \tag{85}$$

Setting each side of the equation equal to the unknown constant $(\overline{E})$, gives two constant coefficient ordinary differential equations.

$$EI\frac{X''''(x)}{X(x)} = \overline{E} \tag{86}$$

$$-\mu A\frac{\ddot{T}(t)}{T(t)} = \overline{E} \tag{87}$$

The assumed form of the temporal ODE, Equation (87), for the case of harmonic forcing is again

$$T(t) = \overline{F}e^{\mathrm{i}\omega t} \tag{88}$$

Substituting the assumed form of the temporal solution, Equation (88), into the governing temporal ODE, Equation (87), gives

$$(-\mu A)(-\omega^2)\overline{F}e^{\mathrm{i}\omega t} - \overline{E}\overline{F}e^{\mathrm{i}\omega t} = 0 \tag{89}$$

Simplifying and solving for the unknown coefficient $\overline{E}$ yields

$$\overline{E} = \mu A\omega^2 \tag{90}$$

The assumed form of the spatial solution to the constant coefficient ODE in Equation (86) is

$$X(x) = \overline{A} e^{\mathbf{i}\alpha x} \tag{91}$$

Substituting the assumed spatial solution, Equation (91), into Equation (86) gives

$$EI\alpha^4 \overline{A} e^{\mathbf{i}\alpha x} - \overline{EA} e^{\mathbf{i}\alpha x} = 0 \tag{92}$$

Substituting the value of $\overline{E}$ found from the temporal ODE in Equation (90) into Equation (92) gives a characteristic equation

$$EI\alpha^4 - \mu A\omega^2 = 0 \tag{93}$$

Solving for the flexural wave number, α, gives the spectral relation(s) for the beam. In this case there are four possible values of spatial wave number that satisfy the characteristic equation and are given as,

$$\begin{aligned} \alpha_1 &= \sqrt[4]{\frac{\mu A\omega^2}{EI}} \\ \alpha_2 &= \mathbf{i}\sqrt[4]{\frac{\mu A\omega^2}{EI}} \\ \alpha_3 &= -\sqrt[4]{\frac{\mu A\omega^2}{EI}} \\ \alpha_4 &= -\mathbf{i}\sqrt[4]{\frac{\mu A\omega^2}{EI}} \end{aligned} \tag{94}$$

Using one exponential function for each possible value of spatial wave number results in a spatial solution of the form

$$X(x) = \overline{A} e^{\mathbf{i}\alpha_1 x} + \overline{B} e^{\mathbf{i}\alpha_2 x} + \overline{C} e^{\mathbf{i}\alpha_3 x} + \overline{D} e^{\mathbf{i}\alpha_4 x} \tag{95}$$

Combining the complete spatial solution, Equation (95), with the temporal solution, Equation (88), and combining unknown coefficients gives the total solution for the displacement field to be

$$w(x,t) = \left(\overline{A}e^{\mathbf{i}\alpha_1 x} + \overline{B}e^{\mathbf{i}\alpha_2 x} + \overline{C}e^{\mathbf{i}\alpha_3 x} + \overline{D}e^{\mathbf{i}\alpha_4 x}\right)e^{\mathbf{i}\omega t} \tag{96}$$

The solution of the beam governing PDE was found through a separation of variables technique. The resulting constant coefficient ODEs were assumed to have exponential solutions. The characteristic equation yielded four possible spatial wave numbers. The four wave numbers were incorporated into the complete spatial solution to form the eigenfunction and the total solution, Equation (96), of the governing PDE, Equation (83). The following section describes the development of the dynamic stiffness matrix from the eigenfunction of the governing PDE.

4.2.3. Dynamic Stiffness

Now that the representation of the displacement field has been established from the governing partial differential equation, the dynamic stiffness can be formulated. The dynamic stiffness is formulated using a direct method. Both the nodal displacements and nodal forces can be written in terms of the unknown coefficients $\left(\overline{A},\overline{B},\overline{C},\overline{D}\right)$. These relations can then be used to form an expression for the dynamic stiffness matrix. The spectral beam element developed will use two nodes with two DOF, transverse displacement $\left(w_1, w_2\right)$ and rotation $\left(\theta_1,\theta_2\right)$, at each node as shown in Figure 6.

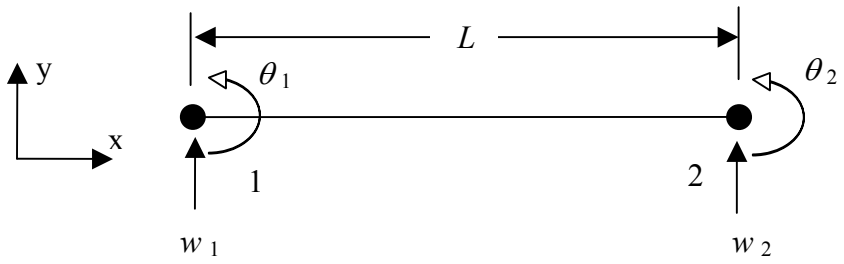

Figure 6. Schematic of Nodal DOF of Spectral Euler-Bernoulli Beam Element

Writing the displacements and rotations at the nodes in matrix form gives

$$\begin{Bmatrix} w(0,t) \\ \theta(0,t) \\ w(L,t) \\ \theta(L,t) \end{Bmatrix} = \begin{Bmatrix} w_1 \\ \theta_1 \\ w_2 \\ \theta_2 \end{Bmatrix} e^{\iota\omega t} = [\mathbf{D}] \begin{Bmatrix} \overline{A} \\ \overline{B} \\ \overline{C} \\ \overline{D} \end{Bmatrix} e^{\iota\omega t} \tag{97}$$

For the case of the Euler-Bernoulli beam elements, $[\mathbf{D}]$ is a 4X4 matrix and has the form

$$[\mathbf{D}] = \begin{bmatrix} 1 & 1 & 1 & 1 \\ \mathbf{i}\alpha_1 & \mathbf{i}\alpha_2 & \mathbf{i}\alpha_3 & \mathbf{i}\alpha_4 \\ e^{\mathbf{i}\alpha_1 L} & e^{\mathbf{i}\alpha_2 L} & e^{\mathbf{i}\alpha_3 L} & e^{\mathbf{i}\alpha_4 L} \\ \mathbf{i}\alpha_1 e^{\mathbf{i}\alpha_1 L} & \mathbf{i}\alpha_2 e^{\mathbf{i}\alpha_2 L} & \mathbf{i}\alpha_3 e^{\mathbf{i}\alpha_3 L} & \mathbf{i}\alpha_4 e^{\mathbf{i}\alpha_4 L} \end{bmatrix} \tag{98}$$

Writing the shears and moments at the nodal locations in matrix form gives

$$\begin{Bmatrix} V(0,t) \\ -M(0,t) \\ -V(L,t) \\ M(L,t) \end{Bmatrix} = \begin{Bmatrix} V_1 \\ M_1 \\ V_2 \\ M_2 \end{Bmatrix} e^{\iota\omega t} = [\mathbf{F}] \begin{Bmatrix} \overline{A} \\ \overline{B} \\ \overline{C} \\ \overline{D} \end{Bmatrix} e^{\iota\omega t} \tag{99}$$

The expressions for the shear, $V(x)$, and the moment, $M(x)$, are as developed in section 4.2.1

$$V(x,t) = \frac{\partial M(x,t)}{\partial x} \tag{80}$$

$$M(x,t) = EI \frac{\partial^2 w(x,t)}{\partial x^2} \tag{82}$$

For the case of the Euler-Bernoulli beam element, $[\mathbf{F}]$ is 4 X 4 matrix and has the form

$$[\mathbf{F}] = EI \begin{bmatrix} -\mathbf{i}\alpha_1^3 & -\mathbf{i}\alpha_2^3 & -\mathbf{i}\alpha_3^3 & -\mathbf{i}\alpha_4^3 \\ \alpha_1^2 & \alpha_2^2 & \alpha_3^2 & \alpha_4^2 \\ \mathbf{i}\alpha_1^3 e^{\mathbf{i}\alpha_1 L} & \mathbf{i}\alpha_2^3 e^{\mathbf{i}\alpha_2 L} & \mathbf{i}\alpha_3^3 e^{\mathbf{i}\alpha_3 L} & \mathbf{i}\alpha_4^3 e^{\mathbf{i}\alpha_4 L} \\ -\alpha_1^2 e^{\mathbf{i}\alpha_1 L} & -\alpha_2^2 e^{\mathbf{i}\alpha_2 L} & -\alpha_3^2 e^{\mathbf{i}\alpha_3 L} & -\alpha_4^2 e^{\mathbf{i}\alpha_4 L} \end{bmatrix} \tag{100}$$

Figure 5 shows the free body diagram of a differential beam element with the shear and moment convention. The minus signs in the expressions for the shear and moment in Equation (99) are to ensure that positive loads will create positive displacements. The transverse displacement and rotation evaluated at the nodes in Equation (97) form the vector of nodal DOF $\{\mathbf{d}\}$

$$\{\mathbf{d}\} = \begin{Bmatrix} w_1 \\ \theta_1 \\ w_2 \\ \theta_2 \end{Bmatrix} e^{i\omega t} \tag{101}$$

The shears and moments evaluated at the nodes in Equation (99) form the vector of nodal forces $\{\mathbf{f}\}$

$$\{\mathbf{f}\} = \begin{Bmatrix} V_1 \\ M_1 \\ V_2 \\ M_2 \end{Bmatrix} e^{i\omega t} \tag{102}$$

The dynamic stiffness matrix $[\mathbf{K}_{Dyn}]$ relates the nodal DOF $\{\mathbf{d}\}$ to the nodal loads $\{\mathbf{f}\}$

$$\{\mathbf{f}\} = [\mathbf{K}_{Dyn}]\{\mathbf{d}\} \tag{103}$$

The dynamic stiffness matrix can be solved from Equations (97) and (99) to be

$$[\mathbf{K}_{Dyn}] = [\mathbf{F}][\mathbf{D}]^{-1} \tag{104}$$

The complete dynamic stiffness for the Euler-Bernoulli spectral beam element is shown in Appendix A. The dynamic stiffness matrix is symmetric and includes the transverse inertial effects. The exponential functions have been converted to trigonometric functions in the matrix shown in Appendix A.

The shape function of the spectral beam element can be expressed in terms of the $[\mathbf{D}]$ matrix. The shape functions for the transverse displacement $[\mathbf{N}_w]$ and the rotation $[\mathbf{N}_\theta]$ are

$$[\mathbf{N}] = \begin{bmatrix} \mathbf{N}_w \\ \mathbf{N}_\theta \end{bmatrix} = \begin{bmatrix} e^{\mathbf{i}\alpha_1 x} & e^{\mathbf{i}\alpha_2 x} & e^{\mathbf{i}\alpha_3 x} & e^{\mathbf{i}\alpha_4 x} \\ \mathbf{i}\alpha_1 e^{\mathbf{i}\alpha_1 x} & \mathbf{i}\alpha_2 e^{\mathbf{i}\alpha_2 x} & \mathbf{i}\alpha_3 e^{\mathbf{i}\alpha_3 x} & \mathbf{i}\alpha_4 e^{\mathbf{i}\alpha_4 x} \end{bmatrix} [\mathbf{D}]^{-1} \tag{105}$$

The complete expression for the displacement field in terms of the nodal DOF $\{\mathbf{d}\}$ and the shape functions $[\mathbf{N}]$ is

$$\begin{bmatrix} w(x) \\ \theta(x) \end{bmatrix} = [\mathbf{N}]\{\mathbf{d}\} \tag{106}$$

In summary, the dynamic stiffness matrix was developed through a direct method using the nodal displacements and forces. The displacement field that the nodal displacements and forces were based on was the exact solution, or eigenfunction, of the governing PDE. Because the dynamic stiffness is based on the exact solution to the governing PDE, the nodal displacements and forces obtained through the use of the dynamic stiffness will also be exact. The exact form of the displacement field was also incorporated into a shape function for the spectral beam element. The following section considers a cantilevered beam example problem to compare the performance of the spectral beam element to that of the conventional beam element.

4.3. Straight Geometry Example Problem

In this section, the conventional and spectral beam elements will be compared using a simple example. A cantilever beam with harmonic loading will be analyzed using both types of elements. A schematic of the example problem is shown in Figure 7.

The material used in the example was aluminum with elastic modulus of 10^6 *psi* and a density of $0.26 \times 10^{-3} \frac{lbf\ s^2}{in^4}$. A harmonic analysis was preformed from 1 *Hz* to 15.915 *kHz* with 300 logarithmically spaced spectral lines. The magnitude of the end load was 100 *lbf*.

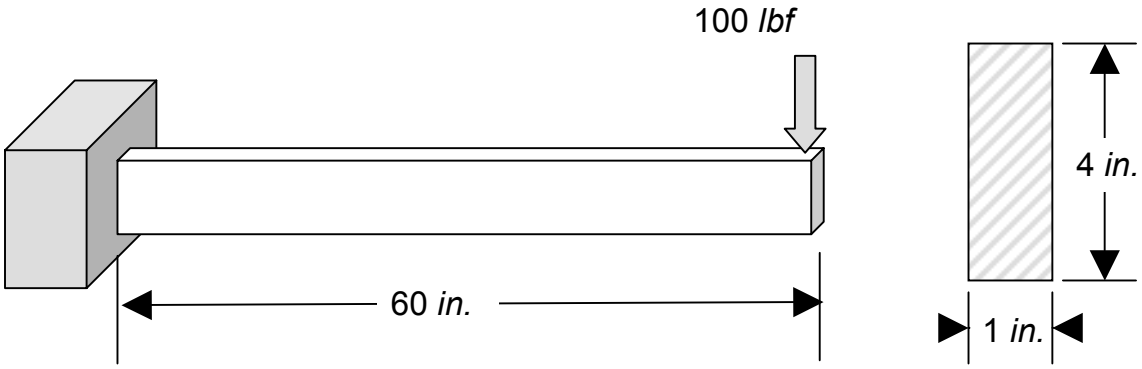

Figure 7. Schematic of Cantilever Beam Example Problem

The number of elements was increased for both the conventional and spectral models until the amplitude of the peaks of the frequency response changed by less than 10%. A summary of the number of elements required to converge the peaks of the frequency response is shown in Table 2. Only one spectral element is needed to converge the peaks of the frequency response, adding an additional element results in the same deflection as with a single spectral element. The required number of conventional elements varied according to which peak was being converged. The frequencies of the peaks are also compared to the natural frequencies calculated from beam theory. The percent difference of the natural frequencies predicted by the element methods is never more than 2.0 % from Euler-Bernoulli beam theory. The peaks of the conventional and spectral element responses occurred at the same frequencies.

Table 2. Summary of Number of Elements Required to Converge the Peaks of the Response

# of Peaks Converged	Number of FEA Elements	Number of Spectral Elements	Frequency (*Hz*)	Frequency From Beam Theory (*Hz*)	% Difference in Frequency
1	3	1	35.72	35.20	1.48%
2	6	1	219.88	220.60	-0.33%
3	7	1	626.90	617.68	1.49%
4	8	1	1196.74	1210.41	-1.13%
5	12	1	2020.69	2000.90	0.99%
6	13	1	3016.47	2989.00	0.92%
7	14	1	4231.55	4174.71	1.36%
8	20	1	5584.70	5558.05	0.48%
9	32	1	7144.96	7139.01	0.08%
10	20	1	8863.39	8917.59	-0.61%
11	22	1	10997.65	10893.78	0.95%
12	23	1	13231.22	13067.60	1.25%
13	34	1	15434.76	15439.03	-0.03%

Figure 8 shows the magnitude of the deflection of the beam tip versus frequency for a single spectral element and five conventional elements. The responses of the two elements match nicely from 10 to 1000 *Hz*. At frequencies above 1000 *Hz* differences in both peak amplitude and location can be seen. The cause of the disagreement at frequencies above 1000 *Hz* is that five conventional elements can't represent the displacement field very well. Figure 9 shows the difference in deformed shape for a 1 element spectral model and a 5 element conventional model for frequencies of 1000, 3000, and 5000 *Hz*. One way to increase the agreement between the two elements at high frequency is to use more conventional elements.

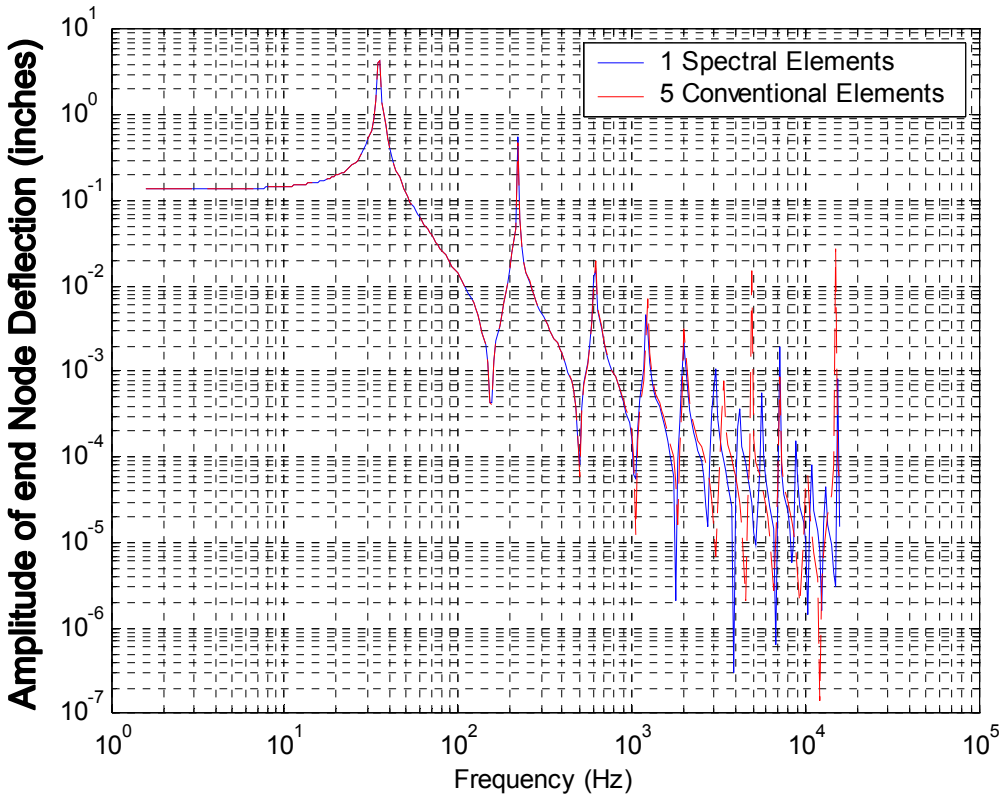

Figure 8. Comparison of End Node Deflection for 5 Conventional Elements and 1 Spectral Element

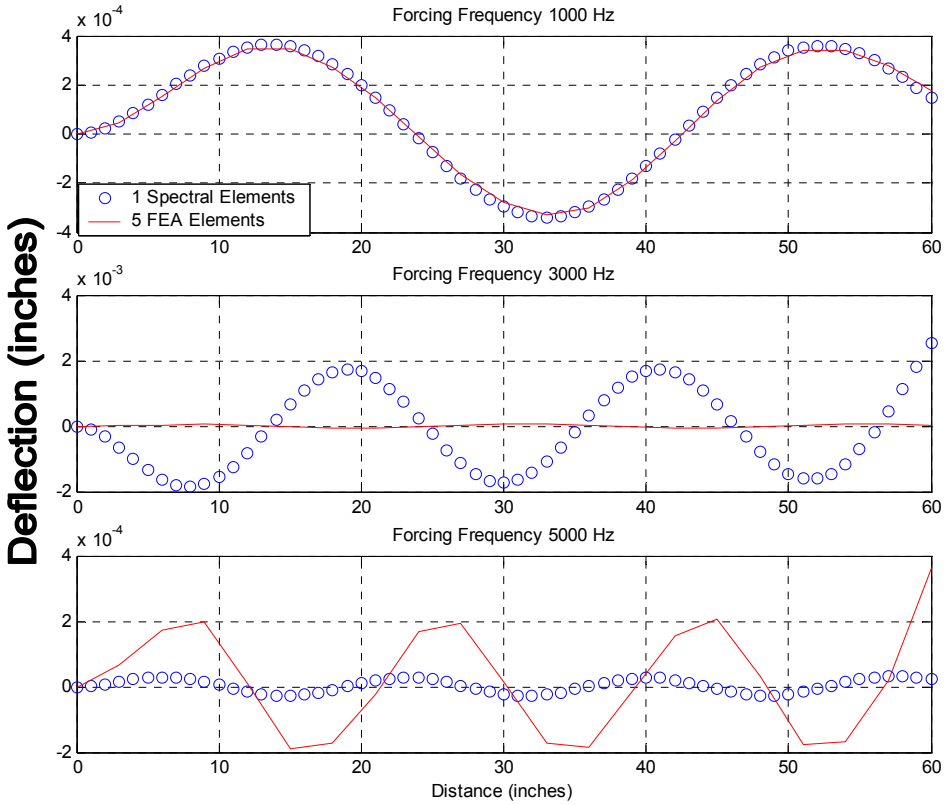

Figure 9. Deformed Shapes for Forcing Frequencies of 1000, 3000, and 5000 *Hz*

When more elements are added to the conventional element solution it more closely matches the spectral element solution. Figure 10 shows the deflection response of the free end of the beam using a single spectral element and 34 conventional elements. It can be seen that the conventional element response more closely matches the spectral response as compared to only using 5 conventional elements, as shown in Figure 8. The peak amplitude and location, of the two responses, match more closely even at high frequency. Figure 11 shows the deformed shapes for forcing frequencies of 1000, 3000, and 5000 *Hz* for 1 spectral element and 34 conventional elements.

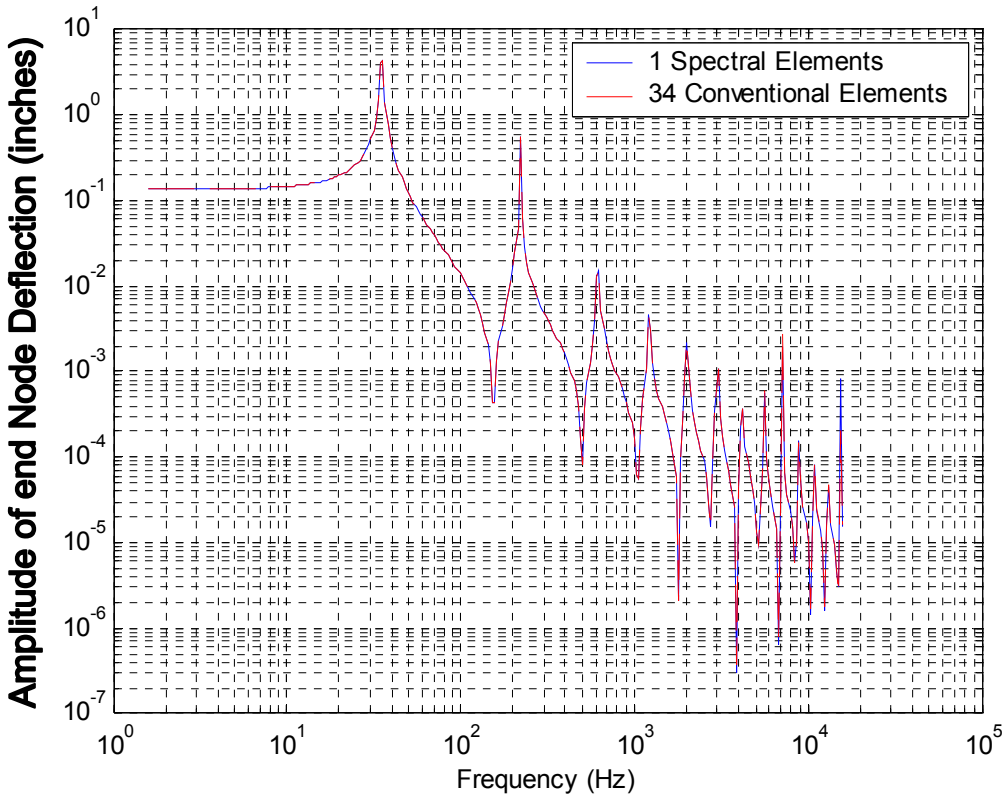

Figure 10. Comparison of End Node Deflection for 34 Conventional Elements and 1 Spectral Element

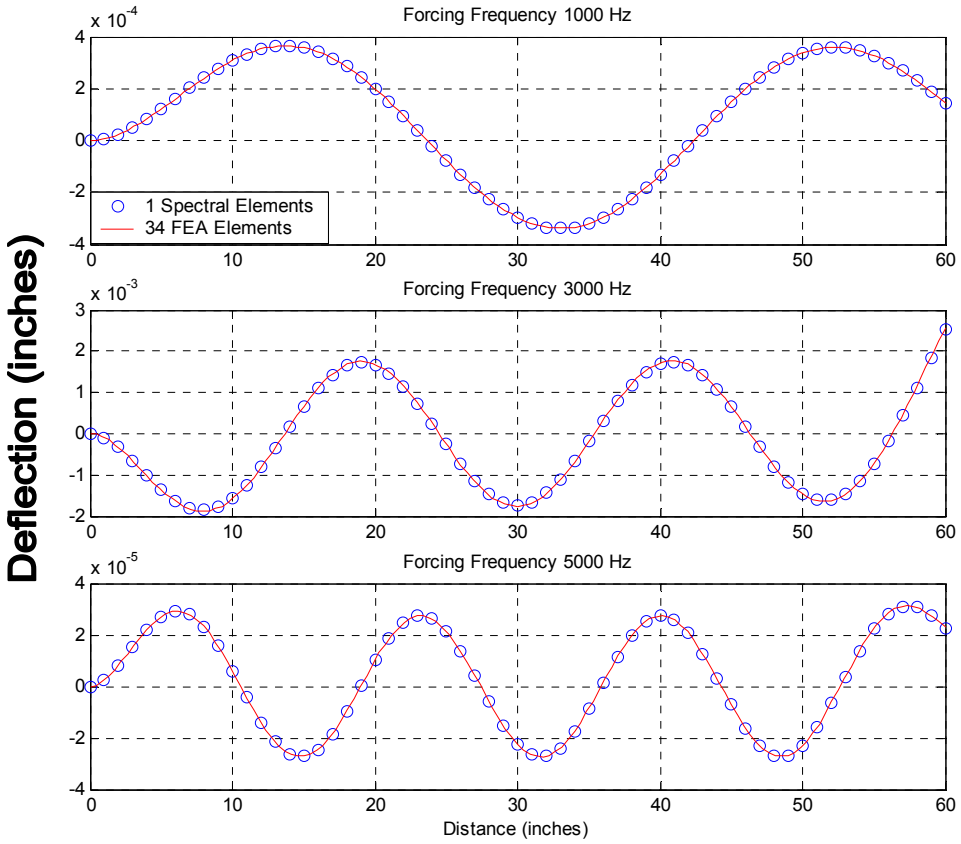

Figure 11. Deformed Shape Comparison for 1000, 3000, and 5000 *Hz* with 1 Spectral and 34 Conventional FE Elements

Figure 12 shows a plot of the percent difference between the spectral and conventional responses using one and 34 elements respectively. The percent difference is near 1% at low frequency and increases up to a maximum of 75%.

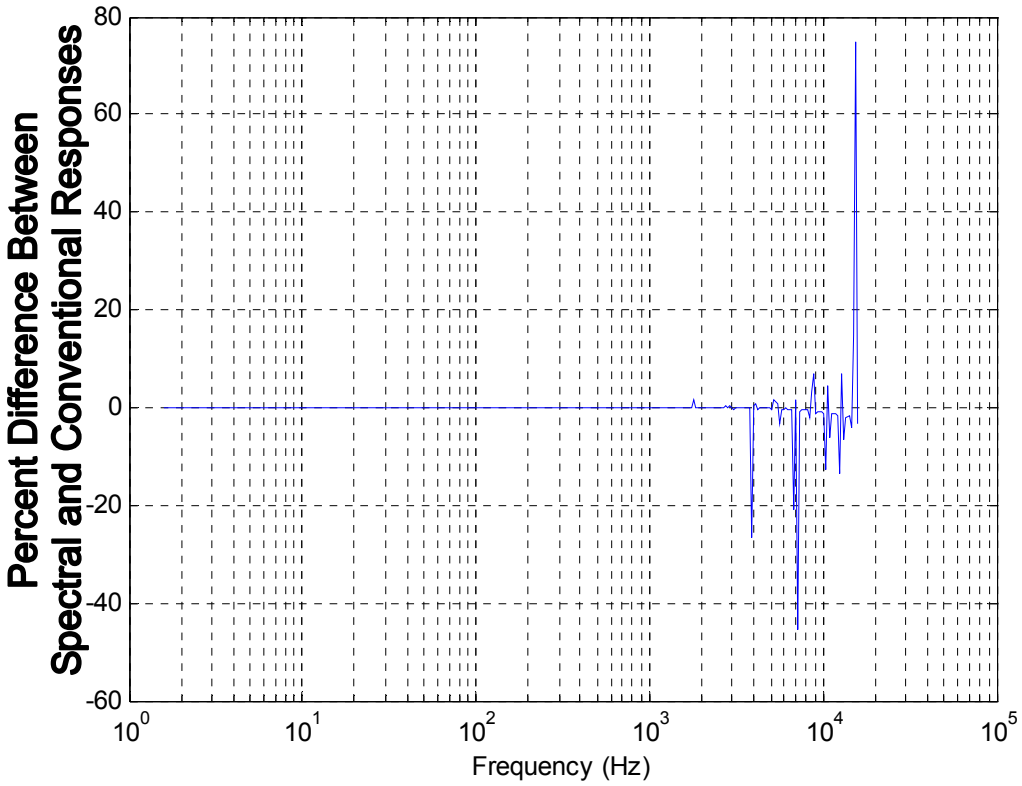

Figure 12. Percent Difference Using 1 Spectral and 34 Conventional Elements

This example illustrates the dynamic modeling power of the spectral beam element. A single spectral element is capable of representing the Euler-Bernoulli beam theory into frequency ranges where the theory is typically considered to depart from reality. The cantilever beam example required 34 conventional elements to give a similar response as a single spectral element at 10 *kHz*. The reduction in elements results in less computer resources required to solve a given problem. Another important result is that the dynamics is not driving the mesh density in the spectral element model. The model mesh only needs to be refined to capture the geometry, boundary conditions, and loading. The following section considers a simply supported curved beam problem to illustrate the effects of geometry on the mesh density of the spectral element model.

4.4. Curved Geometry Example Problem

Another interesting subject is how the spectral beam elements perform on geometry that is curved. To investigate this problem a profile of a parabolic mirror will be analyzed using both spectral and conventional beam elements. Figure 13 shows a schematic of a mirror profile represented with beam elements. The mirror shape is given by the *Sag* Equation as

$$Sag = \frac{(1/\rho)r^2}{1+\sqrt{1-(1+Cc)+(1/\rho)^2 r^2}} \tag{107}$$

where, ρ is the radius of curvature, r is the radial distance from the center, and Cc is the conic constant. The radius of curvature of the mirror is 29.25 *inches* , the conic constant is -1.046. The material properties used in the analysis were again aluminum with an elastic modulus of 10^6 *psi* and a density of $0.26\times10^{-3}\ \frac{lbf\ sec^2}{in^4}$. The magnitude of the load was 100 *lbf* and is applied at center span of the beam.

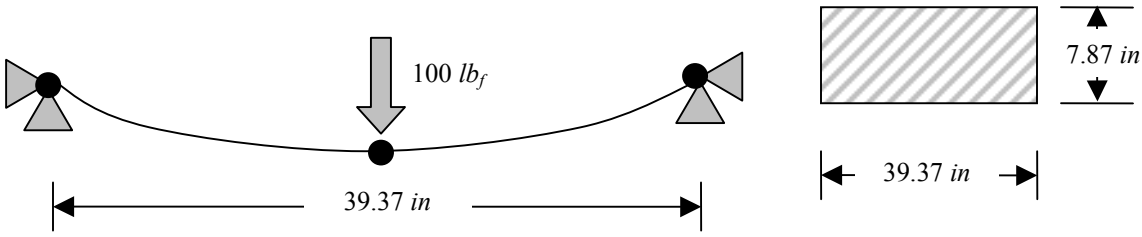

Figure 13. Schematic of Curved Mirror Profile and Beam Cross Section

In order to analyze the curved structure, a beam of arbitrary orientation in the plane must be used. To convert the aligned beam element of section 4.2.3 into an arbitrary

beam, the 2 DOF of the bar element are superimposed over the 4 DOF of the beam. The resulting stiffness matrix must be multiplied by a transformation matrix Doyle[7]. For the arbitrary in-plane beam nodal DOF vector

$$\{\mathbf{d}\} = \{u_1 \quad w_1 \quad \theta_1 \quad u_2 \quad w_2 \quad \theta_2\} \tag{108}$$

the transformation matrix for the dynamic stiffness is given by

$$[\mathbf{T}] = \begin{bmatrix} [\mathbf{R}] & 0 \\ 0 & [\mathbf{R}] \end{bmatrix} \tag{109}$$

where, $[\mathbf{R}]$ is the 3X3 transformation matrix for each node. For the case of the local and global axes having the same origin and only being rotated by some angle β in the x-y plane, $[\mathbf{R}]$ is given by Doyle [7] to be

$$\mathbf{R} = \begin{bmatrix} \cos(\beta) & \cos\left(\beta + \frac{\pi}{2}\right) & 0 \\ \cos\left(\beta + \frac{\pi}{2}\right) & \cos(\beta) & 0 \\ 0 & 0 & 1 \end{bmatrix} \tag{110}$$

The transformed dynamic stiffness matrix is then given by

$$[\mathbf{K}_T] = [\mathbf{T}]^T [\mathbf{K}_{Dyn}][\mathbf{T}] \tag{111}$$

A harmonic analysis was preformed from 100 *Hz* to15.915 *kHz* with 300 logarithmically spaced spectral lines. The number of elements was increased for the conventional and spectral models until the peaks of the receptance frequency

response function (FRF) changed by less than 10%. A summary of the number of elements required to converge the peaks of the receptance FRF is given in Table 3. It takes 10 elements for both the conventional and the spectral models to represent the geometry and capture the first peak of the receptance. The number of conventional elements required to converge successive receptance peaks increases steadily up to 20 for the fifth peak. The number of spectral elements required to converge the peaks remains fairly constant around ten. The number of elements required to converge peaks 2 and 3 are greater than peaks 4 and 5 because of the choice of excitation frequency. It is thought that the excitation frequency is closer to the actual natural frequency for peaks 2 and 3 than it is for peaks 4 and 5. Figure 14 shows a comparison of the deformed shapes for peaks 2 and 3 of the FRF. The conventional and spectral models agree about the shape at 3548 *Hz* and do not agree about the shapes at 4897 *Hz*. It is shown in Table 3 that both conventional and spectral models require more elements for peak 2 than for peak 3.

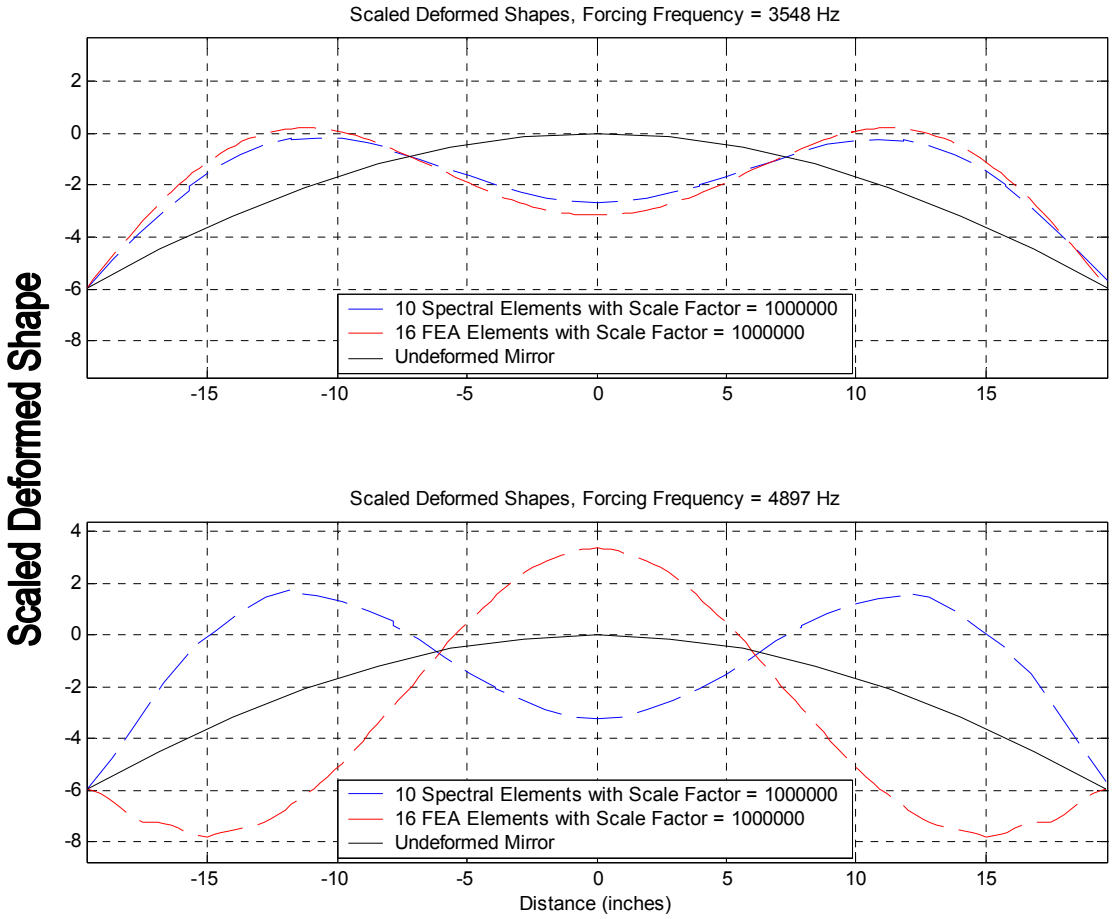

Figure 14. Comparison of Deformed Shape for FRF Peaks 2 and 3 of the Curved Problem

Table 3. Summary of Number of Elements Required to Converge Receptance Peaks

# of Peaks Converged	Frequency (*Hz*)	Number of Conventional Elements	Number of Speactral Elements
1	850.00	10	10
2	3548.00	30	14
3	4897.00	14	12
4	9332.00	16	10
5	10351.00	20	10

Figure 15 shows the receptance of the curved example problem using 10 spectral and 16 conventional elements. Similarly to the straight cantilever example problem, the difference between the conventional and spectral response increases with frequency. In Figure 15 the difference becomes noticeable as the frequency approaches 10 *kHz*.

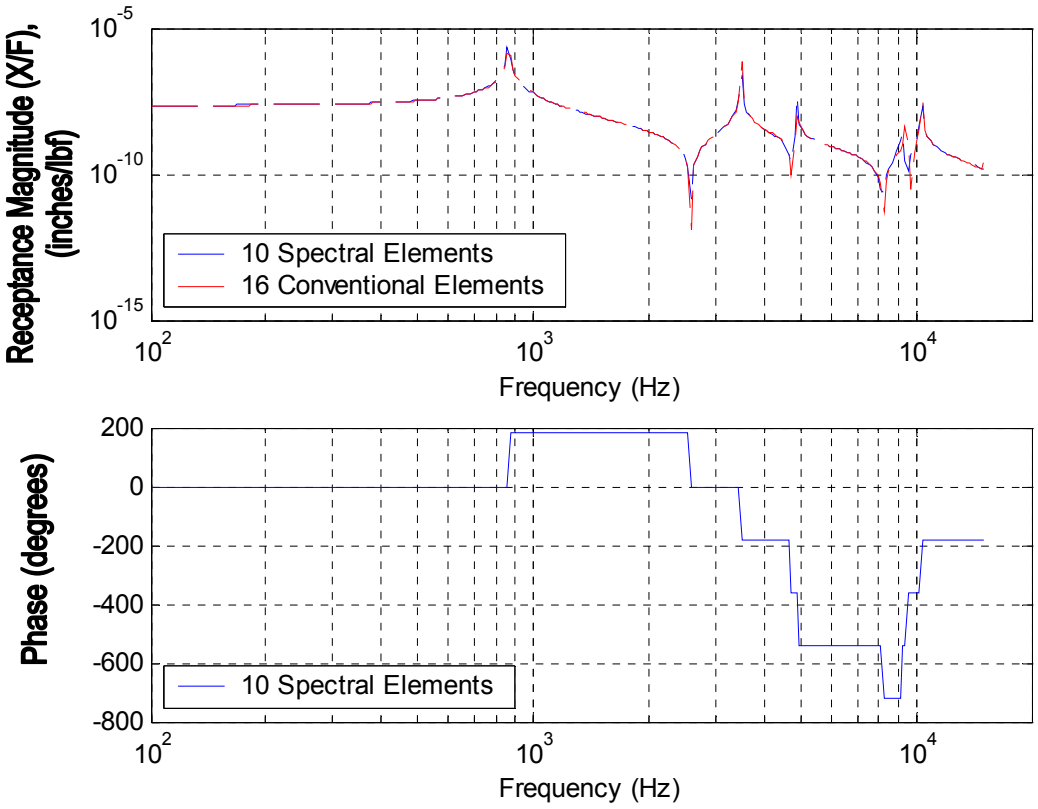

Figure 15. Receptance for Curved Example Using 10 Spectral and 16 Conventional Elements

The major result of the curved example is that the dynamics is not driving the mesh density in the spectral model. Once the geometry, loading, and boundary conditions are converged by refining the mesh, few additional spectral elements were required to analyze higher frequency. In the curved example, the first peak of the response was

converged by increasing the number of elements until the response changed by less than 10%. Only ten spectral elements were required to analyze peaks 1, 4, and 5. Peaks 2 and 3 required 14 and 12 spectral elements, respectively, to converge to less than 10%. The increased number of elements for peaks 2 and 3 was most likely due to the choice of excitation frequency. The general trend was that 10 spectral elements were required to analyze peaks 1 and 5. The conventional formulation required 10 and 20 conventional elements to converge the same two peaks.

4.5. Timoshenko Beam Spectral Element

Typically, as the frequency of the response increases, the assumption of Euler-Bernoulli beam theory, that shear deformation is not important compared to the transverse deformation, fail to accurately represent the mechanics of the beam. At high frequency, the shear forces can largely contribute to the shear deformation of the cross section of the beam. Timoshenko's theory includes the affect of shear deformation and rotatory inertia.

Section 4.5.3 shows that it is possible to formulate spectral elements based on higher order beam theories, such as Timoshenko's beam theory. Formulation of a spectral beam element based on Timoshenko's theory follows a similar procedure as the Euler-Bernoulli spectral element. The elements dynamic stiffness matrix and shape functions are based on the eigenfunctions of the governing differential equation. The formulation of the Timoshenko governing equations starts with a force and moment balance on a differential element. The following subsection describes the development of the governing equations for Timoshenko's beam theory.

4.5.1. Development of Governing Equations

Again the development of the governing equations will start with the free body diagram of a differential element of the beam as shown in Figure 16. The difference

between the Timoshenko and Euler-Bernoulli differential elements is that the Timoshenko element includes the effects of rotatory inertia and shear deformation due to transverse shear forces. The addition of transverse shear deformation leads to an additional independent rotation of the beams cross-section. A rotatory inertia coefficient, K_2, has been introduced to the rotatory inertia term of the beam. A typical value of K_2 for a Timoshenko beam is 1. Setting K_2 to 0 eliminates the rotatory inertia term from the equation.

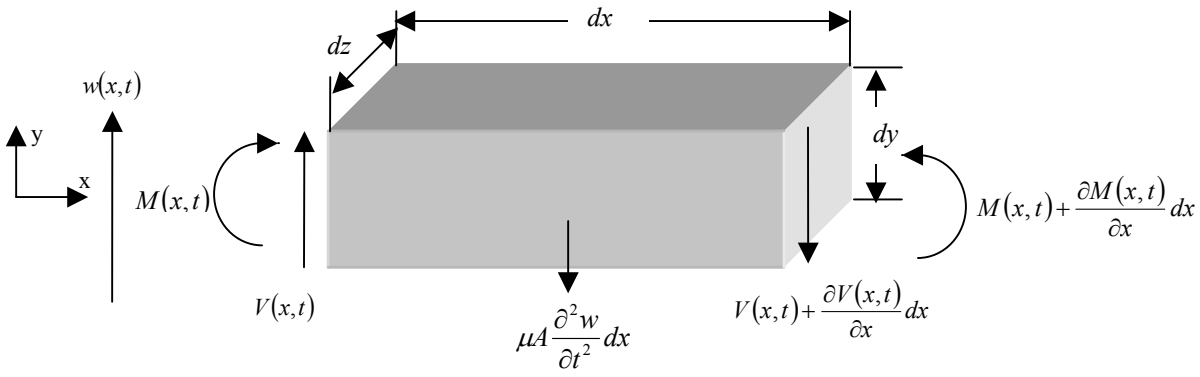

Figure 16. Free Body Diagram of a Differential Element of a Timoshenko Beam

Writing the sum of forces on the differential element yields

$$V(x,t) - V(x,t) - \frac{\partial V(x,t)}{\partial x} dx - \mu A \frac{\partial^2 w(x,t)}{\partial t^2} dx = 0 \qquad (112)$$

Simplifying Equation (112) gives

$$-\frac{\partial V(x,t)}{\partial x}-\mu A\frac{\partial^2 w(x,t)}{\partial t^2}=0 \tag{113}$$

where, A is again the constant cross sectional area. The sum of moments about the center of the differential element yields

$$\begin{aligned}&-M(x,t)+M(x,t)+\frac{\partial M(x,t)}{\partial x}dx-\mu IK_2\frac{\partial^2\psi(x,t)}{\partial t^2}dx \ \ldots\\&-V(x,t)\frac{dx}{2}-V(x,t)\frac{dx}{2}-\frac{\partial V(x,t)}{\partial x}dx\frac{dx}{2}=0\end{aligned} \tag{114}$$

Simplifying Equation (114) and neglecting higher order terms gives

$$\frac{\partial M(x,t)}{\partial x}-V(x,t)-\mu IK_2\frac{\partial^2\psi(x,t)}{\partial t^2}=0 \tag{115}$$

where, $V(x,t)$ is the shear force , $M(x,t)$ is the bending moment, and $w(x,t)$ is the transverse deflection. Similarly, ψ is the slope of the beam due to bending, β is the slope due to shear, and $\frac{dw}{dx}$ is the total slope of the beam. The relation between the slopes is

$$\beta(x,t)=\frac{\partial w(x,t)}{\partial x}-\psi(x,t) \tag{116}$$

Equation (116) also gives the relation between the independent quantities, transverse displacement, $w(x,t)$, and rotation, $\psi(x,t)$. Figure 17 illustrates the meaning of the slopes due to bending and shear.

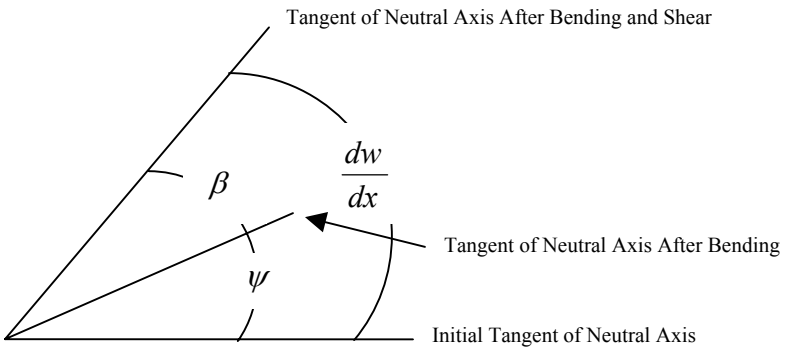

Figure 17. Definitions of Bending, Shear, and Total Slope.

From elementary flexure theory the bending moment is proportional to the bending angle and is given by Timoshenko [20] to be

$$M(x,t) = EI\frac{\partial \psi(x,t)}{\partial x} \tag{117}$$

The Timoshenko expression for the shear force is proportional to the shear angle and is given by

$$V(x,t) = -K_1\beta(x,t)AG \tag{118}$$

where, K_1 is the transverse shear deflection coefficient. A typical value of the shear coefficient is $\frac{\pi^2}{12}$. Setting K_1 equal to infinity makes the shear stiffness very large and the behavior of the beam will approach Euler-Bernoulli theory. Substituting the expressions for shear (Equation (118)), moment (Equation (117)), and shear angle (Equation (116)) into the simplified force and moment balances, given in Equations (113) and (115) respectively, yields one equation of motion for the transverse displacement,

$$K_1 AG\left(\frac{\partial^2 w(x,t)}{\partial x^2} - \frac{\partial \psi(x,t)}{\partial x}\right) - \mu A \frac{\partial^2 w(x,t)}{\partial t^2} = 0 \tag{119}$$

and one equation of motion for the rotation of the cross section,

$$EI\frac{\partial^2 \psi(x,t)}{\partial x^2} + K_1 AG\left(\frac{\partial w(x,t)}{\partial x} - \psi(x,t)\right) - \mu I K_2 \frac{\partial^2 \psi(x,t)}{\partial t^2} = 0 \tag{120}$$

The two coupled, constant coefficient, separable, governing PDEs for the Timoshenko beam were developed from force and moment balances on a differential beam element. Shear deformation and rotatory inertia were incorporated into the force and moment balances. The resulting PDEs are second order in both time and space. The following subsection describes the forms of the solutions for the two dependent variables, transverse displacement $(w(x,t))$ and rotation $(\psi(x,t))$.

4.5.2. Representation of Displacement Field for Timoshenko Element

Similar to the Euler-Bernoulli solution, the solution to the Timoshenko equations can be found using a separable form of the displacement fields. General exponential solutions are assumed for both the transverse displacement and the rotation. The assumed solutions result in a characteristic equation between the spatial wave number and the temporal frequency. The remainder of the section describes the development of the displacement fields for the Timoshenko governing equations.

The governing Timoshenko beam equations have constant coefficients so exponential forms of the solutions for transverse displacement and rotation will be assumed as

$$w(x,t) = \overline{A} e^{\mathbf{i}\alpha x} e^{\mathbf{i}\omega t} \tag{121}$$

$$\psi(x,t) = \overline{B} e^{\mathbf{i}\alpha x} e^{\mathbf{i}\omega t} \tag{122}$$

Substituting theses solutions into the Timoshenko beam governing Equations (119) and (120) yields two equations with two unknowns $\left(\overline{A} \text{ and } \overline{B}\right)$ that can be written in matrix form as

$$\begin{bmatrix} -K_1 AG\alpha^2 + \mu A\omega^2 & -K_1 AG\mathbf{i}\alpha \\ K_1 AG\mathbf{i}\alpha & -EI\alpha^2 - K_1 AG + \mu I K_2 \omega^2 \end{bmatrix} \begin{Bmatrix} \overline{A} \\ \overline{B} \end{Bmatrix} = \begin{Bmatrix} 0 \\ 0 \end{Bmatrix} \tag{123}$$

Setting the determinant of the matrix to zero yields the characteristic equation to be

$$\left(K_1 AGEI\right)\alpha^4 - \left(EIA\mu\omega^2 + \mu I K_2 K_1 AG\omega^2\right)\alpha^2 + \left(IAK_2\mu^2\omega^4 - K_1 A^2 G\mu\omega^2\right) = 0 \tag{124}$$

The characteristic equation is used to define the spectral relation in the same way as in the Euler-Bernoulli theory of section 4.2.2. Equation (124) is quartic in α and can be solved using symbolic software, such as Mathematica [18]. The solution of the characteristic equation yields the spectral relation and four roots for α

$$\alpha_1 = \frac{\sqrt{\frac{AI\left(E+GK_1K_2\right)\mu\omega^2 + \sqrt{A^2I\mu\omega^2\left(4AEG^2K_1^2 + I\left(E+GK_1K_2\right)^2\mu\omega^2\right)}}{AEGIK_1}}}{\sqrt{2}}$$

$$\alpha_2 = \frac{\sqrt{\frac{AI\left(E+GK_1K_2\right)\mu\omega^2 - \sqrt{A^2I\mu\omega^2\left(4AEG^2K_1^2 + I\left(E+GK_1K_2\right)^2\mu\omega^2\right)}}{AEGIK_1}}}{\sqrt{2}}$$

$$\alpha_3 = -\frac{\sqrt{\frac{AI\left(E+GK_1K_2\right)\mu\omega^2 + \sqrt{A^2I\mu\omega^2\left(4AEG^2K_1^2 + I\left(E+GK_1K_2\right)^2\mu\omega^2\right)}}{AEGIK_1}}}{\sqrt{2}} \tag{125}$$

$$\alpha_4 = -\frac{\sqrt{\frac{AI\left(E+GK_1K_2\right)\mu\omega^2 - \sqrt{A^2I\mu\omega^2\left(4AEG^2K_1^2 + I\left(E+GK_1K_2\right)^2\mu\omega^2\right)}}{AEGIK_1}}}{\sqrt{2}}$$

One exponential term must be used for each possible wave number such that there are four terms in the spatial solution of each independent variable. The barred coefficients again represent unknown coefficients and are not necessarily the same as used in the Euler-Bernoulli beam element development.

$$\begin{aligned} X_w(x) &= \widetilde{A}e^{\mathbf{i}\alpha_1 x} + \widetilde{B}e^{\mathbf{i}\alpha_2 x} + \widetilde{C}e^{\mathbf{i}\alpha_3 x} + \widetilde{D}e^{\mathbf{i}\alpha_4 x} \\ X_\psi(x) &= \overline{A}e^{\mathbf{i}\alpha_1 x} + \overline{B}e^{\mathbf{i}\alpha_2 x} + \overline{C}e^{\mathbf{i}\alpha_3 x} + \overline{D}e^{\mathbf{i}\alpha_4 x} \end{aligned} \tag{126}$$

The spatial order of the Timoshenko governing equation is four and thus requires four boundary conditions. The straight and curved barred coefficients of Equations (126) must be related such that the unknown coefficients can be determined from the

application of four boundary conditions. The straight barred and curve barred coefficients can be related using one of the rows of Equation (123). Using the first row of Equation (123) gives the curve barred coefficients in terms of the straight barred coefficients as

$$\begin{aligned}
\widetilde{A} &= \overline{A}\left(\frac{\mathbf{i}K_1 AG\alpha_1}{K_1 AG\alpha_1^2 - \mu A\omega^2}\right) \\
\widetilde{B} &= \overline{B}\left(\frac{\mathbf{i}K_1 AG\alpha_2}{K_1 AG\alpha_2^2 - \mu A\omega^2}\right) \\
\widetilde{C} &= \overline{C}\left(\frac{\mathbf{i}K_1 AG\alpha_3}{K_1 AG\alpha_3^2 - \mu A\omega^2}\right) \\
\widetilde{D} &= \overline{D}\left(\frac{\mathbf{i}K_1 AG\alpha_4}{K_1 AG\alpha_4^2 - \mu A\omega^2}\right)
\end{aligned} \tag{127}$$

Substituting $R_1, R_2, R_3,$ and R_4 for the bracketed expressions in Equation (127), the final form of the spatial component of the displacement field is

$$\begin{aligned}
X_w(x) &= \overline{A}R_1 e^{\mathbf{i}\alpha_1 x} + \overline{B}R_2 e^{\mathbf{i}\alpha_2 x} + \overline{C}R_3 e^{\mathbf{i}\alpha_3 x} + \overline{D}R_4 e^{\mathbf{i}\alpha_4 x} \\
X_\psi(x) &= \overline{A}e^{\mathbf{i}\alpha_1 x} + \overline{B}e^{\mathbf{i}\alpha_2 x} + \overline{C}e^{\mathbf{i}\alpha_3 x} + \overline{D}e^{\mathbf{i}\alpha_4 x}
\end{aligned} \tag{128}$$

As in the Euler-Bernoulli formulation, the temporal component of the separable solution for harmonic excitation is assumed to have the form of

$$\begin{aligned}
T_w(t) &= \overline{E}e^{\mathbf{i}\omega t} \\
T_\psi(t) &= \overline{F}e^{\mathbf{i}\omega t}
\end{aligned} \tag{129}$$

Multiplying the temporal and spatial components and combining coefficients give the complete solutions to be

$$w(x,t) = \left(\overline{A}R_1 e^{\mathbf{i}\alpha_1 x} + \overline{B}R_2 e^{\mathbf{i}\alpha_2 x} + \overline{C}R_3 e^{\mathbf{i}\alpha_3 x} + \overline{D}R_4 e^{\mathbf{i}\alpha_4 x}\right)e^{\mathbf{i}\omega t}$$
$$\psi(x,t) = \left(\overline{A}e^{\mathbf{i}\alpha_1 x} + \overline{B}e^{\mathbf{i}\alpha_2 x} + \overline{C}e^{\mathbf{i}\alpha_3 x} + \overline{D}e^{\mathbf{i}\alpha_4 x}\right)e^{\mathbf{i}\omega t} \tag{130}$$

The solutions to the set of Timoshenko beam governing PDEs were found by assuming a separable solution to the two dependent variables. Exponential solutions were assumed in space because the PDEs have constant coefficients. Exponential solutions were assumed in time because of the interest in only harmonic excitation. The substitution of the assumed forms of the solutions into the governing equations resulted in a system of two equations and two unknowns in the form of an eigenvalue problem. Setting the determinant of the system matrix equal to zero, gave the characteristic equation. The roots of the characteristic equation give the spectral relation between the spatial wave number and the temporal frequency. The four possible spatial wave numbers were incorporated into the complete spatial solution to form the eigenfunction. Finally, the coefficients of the two dependent variables were related using one of the governing equations. The solutions for the displacement fields can now be used to form the dynamic stiffness matrix. The following section describes the development of the dynamic stiffness matrix using the solutions to the governing PDEs.

4.5.3. Dynamic Stiffness for Timoshenko Element

The dynamic stiffness matrix for the spectral Timoshenko beam element is formulated following the same direct method as the spectral Euler-Bernoulli dynamic stiffness. The displacements and forces at each node are written in terms of the

unknown coefficients, $\overline{A}, \overline{B}, \overline{C}, \text{and } \overline{D}$. These relations can then be used to form an expression for the dynamic stiffness matrix. The nodal DOF for the Timoshenko beam element are shown in Figure 18.

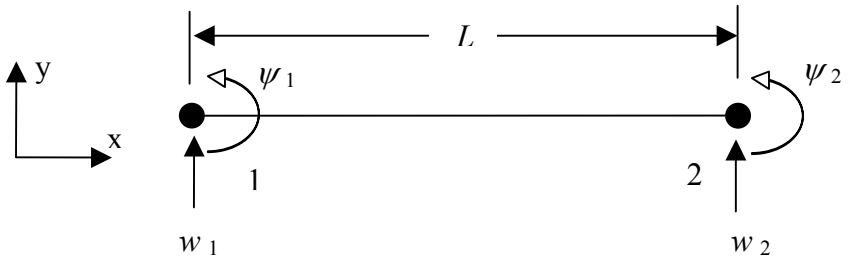

Figure 18. Nodal DOF of Spectral Timoshenko Beam Element

Evaluating the transverse displacement and rotation, in Equation (130), at the nodes and writing in matrix form gives

$$\begin{Bmatrix} w(0,t) \\ \psi(0,t) \\ w(L,t) \\ \psi(L,t) \end{Bmatrix} = \begin{Bmatrix} w_1 \\ \psi_1 \\ w_2 \\ \psi_2 \end{Bmatrix} = [\mathbf{D}] \begin{Bmatrix} \overline{A} \\ \overline{B} \\ \overline{C} \\ \overline{D} \end{Bmatrix} e^{\mathbf{i}\omega t} \tag{131}$$

For the case of the Timoshenko beam element, $[\mathbf{D}]$ is a 4X4 matrix and has the form

$$[\mathbf{D}] = \begin{bmatrix} R_1 & R_2 & R_3 & R_4 \\ 1 & 1 & 1 & 1 \\ R_1 e^{\mathbf{i}\alpha_1 L} & R_2 e^{\mathbf{i}\alpha_2 L} & R_3 e^{\mathbf{i}\alpha_3 L} & R_4 e^{\mathbf{i}\alpha_4 L} \\ e^{\mathbf{i}\alpha_1 L} & e^{\mathbf{i}\alpha_2 L} & e^{\mathbf{i}\alpha_3 L} & e^{\mathbf{i}\alpha_4 L} \end{bmatrix} \tag{132}$$

Writing the nodal shear and moment forces, given in Equations (118) and (117) respectively, in matrix form gives

$$\begin{Bmatrix} V(0,t) \\ -M(0,t) \\ -V(L,t) \\ M(L,t) \end{Bmatrix} = \begin{Bmatrix} V_1 \\ M_1 \\ V_2 \\ M_2 \end{Bmatrix} = [\mathbf{F}] \begin{Bmatrix} \overline{A} \\ \overline{B} \\ \overline{C} \\ \overline{D} \end{Bmatrix} e^{\mathbf{i}\omega t} \tag{133}$$

For the case of the Timoshenko beam element, $[\mathbf{F}]$ is a 4X4 matrix and has the form

$$[\mathbf{F}] = \begin{bmatrix} (\mathbf{i}\alpha_1 R_1 - 1) & (\mathbf{i}\alpha_2 R_2 - 1) & (\mathbf{i}\alpha_3 R_3 - 1) & (\mathbf{i}\alpha_4 R_4 - 1) \\ \mathbf{i}\alpha_1 & \mathbf{i}\alpha_2 & \mathbf{i}\alpha_3 & \mathbf{i}\alpha_4 \\ (\mathbf{i}\alpha_1 R_1 - 1)e^{\mathbf{i}\alpha_1 L} & (\mathbf{i}\alpha_2 R_2 - 1)e^{\mathbf{i}\alpha_2 L} & (\mathbf{i}\alpha_3 R_3 - 1)e^{\mathbf{i}\alpha_3 L} & (\mathbf{i}\alpha_4 R_4 - 1)e^{\mathbf{i}\alpha_4 L} \\ \mathbf{i}\alpha_1 e^{\mathbf{i}\alpha_1 L} & \mathbf{i}\alpha_2 e^{\mathbf{i}\alpha_2 L} & \mathbf{i}\alpha_3 e^{\mathbf{i}\alpha_3 L} & \mathbf{i}\alpha_4 e^{\mathbf{i}\alpha_4 L} \end{bmatrix} \bullet \begin{Bmatrix} -K_1 AG \\ -EI \\ K_1 AG \\ EI \end{Bmatrix} \tag{134}$$

where, each row of the vector on the right represents the coefficient of each term in the corresponding row of the matrix on the left. The minus signs for the shear and moment in Equation (133) are to ensure that a positive force will cause a positive displacement.

The transverse displacement and rotation evaluated at the nodes in Equation (131) form the vector of nodal DOF $\{\mathbf{d}\}$ as

$$\{\mathbf{d}\} = \begin{Bmatrix} w_1 \\ \psi_1 \\ w_2 \\ \psi_2 \end{Bmatrix} e^{\mathbf{i}\omega t} \tag{135}$$

The shear and moment evaluated at the nodes in Equation (133) form the vector of nodal forces $\{\mathbf{f}\}$ as

$$\{\mathbf{f}\} = \begin{Bmatrix} V_1 \\ M_1 \\ V_2 \\ M_2 \end{Bmatrix} e^{\mathbf{i}\omega t} \tag{136}$$

The dynamic stiffness matrix relates the dynamic nodal DOF $\{\mathbf{d}\}$ to the dynamic nodal loads $\{\mathbf{f}\}$.

$$\{\mathbf{f}\} = [\mathbf{K}_{Dyn}]\{\mathbf{d}\} \tag{137}$$

The dynamics stiffness matrix can be solved from Equations (131) and (133) to be

$$[\mathbf{K}_{Dyn}] = [\mathbf{F}][\mathbf{D}]^{-1} \tag{138}$$

The shape functions for the spectral Timoshenko beam element can be expressed in terms of the $[\mathbf{D}]$ matrix. The shape functions for the transverse displacement $[\mathbf{N}_w]$ and rotation $[\mathbf{N}_\psi]$ are

$$[\mathbf{N}] = \begin{bmatrix} \mathbf{N}_w \\ \mathbf{N}_\psi \end{bmatrix} = \begin{bmatrix} R_1 e^{\mathbf{i}\alpha_1 x} & R_2 e^{\mathbf{i}\alpha_2 x} & R_3 e^{\mathbf{i}\alpha_3 x} & R_4 e^{\mathbf{i}\alpha_4 x} \\ e^{\mathbf{i}\alpha_1 x} & e^{\mathbf{i}\alpha_2 x} & e^{\mathbf{i}\alpha_3 x} & e^{\mathbf{i}\alpha_4 x} \end{bmatrix} [\mathbf{D}]^{-1} \tag{139}$$

The complete expression for the transverse displacement and rotation in terms of the nodal DOF and the shape function is

$$\begin{Bmatrix} w(x) \\ \psi(x) \end{Bmatrix} = [\mathbf{N}]\{\mathbf{d}\} \tag{140}$$

In summary, the dynamic stiffness matrix was developed through a direct method using the nodal DOF and nodal forces. The displacement field that the nodal displacements and forces were based on was the exact solution, or eigenfunction, of the governing PDEs. The symmetric dynamic stiffness matrix includes the effects of transverse inertia, rotatory inertia, shear deformation, and bending. The eignefunctions were also incorporated into the shape functions for the element. The following section revisits the curved geometry example of section 4.4 to investigate the effect of shear deformation and rotatory inertia. The results of the spectral Timoshenko beam and compared to the results of the spectral Euler-Bernoulli beam.

4.5.4. Curved Geometry Example Revisited

To show the effect of rotatory inertia and shear deformation on the vibration of beams that have a slenderness ratio (L/h) less than 10, the curved example problem of section 4.4 will now be analyzed using Timoshenko beam elements.

Figure 19 shows the dimensions of the curved example problem. The material properties used in the analysis were again aluminum with an elastic modulus of 10^6 *psi* and a density of $0.26\times10^{-3}\ \frac{lbf\ s^2}{in^4}$. The magnitude of the load was 100 *lbf* and was applied at center span of the beam. The slenderness ratios for the problem are

$$\frac{L}{h_y} = \frac{39.37}{7.87} = 5, \qquad \frac{L}{h_z} = \frac{39.37}{39.37} = 1 \tag{141}$$

The slenderness ratios in both the y-direction and the z-direction are both less than 10. This means that the beam cannot be considered slender and, shear deformation and rotatory inertia may have a significant contribution to the solution.

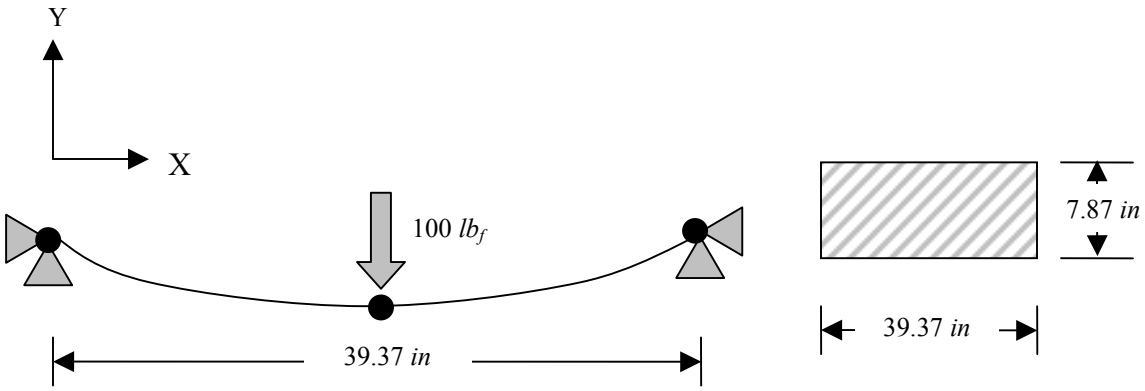

Figure 19. Schematic of Curved Mirror Cross-Section

Figure 20 shows the receptance of the curved geometry problem using both Euler-Bernoulli and Timoshenko beam theories. Notice the large shifts in the receptance peaks. The low slenderness ratios indicate the effects of shear deformation and rotatory inertia will be important and thus have an effect on the response.

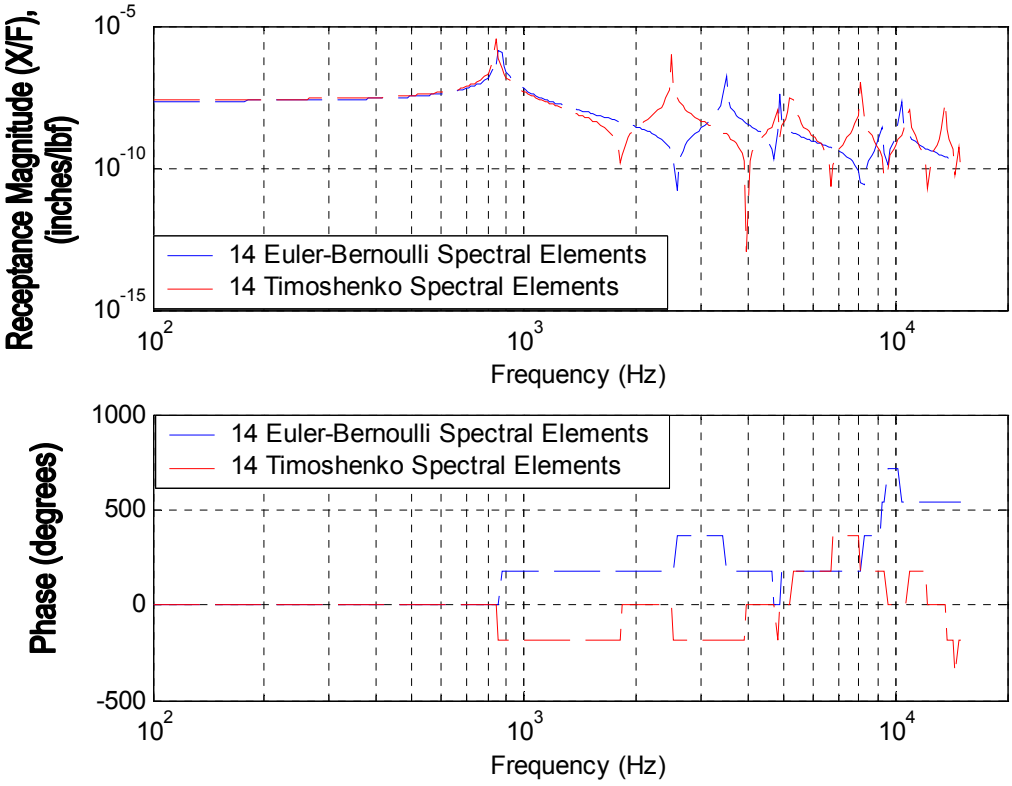

Figure 20. Euler-Bernoulli, Timoshenko Receptance Comparison

Table 4 shows the percent change in natural frequency from including the rotatory inertia and shear deformation for the first two peaks in the receptance. The change in the first peak is 1.83% but, the change in the second peak (3rd bending mode) is much more substantial at 28.50%. The effects of rotatory inertia and shear deformation become even more important as frequency increases.

Table 4. Percent Change Due to Rotatory Inertia and Shear Deformation in FRF Peaks

Peak #	Euler-Bernoulli (*Hz*)	Timoshenko (*Hz*)	% Difference
1	853.10	837.53	-1.83%
2	3490.60	2495.74	-28.50%

The natural frequencies predicted by the Timoshenko element are lower than those predicted by the Euler-Bernoulli element because of the effects of rotatory inertia over power the effects of shear deformation. The rotatory inertia adds to the mass effect of the beam and the shear deformation adds to the stiffness of the beam. Looking at the natural frequency as the square root of the ratio of mass effects to stiffness effects $\left(\omega_n = \sqrt{k/m}\right)$, it can be seen that if the increase in the mass effects is greater than the increase in stiffness the natural frequency will decrease.

4.6. Chapter Summary

Similar to the bar element, the interpolation functions for a conventional beam element are based on the static beam displacement field. A major difference in the spectral element interpolation function is that it is based on the dynamic beam displacement field. The conventional interpolation function uses polynomial functions, which is the exact solution to the static problem and thus an approximation to the dynamic problem. The spectral interpolation function contains trigonometric functions, which are the exact solution to the dynamic problem. This enables the spectral element to represent the dynamics of a beam exactly, as was shown in the straight example problem of section 4.3. Table 5 shows a side-by-side comparison of the major formulation differences between conventional and spectral Euler-Bernoulli beam elements.

Table 5. Summary of Formulation Differences Between Conventional and Spectral Euler-Bernoulli Beams

	Conventional Beam	Spectral Beam
Governing Equation	$[\mathbf{m}]\{\ddot{\mathbf{d}}\}+[\mathbf{k}]\{\mathbf{d}\}=\{\mathbf{r}_{ext}\}$	$EI\frac{\partial^4 w(x,t)}{\partial x^4}=-\mu A\frac{\partial^2 w(x,t)}{\partial t^2}$
Basis Function	$w(x,t)=\left(\overline{A}x^3+\overline{B}x^2+\overline{C}x+\overline{D}\right)e^{i\omega t}$	$w(x,t)=\left(\overline{A}e^{i\alpha_1 x}+\overline{B}e^{i\alpha_2 x}+\overline{C}e^{i\alpha_3 x}+\overline{D}e^{i\alpha_4 x}\right)e^{i\omega t}$
Dynamic Stiffness Formulation	$[\mathbf{K}_{Dyn}]=-\omega^2[\mathbf{m}]+[\mathbf{k}]$	$[\mathbf{K}_{Dyn}]=[\mathbf{F}][\mathbf{D}]^{-1}$
Conventional Beam Shape Function		
$[\mathbf{N}]=\begin{bmatrix}\mathbf{N}_w\\ \mathbf{N}_\theta\end{bmatrix}=\begin{bmatrix}1-\frac{3x^2}{L^2}+\frac{2x^3}{L^3}, & x-\frac{2x^2}{L}+\frac{x^3}{L^2}, & \frac{3x^2}{L^2}-\frac{2x^3}{L^3}, & -\frac{x^2}{L}+\frac{x^3}{L^2}\\ 6\left(\frac{x^2}{L^3}-\frac{x}{L^2}\right), & \frac{3x^2}{L^2}-\frac{4x}{L}+1, & 6\left(\frac{x}{L^2}-\frac{x^2}{L^3}\right), & \frac{3x^2}{L^2}-\frac{2x}{L}\end{bmatrix}$		
Spectral Beam Shape Function		
$[\mathbf{N}]=\begin{bmatrix}\mathbf{N}_w\\ \mathbf{N}_\theta\end{bmatrix}=\begin{bmatrix}e^{i\alpha_1 x} & e^{i\alpha_2 x} & e^{i\alpha_3 x} & e^{i\alpha_4 x}\\ i\alpha_1 e^{i\alpha_1 x} & i\alpha_2 e^{i\alpha_2 x} & i\alpha_3 e^{i\alpha_3 x} & i\alpha_4 e^{i\alpha_4 x}\end{bmatrix}[\mathbf{D}]^{-1}$		

The first 13 natural frequencies of the straight cantilever example problem, for both the spectral and conventional models, differed by less than 2% from the natural frequencies predicted by the analytic solution for beam theory. A single spectral element was able to predict natural frequencies and amplitude of the displacement response out to 15 kHz. It required 34 conventional elements to converge the amplitude of the displacement response to the level achieved by the spectral element at 15 kHz.

It was also shown that higher order Timoshenko beam theory could be incorporated into a spectral element. The element formulation and spectral relation is more complicated for the Timoshenko element than for the Euler-Bernoulli element. The Timoshenko element, like the Euler-Bernoulli element, incorporated the exact solution of the dynamic governing equations into the element formulation. The

addition of rotatory inertia and shear deformation resulted in a 28% difference in the natural frequencies between the Euler-Bernoulli and Timoshenko curved geometry models for the third bending mode at frequencies between 2500 and 3500 Hz.

Another benefit of the spectral elements is the C^n continuity of the shape functions. The shape functions of the spectral beam element are infinitely differentiable. Any number of derivatives may be calculated without the loss of information. The shear forces and moments can be calculated accurately anywhere in the element. In addition, accurate values of the slope and curvature can be obtained over the entire frequency range with very few elements. The slope and curvature calculations would be very useful in the satellite mirror analysis.

Over all, the spectral beam element fits into the existing FEA framework very well. The same procedures for matrix assembly and plotting used in conventional FEA can be utilized in spectral element analysis. The greatest advantages of spectral element analysis are the reduced number of DOF in the model and the powerful interpolation functions, resulting in less solution time and a more accurate solution into higher frequency ranges. The C^n continuity and the prediction of internal forces and resulting stresses is another important advantage of spectral elements. The performance of the spectral element cannot be obtained using polynomial based shape functions over the frequency range studied.

5. Levy-Type Kirchhoff Plate Element

The chapter contains the development of a conventional four node Kirchhoff plate elements and a two edge spectral Levy-type Kirchhoff plate elements in sections 5.1 and 5.2 respectively. Each development section consists of subsections that cover the governing equation, displacement field, and dynamic stiffness. After the developments of the conventional and spectral elements are discussed, an example problem is used to demonstrate the performance differences between the two elements. A simply supported Levy-type plate with uniform loading on the free edges is used as the example. The example has the same geometry and material properties as an example used in Kevorkian [15]. Section 5.4 contains a comparison of the results between the conventional and spectral models. Finally, differences in the spectral analysis between beam elements and Levy-type plate elements are summarized.

5.1. Conventional Plate Elements

5.1.1. Development of Governing Equation

Typically, the conventional plate element has 4 nodes with 3 DOF at each node. Figure 21 shows the nodal DOF of a typical plate element with positive orientations of the displacements and rotations. The 3 DOF used at each node were the transverse displacement (w), the rotation about the x-direction (θ_y), and the rotation about the y-direction (θ_x).

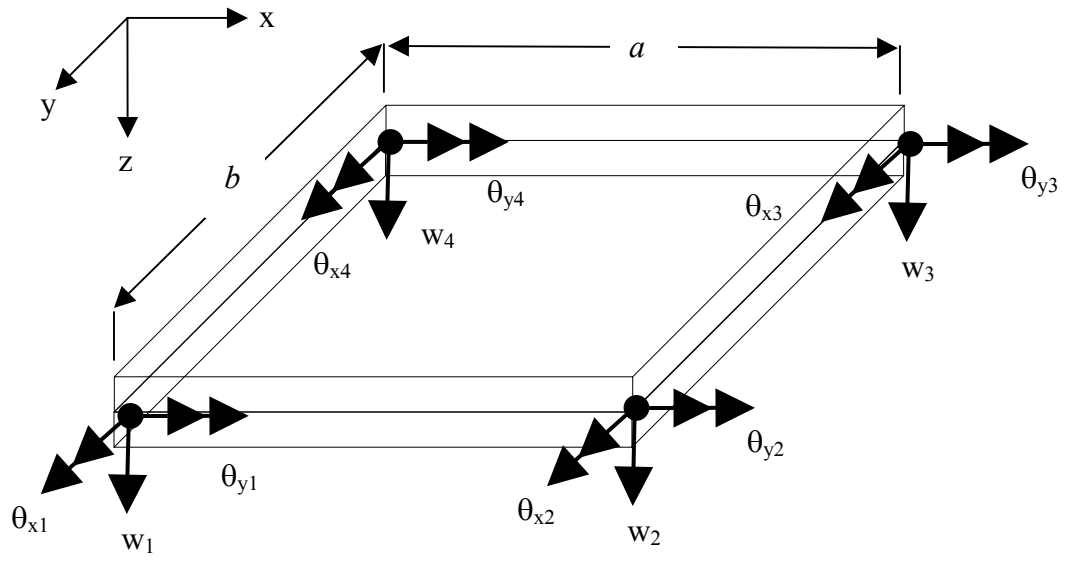

Figure 21. Positive Orientation of Nodal DOF for Kirchhoff Plate Element

The development of the governing equation for a conventional plate element is the same as the conventional bar element. The governing equation is obtained by minimizing the sum of the kinetic and potential energies in the system. Section 3.1.1 gives the development of the governing structural dynamics equation for conventional elements. The governing structural dynamics equation for the plate element is repeated here for convenience

$$[\mathbf{m}]\{\ddot{\mathbf{d}}\}+[\mathbf{k}]\{\mathbf{d}\}=\{\mathbf{r}_{ext}\} \tag{9}$$

where, $[\mathbf{m}]$ is the mass matrix, $[\mathbf{k}]$ is the stiffness matrix, $\{\mathbf{r}_{ext}\}$ is a vector of external loads, and $\{\mathbf{d}\}$ is a vector of the DOF of the beam element. The difference from the bar element is that different DOF have been chosen to form $\{\mathbf{d}\}$ and a different shape function will be formulated to be the basis of the mass matrix, $[\mathbf{m}]$, and stiffness matrix, $[\mathbf{k}]$. The shape functions capture the bending mechanics of the plate. The

following section describes the choice of basis function and the development of the shape function for the conventional plate element shown in Figure 21.

5.1.2. Representation of the Displacement Field

Applying Equation (9) to the plate element shown in Figure 21, requires choosing a basis function to represent the spatial and temporal components of the assumed separable solution, given in Equation (2). The basis function can then be used to form the shape function matrix, $[\mathbf{N}]$, that will satisfy arbitrary nodal boundary conditions. The shape function is then used in the formulation of the mass and stiffness matrices, as shown in Equations (7) and (8) respectively.

In conventional finite element analysis the incomplete quartic polynomial,

$$X(x,y) = \overline{A} + \overline{B}x + \overline{C}y + \overline{D}x^2 + \overline{E}xy + \overline{F}y^2 + \overline{G}x^3 + \ldots \\ \overline{H}x^2y + \overline{I}xy^2 + \overline{J}y^3 + \overline{K}x^3y + \overline{L}xy^3 \tag{142}$$

is chosen for the basis of the shape function formulation. The 12 unknown coefficients, $\overline{A},\overline{B},\overline{C},\ldots,\overline{L}$, are to be determined by applying boundary conditions. For the case of harmonic excitation, the basis of the temporal component of the separable solution is assumed to have the form

$$T(t) = \overline{M}e^{\mathbf{i}\omega t} \tag{143}$$

where, ω is the circular forcing frequency. Multiplying the spatial solution, Equation (142), by the temporal solution, Equation (143), and combining coefficients gives the total representation of the basis function for the transverse displacement field.

$$w(x,y,t) = (\,\overline{A} + \overline{B}x + \overline{C}y + \overline{D}x^2 + \overline{E}xy + \overline{F}y^2 + \overline{G}x^3 \ldots + \overline{H}x^2y + \overline{I}xy^2 + \overline{J}y^3 + \overline{K}x^3y + \overline{L}xy^3\,)\,e^{\mathbf{i}\omega t} \tag{144}$$

The rotations about the x-direction $(\theta_y(x,y,t))$ and y-direction $(\theta_x(x,y,t))$ are then given by the derivatives of the transverse displacement with respect to the x-direction and y-direction respectively.

$$\theta_x(x,y,t) = -\frac{\partial w(x,y,t)}{\partial x} \qquad \theta_y(x,y,t) = \frac{\partial w(x,y,t)}{\partial y} \tag{145}$$

The shape function for the transverse displacement and rotations can be formulated following the same procedure as the conventional bar element. Writing the assumed solutions from Equations (144) and (145) in matrix form gives

$$\begin{Bmatrix} w(x,y,t) \\ \theta_x(x,y,t) \\ \theta_y(x,y,t) \end{Bmatrix} = [\mathbf{X}]\{\mathbf{a}\}e^{\mathbf{i}\omega t} \tag{146}$$

The matrix $[\mathbf{X}]$ is a 3X12 matrix formed from the spatial solution and it derivatives with respect to x and y and is written as

$$[\mathbf{X}] = \begin{bmatrix} 1 & x & y & x^2 & xy & y^2 & x^3 & x^2y & xy^2 & y^3 & x^3y & xy^3 \\ 0 & -1 & 0 & -2x & -y & 0 & -3x^2 & -2xy & -y^2 & 0 & -3x^2y & -y^3 \\ 0 & 0 & 1 & 0 & x & 2y & 0 & x^2 & 2xy & 3y^2 & x^3 & 3xy^2 \end{bmatrix} \tag{147}$$

The column vector $\{\mathbf{a}\}$ is the vector of 12 unknown coefficients

$$\{\mathbf{a}\} = \begin{bmatrix} \overline{A} & \overline{B} & \overline{C} & \overline{D} & \overline{E} & \overline{F} & \overline{G} & \overline{H} & \overline{I} & \overline{J} & \overline{K} & \overline{L} \end{bmatrix}^T \tag{148}$$

The transverse displacement and rotations about the x and y-directions at the nodes, shown as $w_1, \theta_{x1}, \theta_{y1}$ in Figure 21, were chosen as the nodal DOF. The vector $\{\mathbf{d}\}$, from Equation (2), is then defined as the temporal solution of the nodal DOF.

$$\{\mathbf{d}\} = \begin{bmatrix} w_1 & \theta_{x1} & \theta_{y1} & w_2 & \theta_{x2} & \theta_{y2} & w_3 & \theta_{x3} & \theta_{y3} & w_4 & \theta_{x4} & \theta_{y4} \end{bmatrix}^T e^{\mathbf{i}\omega t} \quad (149)$$

Evaluating the displacement fields, Equations (144) and (145) for the case that the local coordinate system is located at node 1, at the nodes and writing in matrix form gives

$$\begin{Bmatrix} w(0,0,t) \\ \theta_x(0,0,t) \\ \theta_y(0,0,t) \\ w(a,0,t) \\ \theta_x(a,0,t) \\ \theta_y(a,0,t) \\ w(a,b,t) \\ \theta_x(a,b,t) \\ \theta_y(a,b,t) \\ w(0,b,t) \\ \theta_x(0,b,t) \\ \theta_y(0,b,t) \end{Bmatrix} = \underbrace{\begin{bmatrix} 1 & 0 & 0 & 0 & 0 & 0 & 0 & 0 & 0 & 0 & 0 & 0 \\ 0 & -1 & 0 & 0 & 0 & 0 & 0 & 0 & 0 & 0 & 0 & 0 \\ 0 & 0 & 1 & 0 & 0 & 0 & 0 & 0 & 0 & 0 & 0 & 0 \\ 1 & a & 0 & a^2 & 0 & 0 & a^3 & 0 & 0 & 0 & 0 & 0 \\ 0 & -1 & 0 & -2a & 0 & 0 & -3a^2 & 0 & 0 & 0 & 0 & 0 \\ 0 & 0 & 1 & 0 & a & 0 & 0 & a^2 & 0 & 0 & a^3 & 0 \\ 1 & a & b & b^2 & ab & b^2 & a^3 & a^2b & ab^2 & b^3 & a^3b & ab^3 \\ 0 & -1 & 0 & -2a & -b & 0 & -3a^2 & -2ab & -b^2 & 0 & -3a^2b & -b^3 \\ 0 & 0 & 1 & 0 & a & 2b & 0 & a^2 & 2ab & 3b^2 & a^3 & 3ab^2 \\ 1 & 0 & b & 0 & 0 & b^2 & 0 & 0 & 0 & b^3 & 0 & 0 \\ 0 & -1 & 0 & 0 & -b & 0 & 0 & 0 & -b^2 & 0 & 0 & -b^3 \\ 0 & 0 & 1 & 0 & 0 & 2b & 0 & 0 & 0 & 3b^2 & 0 & 0 \end{bmatrix}}_{[\mathbf{A}]} \{\mathbf{a}\} e^{\mathbf{i}\omega t} \quad (150)$$

where, $[\mathbf{A}]$ is a 12 X 12 matrix of the displacement fields evaluated at each of the nodes. The shape functions for the plate element can be expressed using Equation (22) as,

$$[\mathbf{N}] = \begin{bmatrix} \mathbf{N}_w \\ \mathbf{N}_{\theta_x} \\ \mathbf{N}_{\theta_y} \end{bmatrix} = \begin{bmatrix} 1 & x & y & x^2 & xy & y^2 & x^3 & x^2y & xy^2 & y^3 & x^3y & xy^3 \\ 0 & -1 & 0 & -2x & -y & 0 & -3x^2 & -2xy & -y^2 & 0 & -3x^2y & -y^3 \\ 0 & 0 & 1 & 0 & x & 2y & 0 & x^2 & 2xy & 3y^2 & x^3 & 3xy^2 \end{bmatrix} [\mathbf{A}]^{-1} \quad (151)$$

The Kirchhoff plate shape functions were formed from the spatial basis function. An incomplete quartic polynomial in *x* and *y* was used as the basis function for the spatial component of the separable solution. A complex exponential was used for the temporal solution because of the interest in harmonic excitation. The basis function was then incorporated into the shape function such that the displacement field could be calculated through the nodal displacements. The following section describes the details in forming the dynamic stiffness matrix from the shape function developed in this section.

5.1.3. Dynamic Stiffness

The dynamic stiffness matrix for a harmonically forced plate element can be found by substituting the temporal solution of the nodal DOF into the governing structural dynamics equation and regrouping terms. The resulting dynamic stiffness is a single matrix that can be used to calculate the harmonic response of the nodal displacements and loads. The mass and stiffness matrices that make up the dynamic stiffness matrix are defined by the shape functions developed in section 5.1.2.

The mass matrix, $[\mathbf{m}]$, and the stiffness matrix, $[\mathbf{k}]$, from Equations (7) and (8) respectively, simplified for the plate element are

$$[\mathbf{m}] = \int \mu h_z [\mathbf{N}]^T [\mathbf{N}] dA \quad (152)$$

$$[\mathbf{k}] = \int [\mathbf{B}]^T [\mathbf{D}][\mathbf{B}] dA \quad (153)$$

where, $[\mathbf{N}]$ is the shape function matrix of the plate, μ is the mass density, h_z is the plate thickness, and dA is the differential area, equivalent to $dxdy$. The moment-curvature matrix, $[\mathbf{D}]$, for homogeneous and isotropic materials is given by

$$[\mathbf{D}] = \begin{bmatrix} D & vD & 0 \\ vD & D & 0 \\ 0 & 0 & \dfrac{(1-v)D}{2} \end{bmatrix} \tag{154}$$

where, D is the flexural rigidity as is written as

$$D = \frac{Eh_z^{\,3}}{12(1-\nu^2)} \tag{155}$$

where, ν is Poisson's ratio and E is the elastic modulus. The strain displacement matrix, $[\mathbf{B}]$, for the Kirchhoff plate element can be written in terms of the derivatives of the shape function matrix as

$$[\mathbf{B}] = \begin{Bmatrix} \partial^2/\partial x^2 \\ \partial^2/\partial y^2 \\ 2\partial^2/\partial x \partial y \end{Bmatrix} [\mathbf{N}] \tag{156}$$

Substituting the temporal nodal DOF solution, Equation (149) , into the governing structural dynamics equation, Equation (9), gives

$$-\omega^2[\mathbf{m}]\{\mathbf{d}\} + [\mathbf{k}]\{\mathbf{d}\} = \{\mathbf{r}_{ext}\} \tag{157}$$

where, the exponential term $e^{i\omega t}$ has been cancelled from both sides of the equation. The dynamic stiffness, $\mathbf{K}_{Dyn}$, of the conventional plate element can then be written as

$$\left[\mathbf{K}_{Dyn}\right] = -\omega^2\left[\mathbf{m}\right] + \left[\mathbf{k}\right] \tag{158}$$

such that,

$$\left[\mathbf{K}_{dyn}\right]\{\mathbf{d}\} = \{\mathbf{r}_{ext}\} \tag{159}$$

The dynamic stiffness matrix, given in Equation (158), was formed by incorporating the assumed temporal solution into the governing structural dynamic equation. Notice that the mass and stiffness matrices are computed separately, from the shape function, and then added together. The inertia effects are incorporated through scaling the mass matrix by the forcing frequency squared. The following section develops the governing equation, displacement field, and dynamic stiffness matrix for a spectral Levy-type plate element.

5.2. Levy-Type Spectral Plate Elements

5.2.1. Governing Equation

The formulation of the governing equation for the Kirchhoff rectangular plate begins with the free body diagram of a differential element, shown in Figure 22, Venstel [23]. The inertial force associated with transverse acceleration has been included in the free body diagram. The shear and moment pairs shown in Figure 22 establish the positive sign convention used in the formulation. Positive bending moments are defined as moments that cause the bottom of the plate to be under tension. Shear

forces are determined by the product of the signs of the direction of the shear force and the direction of the outward normal of the face.

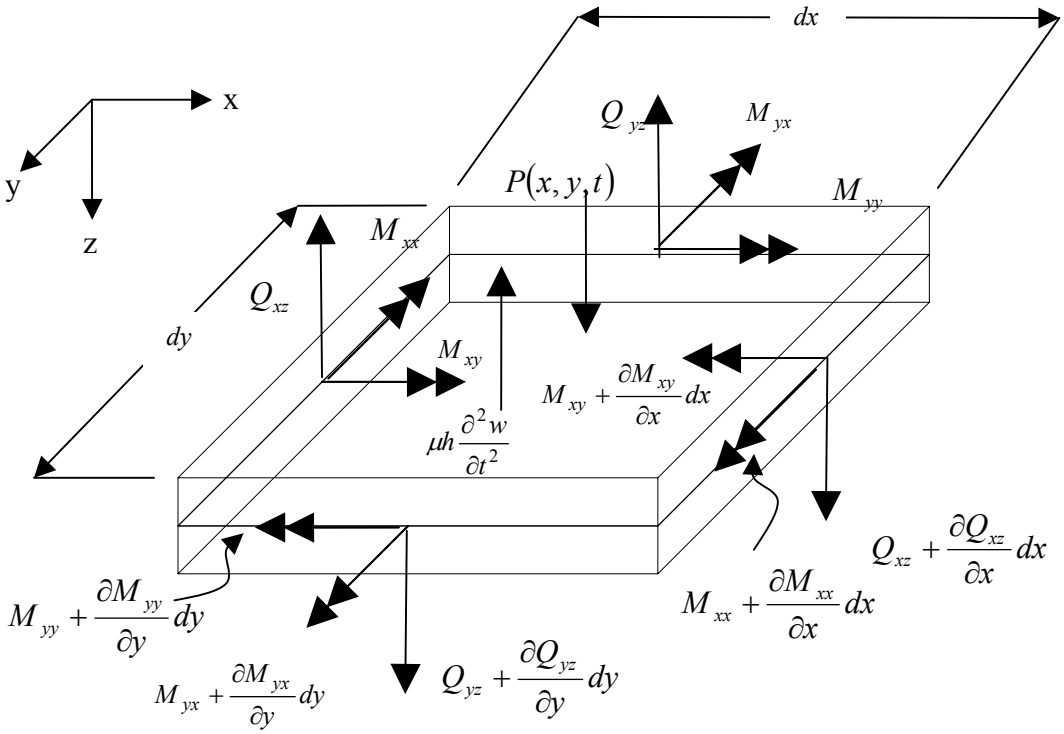

Figure 22. Free Body Diagram of Differential Kirchhoff Plate with Positive Shear and Moment Orientation

The Kirchhoff assumptions are implied throughout the rest of the section. The Kirchhoff assumptions being: homogeneous and isotropic material, the plate is initially flat, deflections of the mid-plane are small compared to the thickness of the plate such that the square of the slope is negligible, lines normal to the mid-plane remain normal after deformation such that shear strains are negligible, the stress normal to the mid-plane is small and may be neglected, since in-plane displacements are assumed to be zero the mid-plane remains unstrained after bending.

The shear resultant per unit length, Q_{xz} and Q_{yz}, and moments per unit length, M_{xx}, M_{yy}, and M_{xy}, are determined as the stress components integrated over the thickness as

$$\begin{Bmatrix} Q_{xz} \\ Q_{yz} \end{Bmatrix} = \int_{-h/2}^{h/2} \begin{Bmatrix} \tau_{xz} \\ \tau_{yz} \end{Bmatrix} dz \tag{160}$$

$$\begin{Bmatrix} M_{xx} \\ M_{yy} \\ M_{xy} \end{Bmatrix} = \int_{-h/2}^{h/2} \begin{Bmatrix} \sigma_{xx} \\ \sigma_{yy} \\ \tau_{xy} \end{Bmatrix} z dz \tag{161}$$

where, the positive orientations of the stresses are defined as shown in

Figure 23. The first subscript for the stresses $(\tau_{xz}, \tau_{yz}, \tau_{xy}, \sigma_{xx}, \sigma_{yy})$ and shear resultants (Q_{yz}, Q_{xz}) indicates the direction of the outward normal of the face on which the component acts. The second subscript indicates the direction in which the component itself acts. The subscripts for the moment resultants (M_{xx}, M_{yy}, M_{xy}) indicate which stress component causes them. The moment resultant M_{xx} is caused by stress component σ_{xx} with a face normal in the x-direction and the stress component acting in the x-direction.

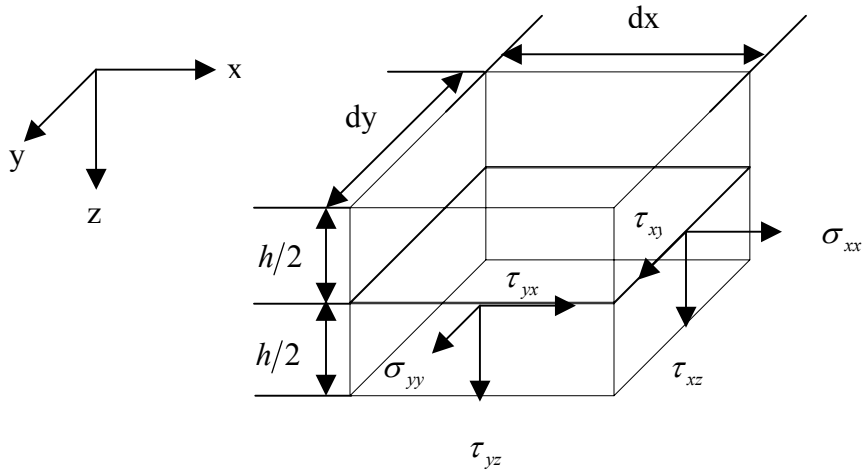

Figure 23. Stress Components for the Visible Faces of a Differential Plate Element

The development of the governing Kirchhoff plate equation follows from the free body diagram of the differential plate element shown in Figure 22. The summation of forces in the z-direction yields

$$\frac{\partial Q_{xz}}{\partial x}dxdy + \frac{\partial Q_{yz}}{\partial y}dxdy + P(x.y.t)dxdy - \mu h\frac{\partial^2 w(x,y,t)}{\partial t^2}dxdy = 0 \qquad (162)$$

The summation of moments about the x-axis, omitting terms with higher order smallness, yields

$$\frac{\partial M_{xy}}{\partial x}dxdy + \frac{\partial M_{yy}}{\partial y}dxdy - Q_{yz}dxdy = 0 \qquad (163)$$

Equation (163) can yield an expression for the shear resultant as

$$Q_{yz} = \frac{\partial M_{xy}}{\partial x} + \frac{\partial M_{yy}}{\partial y} \tag{164}$$

The summation of moments about the y-axis results in

$$\frac{\partial M_{yx}}{\partial y} + \frac{\partial M_{xx}}{\partial x} - Q_{xz} = 0 \tag{165}$$

Equation (165) can yield an expression for the shear resultant

$$Q_{xz} = \frac{\partial M_{yx}}{\partial y} + \frac{\partial M_{xx}}{\partial x} \tag{166}$$

The expressions for the moments are given by Vestel [23] as

$$\begin{aligned} M_{xx} &= -D\left(\frac{\partial^2 w(x,y,t)}{\partial x^2} + \nu \frac{\partial^2 w(x,y,t)}{\partial y^2} \right) \\ M_{yy} &= -D\left(\frac{\partial^2 w(x,y,t)}{\partial y^2} + \nu \frac{\partial^2 w(x,y,t)}{\partial x^2} \right) \\ M_{xy} &= M_{yx} = -D(1-\nu)\frac{\partial^2 w(x,y,t)}{\partial x \partial y} \end{aligned} \tag{167}$$

Substituting the resulting expressions for Q_{yz} and Q_{xz}, from Equations (164) and (166), into the z-direction force balance, Equation (162), yields an expression entirely in terms of the moments.

$$\frac{\partial}{\partial x}\left[\frac{\partial M_{yx}}{\partial y} + \frac{\partial M_{xx}}{\partial x} \right] + \frac{\partial}{\partial y}\left[\frac{\partial M_{xy}}{\partial x} + \frac{\partial M_{yy}}{\partial y} \right] + P(x,y,t) - \mu h \frac{\partial^2 w(x,y,t)}{\partial t^2} = 0 \tag{168}$$

Using the expressions for the moments from Equation (167) into Equation (168) yields the common form of the dynamic governing Kirchhoff plate equation including external load, $P(x,y,t)$, to be

$$D\left(\frac{\partial^4 w(x,y,t)}{\partial x^4}+2\frac{\partial^4 w(x,y,t)}{\partial x^2\partial y^2}+\frac{\partial^4 w(x,y,t)}{\partial y^4}\right)-P(x,y,t)+\mu h\frac{\partial^2 w(x,y,t)}{\partial t^2}=0 \quad (169)$$

where, D is the flexural rigidity, μ is the mass density, h is the thickness of the plate, and $P(x,y,t)$ is the applied load.

The governing Kirchhoff PDE was determined through balancing forces, in the z-direction, and moments, about the x and y-directions, of a differential plate element. The governing PDE is fourth order in both *x* and *y*, and second order in time. The space and time variables of the PDE are separable but the two space variables $(x \text{ and } y)$ are generally not separable. The inseparability of the spatial variables makes the general dynamic plate solution difficult to obtain for arbitrary boundary conditions. The following section describes the development of a Levy-type solution to Kirchhoff plate equation. The two opposing simply supported edges of the Levy-type plate allow a separable solution to satisfy the governing PDE and the specific boundary conditions.

5.2.2. Representation of the Displacement Field

Levy introduced a method for solving rectangular plate bending problems where two opposing edges are simply supported with arbitrary boundary conditions on the remaining two edges. Levy's method uses a separable single Fourier series to satisfy both the governing PDE and the boundary conditions. The following section describes the development of a Levy-type solution for the simply supported plate

shown in Figure 24. The edges at $y = 0$ and $y = b$ have a simply supported boundary condition. The edges at $x = 0$ and $x = a$ are currently considered to have arbitrary boundary conditions.

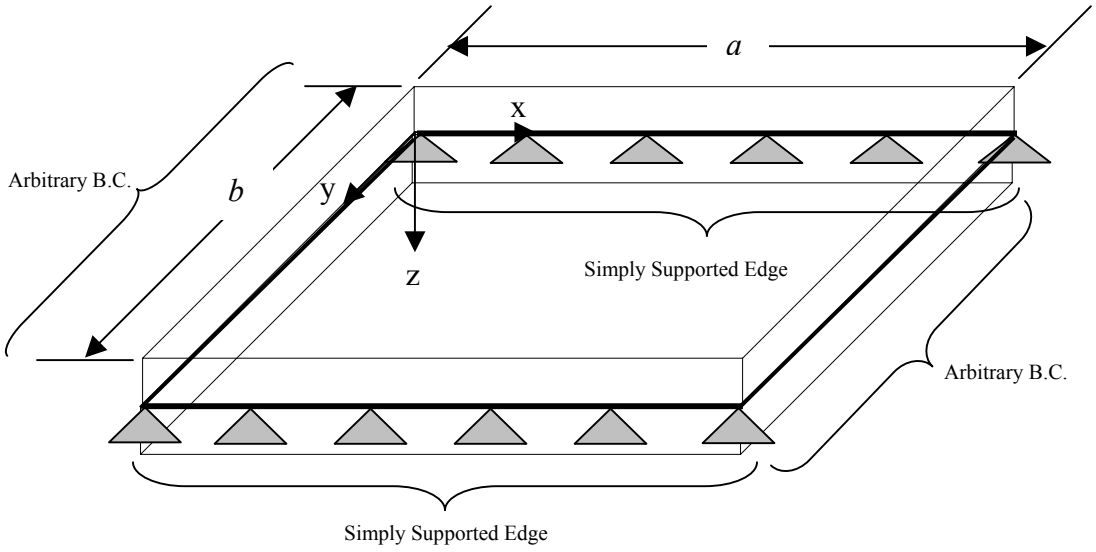

Figure 24. Schematic of Boundary Conditions for Levy-type Plate

One consequence of the simply supported boundary is zero displacement of the supported edge or mathematically for the case shown in Figure 24,

$$w = 0\big|_{y=0,b} \tag{170}$$

which, also implies that all derivatives of w with respect to x are zero at $y = 0, b$.

$$\frac{\partial w}{\partial x} = \frac{\partial^2 w}{\partial x^2} = 0\big|_{y=0,b} \tag{171}$$

Another consequence of the simply supported boundary is zero bending moment about the supported edge or mathematically for the case shown in Figure 24,

$$M_{yy} = -D\left(\frac{\partial^2 w}{\partial y^2} + \nu \frac{\partial^2 w}{\partial x^2}\right) = 0\Big|_{y=0,b} \tag{172}$$

Using the boundary condition of Equation (171) into the boundary condition of Equation (172) gives another consequence of the simply supported boundary condition, zero curvature in the y-direction at the simply supported edge.

$$\frac{\partial^2 w}{\partial y^2} = 0\Big|_{y=0,b} \tag{173}$$

The separable Levy-type solution for the simply supported boundary conditions is typically taken to be

$$w(x,y,t) = \sum_{m=1}^{\infty} f_m(x)\sin\left(\frac{m\pi y}{b}\right)e^{i\omega t} \tag{174}$$

where, the temporal solution has again been assumed to be a complex exponential for the case of harmonic excitation. It can be seen that $\sin\left(\frac{m\pi y}{b}\right)$ indeed satisfies the boundary conditions specified by Equations (170), (171), and (173) for all x, t, and m.

$$w\left(x,\{y=0,b\},t\right)=\sum_{m=1}^{\infty}f_m\left(x\right)sin\left(m\pi\right)e^{\mathbf{i}\omega t}=0$$

$$\frac{\partial w\left(x,\{y=0,b\},t\right)}{\partial x}=\sum_{m=1}^{\infty}\frac{d\,f_m\left(x\right)}{dx}sin\left(m\pi\right)e^{\mathbf{i}\omega t}=0 \tag{175}$$

$$\frac{\partial^2 w\left(x,\{y=0,b\},t\right)}{\partial y^2}=-\sum_{m=1}^{\infty}f_m\left(x\right)\left(\frac{m\pi}{b}\right)^2 sin\left(m\pi\right)e^{\mathbf{i}\omega t}=0$$

Now the x-component of the Levy-type solution can be determined through the used of the Kirchhoff governing equation. Substituting the Levy-type solution from Equation (174) into the homogeneous, i.e. $P\left(x,y,t\right)=0$, governing PDE from Equation (169) gives

$$\left[\frac{d^4 f_m\left(x\right)}{dx^4}-2\left(\frac{m\pi}{b}\right)^2\frac{d^2 f_m\left(x\right)}{dx^2}+\left(\left(\frac{m\pi}{b}\right)^2-\frac{\mu h\omega^2}{D}\right)f_m\left(x\right)\right]\sin\left(\frac{m\pi y}{b}\right)e^{\mathbf{i}\omega t}=0 \tag{176}$$

The useful information from Equation (176) comes when the bracketed term is zero such that the resulting fourth order constant coefficient ODE in $f_m\left(x\right)$ is

$$\frac{d^4 f_m\left(x\right)}{dx^4}-2\left(\frac{m\pi}{b}\right)^2\frac{d^2 f_m\left(x\right)}{dx^2}+\left(\left(\frac{m\pi}{b}\right)^2-\frac{\mu h\omega^2}{D}\right)f_m\left(x\right)=0 \tag{177}$$

An exponential form of $f_m\left(x\right)$ can be assumed, as before with constant coefficient ODEs,

$$f_m\left(x\right)=\overline{A}e^{px} \tag{178}$$

Substituting the assumed form of $f_m(x)$ into Equation (177) and simplifying yields a characteristic equation of the form

$$p^4 - 2\left(\frac{m\pi}{b}\right)^2 p^2 + \left(\frac{m\pi}{b}\right)^4 - \frac{\mu h\omega^2}{D} = 0 \tag{179}$$

Factoring the polynomial in p and rearranging gives

$$\left(p^2 - \left(\frac{m\pi}{b}\right)^2\right)^2 = \frac{\mu h\omega^2}{D} \tag{180}$$

Solving for p gives

$$p = \pm\sqrt{\pm\sqrt{\frac{\mu h\omega^2}{D}} + \left(\frac{m\pi}{b}\right)^2} \tag{181}$$

Such that there are four possible values of p, for each value of m, that will satisfy the characteristic equation

$$\begin{aligned} p_1 &= \sqrt{\sqrt{\frac{\mu h\omega^2}{D}} + \left(\frac{m\pi}{b}\right)^2} \\ p_2 &= \sqrt{-\sqrt{\frac{\mu h\omega^2}{D}} + \left(\frac{m\pi}{b}\right)^2} \\ p_3 &= -\sqrt{\sqrt{\frac{\mu h\omega^2}{D}} + \left(\frac{m\pi}{b}\right)^2} \\ p_4 &= -\sqrt{-\sqrt{\frac{\mu h\omega^2}{D}} + \left(\frac{m\pi}{b}\right)^2} \end{aligned} \tag{182}$$

Incorporating all four wave numbers into the assumed Levy-type plate solution, Equation (174), yields the general form of the transverse displacement field

$$w(x,y,t)=\sum_{m=1}^{\infty}\left[\overline{A}e^{p_1 x}+\overline{B}e^{p_2 x}+\overline{C}e^{p_3 x}+\overline{D}e^{p_4 x}\right]\sin\left(\frac{m\pi y}{b}\right)e^{\mathrm{i}\omega t} \tag{183}$$

The rotation about the y-direction $(\theta_x(x,y,t))$ is given by the derivative of the transverse displacement with respect to x as

$$\theta_x(x,y,t)=-\frac{\partial w(x,y,t)}{\partial x} \tag{184}$$

The solution to the Kirchhoff plate governing PDE was found by assuming a separable solution. A single Fourier series in the y-direction with an undetermined function in the x-direction was assumed as the separable solution. Substituting the assumed solution into the governing PDE resulted in a fourth order constant coefficient ODE in the undetermined function, $f_m(x)$. Assuming an exponential form of the unknown function gave a characteristic equation with four roots. Incorporating the four roots into the assumed solution resulted in the total solution to the Kirchhoff PDE. The assumed solution was shown to satisfy the specific Levy-type boundary condition as well as the Kirchhoff governing PDE. The following section describes the development of the dynamic stiffness matrix for a Levy-type Kirchhoff plate element using the displacement field developed in Equation (183).

5.2.3. Dynamic Stiffness

A major difference in the formulation of the spectral Levy-type plate element compared to the spectral beam element is that the plate element must satisfy boundary conditions along an edge opposed to at a single point. The spectral Levy-type plate element must specify a function for the displacement and rotation along the edge to specify the arbitrary boundary conditions of Figure 24 as edge-DOF. The edge-DOF

of the Levy-type element will be represented as a Fourier series expansions of the transverse displacement (w_1, w_2) and rotation about the y-direction $(\theta_{x1}, \theta_{x2})$, shown in Figure 25 with positive orientation.

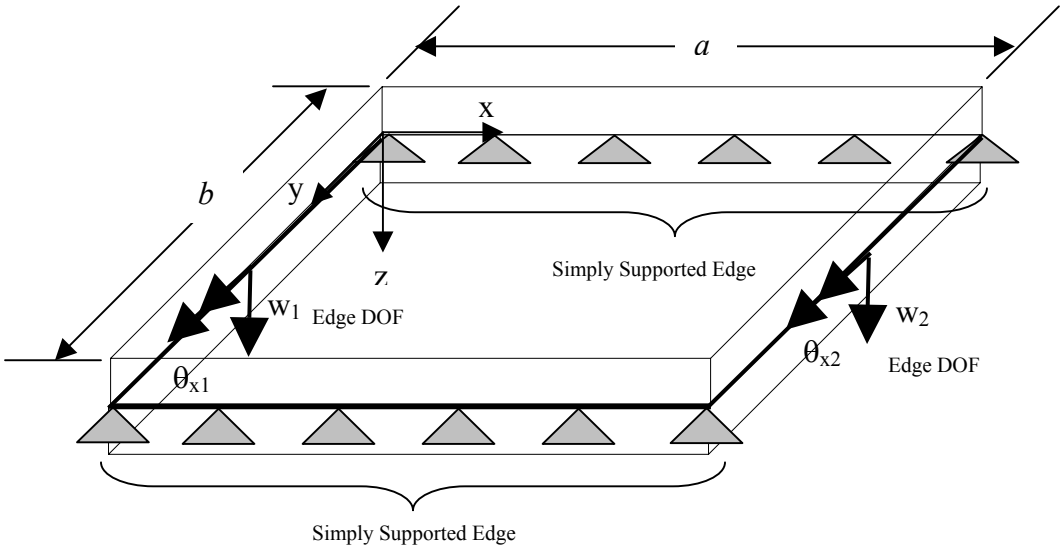

Figure 25. Edge DOF of Levy-type Spectral Plate Element

The dynamic stiffness matrix for the Levy-type element can be formulated using the displacement field developed in Equation (183). The method to develop the dynamic stiffness is similar to that of the spectral beam element. The fundamental difference is that a spatial Fourier series representation of the edge loading, displacement, and rotation boundary conditions is used to form the dynamic stiffness, Kevorkian [12]. The relations between the Fourier expanded displacements and forces can then be used to eliminate the unknown coefficients and form an expression for the dynamic stiffness matrix.

A single term of the Fourier series expansion, shown as $\mathcal{F}$, of the displacements and rotations, given in Equations (183) and (184) respectively, is

$$\mathcal{F}\begin{Bmatrix} w(0,y,t) \\ \theta_x(0,y,t) \\ w(a,y,t) \\ \theta_x(a,y,t) \end{Bmatrix} = \left[\frac{2}{b}\int_0^b sin\left(\frac{m\pi y}{b}\right)\begin{Bmatrix} w(0,y,t) \\ \theta_x(0,y,t) \\ w(a,y,t) \\ \theta_x(a,y,t) \end{Bmatrix} dy \right] sin\left(\frac{m\pi y}{b}\right) \tag{185}$$

where, the bracketed terms are the Fourier series expansion coefficients of the edge displacements. Defining the edge DOF as the $\sin\left(\frac{m\pi y}{b}\right)$ Fourier coefficients such that,

$$\begin{Bmatrix} w_1 \\ \theta_{x1} \\ w_2 \\ \theta_{x2} \end{Bmatrix} sin\left(\frac{m\pi y}{b}\right) e^{i\omega t} = \left[\frac{2}{b}\int_0^b sin\left(\frac{m\pi y}{b}\right)\begin{Bmatrix} w(0,y,t) \\ \theta_x(0,y,t) \\ w(a,y,t) \\ \theta_x(a,y,t) \end{Bmatrix} dy \right] sin\left(\frac{m\pi y}{b}\right) \tag{186}$$

Regrouping the expression for the edge displacement Fourier expansion coefficients into the matrix $[\mathbf{D}_m]$ such that

$$\begin{bmatrix} \frac{2}{b}\int_0^b sin\left(\frac{m\pi y}{b}\right) w(0,y,t)dy \\ \frac{2}{b}\int_0^b sin\left(\frac{m\pi y}{b}\right) \theta_x(0,y,t)dy \\ \frac{2}{b}\int_0^b sin\left(\frac{m\pi y}{b}\right) w(a,y,t)dy \\ \frac{2}{b}\int_0^b sin\left(\frac{m\pi y}{b}\right) \theta_x(a,y,t)dy \end{bmatrix} = [\mathbf{D}_m]\{\mathbf{a}\}e^{\mathbf{i}\omega t} \tag{187}$$

Substituting $[\mathbf{D}_m]\{\mathbf{a}\}e^{\mathbf{i}\omega t}$, from Equation (187), for the bracketed expression in Equation (186) gives

$$\begin{Bmatrix} w_1 \\ \theta_{x1} \\ w_2 \\ \theta_{x2} \end{Bmatrix} \sin\left(\frac{m\pi y}{b}\right) e^{\mathbf{i}\omega t} = [\mathbf{D}_m]\{\mathbf{a}\}\sin\left(\frac{m\pi y}{b}\right) e^{\mathbf{i}\omega t} \tag{188}$$

where, $\{\mathbf{a}\}$ is the vector of unknown coefficients

$$\{\mathbf{a}\} = \begin{bmatrix} \overline{A} & \overline{B} & \overline{C} & \overline{D} \end{bmatrix}^T \tag{189}$$

The explicit form of the matrix of Fourier coefficients $[\mathbf{D}_m]$ is

$$[\mathbf{D}_m] = \begin{bmatrix} 1 & 1 & 1 & 1 \\ -p_1 & -p_2 & -p_3 & -p_4 \\ e^{p_1 a} & e^{p_2 a} & e^{p_3 a} & e^{p_4 a} \\ -p_1 e^{p_1 a} & -p_2 e^{p_2 a} & -p_3 e^{p_3 a} & -p_4 e^{p_4 a} \end{bmatrix} \tag{190}$$

The effective Kirchhoff shear forces and moments are given by Venstel [23] to be

$$V_{xz}(x,y,t) = -D\left[\frac{\partial^3 w(x,y,t)}{\partial x^3} + (2-\nu)\frac{\partial^3 w(x,y,t)}{\partial y^2 x}\right] \tag{191}$$

$$M_{xx}(x,y,t) = -D\left[\frac{\partial^2 w(x,y,t)}{\partial x^2} + \nu\frac{\partial^2 w(x,y,t)}{\partial y^2}\right] \tag{192}$$

The $\sin\left(\frac{m\pi y}{b}\right)$ Fourier series expanded edge forces and moments for a single Fourier series value, m, can be written as,

$$\mathcal{F}\begin{Bmatrix} V_{xz}(0,y,t) \\ M_{xx}(0,y,t) \\ V_{xz}(a,y,t) \\ M_{xx}(a,y,t) \end{Bmatrix} = \left[\frac{2}{b}\int_0^b sin\left(\frac{m\pi y}{b}\right)\begin{Bmatrix} V_{xz}(0,y,t) \\ M_{xx}(0,y,t) \\ V_{xz}(a,y,t) \\ M_{xx}(a,y,t) \end{Bmatrix} dy\right] sin\left(\frac{m\pi y}{b}\right) \tag{193}$$

where, the bracketed expressions are the Fourier expansion coefficients of the edge forces and moments. Defining the vector of edge load Fourier coefficients such that,

$$\begin{Bmatrix} V_1 \\ M_1 \\ V_2 \\ M_2 \end{Bmatrix} sin\left(\frac{m\pi y}{b}\right)e^{i\omega t} = \left[\frac{2}{b}\int_0^b sin\left(\frac{m\pi y}{b}\right)\begin{Bmatrix} -V_{xz}(0,y,t) \\ -M_{xx}(0,y,t) \\ V_{xz}(a,y,t) \\ M_{xx}(a,y,t) \end{Bmatrix} dy\right] sin\left(\frac{m\pi y}{b}\right) \tag{194}$$

where, the minus signs ensure that a positive load will create a positive displacement. Regrouping the edge load Fourier expansion coefficients into the matrix $[\mathbf{F}_m]$ as,

$$\begin{bmatrix} -\frac{2}{b}\int_0^b \sin\left(\frac{m\pi y}{b}\right) V_{xz}(0,y,t)\,dy \\ -\frac{2}{b}\int_0^b \sin\left(\frac{m\pi y}{b}\right) M_{xx}(0,y,t)\,dy \\ \frac{2}{b}\int_0^b \sin\left(\frac{m\pi y}{b}\right) V_{xz}(a,y,t)\,dy \\ \frac{2}{b}\int_0^b \sin\left(\frac{m\pi y}{b}\right) M_{xx}(a,y,t)\,dy \end{bmatrix} = [\mathbf{F}_m]\{\mathbf{a}\}e^{\mathbf{i}\omega t} \tag{195}$$

Substituting the expression for $[\mathbf{F}_m]$, from Equation (195), into the expression for the Fourier expanded edge loads, from Equation (194), gives

$$\begin{Bmatrix} V_1 \\ M_1 \\ V_2 \\ M_2 \end{Bmatrix} \sin\left(\frac{m\pi y}{b}\right) e^{\mathbf{i}\omega t} = [\mathbf{F}_m]\{\mathbf{a}\}\sin\left(\frac{m\pi y}{b}\right) e^{\mathbf{i}\omega t} \tag{196}$$

where, $\{\mathbf{a}\}$ is again the vector of unknown coefficients, as shown in Equation (189). The explicit form of $[\mathbf{F}_m]$, for the Fourier coefficients of the edge loads is,

$$[\mathbf{F}_m] = -D\begin{bmatrix} -p_1^3 + (2-\nu)\left(\frac{m\pi}{b}\right)^2 p_1 & \dots & \dots & \dots \\ -p_1^2 + \nu\left(\frac{m\pi}{b}\right)^2 & \dots & \dots & \dots \\ p_1^3 e^{p_1 a} - (2-\nu)\left(\frac{m\pi}{b}\right)^2 p_1 e^{p_1 a} & \dots & \dots & \dots \\ p_1^2 e^{p_1 a} - \nu\left(\frac{m\pi}{b}\right)^2 e^{p_1 a} & \dots & \dots & \dots \end{bmatrix} \tag{197}$$

where, the remaining three columns can be found by simply changing the subscript on the wave number (p_{column}) to the column of interest.

Defining the Fourier coefficients of the edge DOF for each value of m, from Equation (188), as $\{\mathbf{d}_m\}$ such that,

$$\{\mathbf{d}_m\} = \begin{Bmatrix} w_1 \\ \theta_{x1} \\ w_2 \\ \theta_{x2} \end{Bmatrix} \tag{198}$$

Similarly, defining the Fourier coefficients of the edge loads for each value of m, from Equation (196), as $\{\mathbf{f}_m\}$ such that,

$$\{\mathbf{f}_m\} = \begin{Bmatrix} V_1 \\ M_1 \\ V_2 \\ M_2 \end{Bmatrix} \tag{199}$$

The dynamic stiffness matrix $[\mathbf{K}_{Dyn\ m}]$ relates the DOF Fourier coefficients $\{\mathbf{d}_m\}$ to the load Fourier coefficients $\{\mathbf{f}_m\}$, for each value of m such that

$$\{\mathbf{f}_m\} = [\mathbf{K}_{Dyn\ m}]\{\mathbf{d}_m\} \tag{200}$$

The dynamic stiffness relation can be found by solving Equation (188) for $\{\mathbf{a}\}$ as,

$$\{\mathbf{a}\} = [\mathbf{D}_m]^{-1}\{\mathbf{d}_m\} \tag{201}$$

Substituting the expression for $\{\mathbf{a}\}$ in Equation (201) into Equation (196) gives

$$\{\mathbf{f}_m\} = [\mathbf{F}_m][\mathbf{D}_m]^{-1}\{\mathbf{d}_m\} \tag{202}$$

The dynamic stiffness of the Levy-type spectral plate element can be extracted from Equation (202) . The formulation of the dynamic stiffness for each *m*-value is,

$$[\mathbf{K}_{Dyn\ m}] = [\mathbf{F}_m][\mathbf{D}_m]^{-1} \tag{203}$$

The dynamic stiffness for each value of *m* is symmetric and includes the effects of transverse inertia.

The shape functions of the Levy-type spectral plate element can be expressed in terms of the $[\mathbf{D}_m]$ matrix. The shape functions for the transverse displacement $[\mathbf{N}_{w\,m}]$ and rotation $[\mathbf{N}_{\theta_x\ m}]$ are given by,

$$[\mathbf{N}_m] = \begin{bmatrix} \mathbf{N}_{w\,m} \\ \mathbf{N}_{\theta_x m} \end{bmatrix} = sin\left(\frac{m\pi y}{b}\right) e^{\mathrm{i}\omega t} \begin{bmatrix} e^{p_1 x} & e^{p_2 x} & e^{p_3 x} & e^{p_4 x} \\ -p_1 e^{p_1 x} & -p_2 e^{p_2 x} & -p_3 e^{p_3 x} & -p_4 e^{p_4 x} \end{bmatrix} [\mathbf{D}_m]^{-1} \tag{204}$$

The representation of the displacement field in terms of the edge DOF $\{\mathbf{d}_m\}$ and the shape function $[\mathbf{N}_m]$ for each *m* value is then

$$\begin{bmatrix} w_m(x,y,t) \\ \theta_{x\,m}(x,y,t) \end{bmatrix} = [\mathbf{N}_m]\{\mathbf{d}_m\} \tag{205}$$

The total solution is then the summation over all the *m* values used in the model,

$$\begin{bmatrix} w(x,y,t) \\ \theta_x(x,y,t) \end{bmatrix} = \sum_{m=1}^{\infty} [\mathbf{N}_m]\{\mathbf{d}_m\} \tag{206}$$

The dynamic stiffness matrix of the Levy-type spectral plate element was formed through a variation of the direct method used in sections 3.2.3 and 4.2.3 for the bar and beam elements. The Levy-type plate dynamic stiffness relates the Fourier expansion of the edge displacement functions to the Fourier expansion of the edge load functions. The dynamic stiffness of the bar and beam spectral elements related nodal displacements to nodal loads.

Relating the edge displacement function and edge load function Fourier expansions on a term-by-term basis resulted in a dynamic stiffness matrix for each Fourier term in the series expansion. It is worth noting that each set of Equations (202) for a given *m*-value is independent from (or orthogonal to) all other *m*-values, just as in a conventional Fourier series analysis. Thus, the effects of each *m*-value can be calculated separately and added together at the end of the analysis.

The Levy-type spectral element shape function was also formed through the Fourier expansion of the edge displacements. The shape functions for each *m*-value relates the displacement field to the edge DOF for each *m*-value of the Fourier expansion. Thus, there is a different shape function for each *m*-value of the series. The number of *m*-values in the Fourier series can be increased until the displacement field results converge to an acceptable level. Thus, the spectral Levy-type plate element is not an exact formulation in the same sense that the spectral bar and beam were exact. The convergence of the Fourier series is strongly affected by the presence of discontinuities, which may occur at the edge of an element, Venstel [23]. Thus, the geometry, loading, and boundary conditions will all affect the convergence of the series. The following section uses a Levy-type plate with uniform loads on the free edges to investigate the performance of the Levy-type spectral element compared to the conventional element developed in section 5.1.3.

5.3. Straight Example Problem

A simply supported plate example is used to illustrate the modeling differences between conventional finite elements and Levy-type spectral elements. SI units are used in the example along with the same geometry, loading, and material properties used in the example by Kevorkian [12]. Figure 26 shows a schematic of the plate geometry and loading used in the example. The example uses material properties of aluminum with a modulus of elasticity (E) of $68948 \times 10^6\ Pa$, a density of $2700\, kg/m^3$, and a Poisson's ratio (ν) of 0.33. The length of the plate between the supports (b) is $0.381\, m$, the width of the plate (a) is $0.254\, m$, and the plate thickness (h) is $0.003175\, m$. A harmonic edge load with uniform amplitude (p_0) of $6561.67\ N/m$ was applied to each of the free edges. The Fourier series expansion of a uniform edge load is given by Ventsel [23] to be

$$p_m = \frac{2p_0}{b}\int_0^b \sin\left(\frac{m\pi y}{b}\right)dy = \frac{4p_0}{m\pi} \qquad m = 1,3,5,\ldots\ odd \tag{207}$$

where p_0 is the magnitude of the applied load and m is the Fourier series summation index.

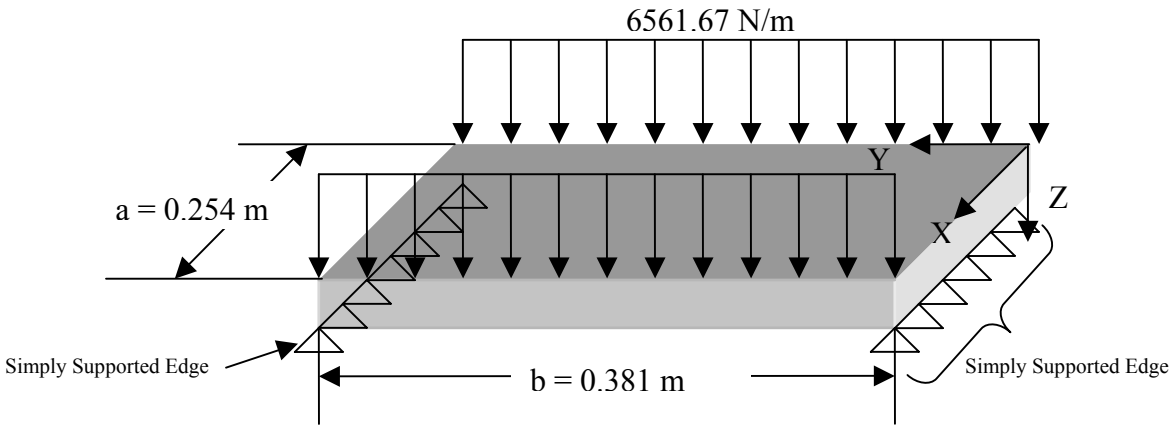

Figure 26. Schematic of Simply Supported Plate

5.3.1. Single Point Response Comparison

A finite element model, created in ANSYS using SHELL63 elements, was used to compare the dynamic response of a plate modeled with conventional finite elements to that of a plate modeled with spectral elements. The ANSYS model used mapped element meshes ranging from 2X2 to 96X96 with loading and geometry as shown in Figure 26. The location selected for the comparison was the center of the free edge of the simply supported plate, as shown in Figure 27.

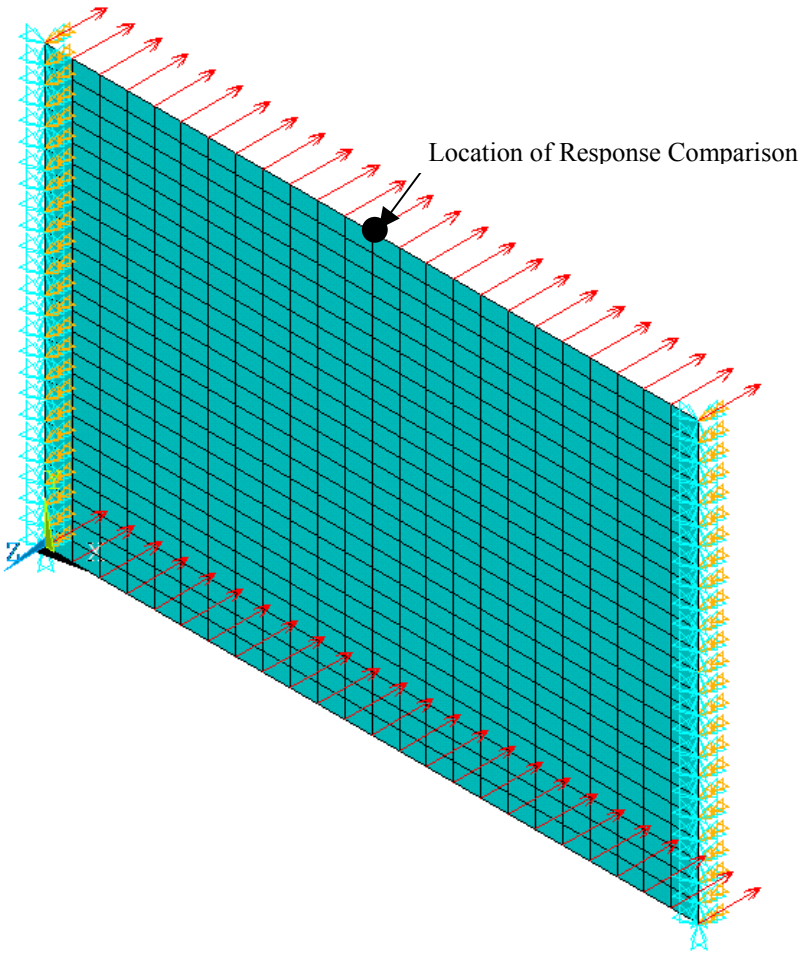

Figure 27. 24X24 Element ANSYS Model with Single Comparison Point

The number of elements in the FEA model were increased by 2 elements per edge from 2X2 to 12X12, and then increased by 4 elements per edge from 12X12 to 24X24. Finally the number of elements per edge was doubled from 24X24 to 96X96. Table 6 gives a summary of the ANSYS models used in the comparison including the number of elements and number of nodes. The uniform edge load was divided equally over the nodes such that the load on each node was

$$Load\ per\ Node = \frac{6561.67\ N/m \times 0.381 m}{Number\ of\ Nodes\ per\ Edge} \tag{208}$$

The response of the center of the free edge was recorded for each mesh at frequencies of 10, 100, 300, 600, 1500, 2000, and 4500 *Hz*. As a measure of convergence, the percent difference was calculated between each mesh for a given frequency. The difference was calculated as

$$Percent\ Differnce = \frac{mesh_{m+1} - mesh_m}{mesh_m} \times 100 \tag{209}$$

where, $mesh_m$ is the previous mesh with fewer elements and $mesh_{m+1}$ is the refined mesh with a higher number of elements than $mesh_m$. The percent difference between mesh sizes decreases to below 3% for a mesh size of 96X96, even for the 4500 Hz case. Figure 28 shows a plot of the percent difference between the mesh sizes for the frequencies given above.

Table 6. ANSYS Models Used in Comparison of Conventional and Spectral Response

ANSYS Model Summary			
Mesh	**Mesh Size**	**Number of Elements**	**Number of Nodes**
1	2X2	4	9
2	4X4	16	25
3	6X6	36	49
4	8X8	64	81
5	10X10	100	121
6	12X12	144	169
7	16X16	256	289
8	20X20	400	441
9	24X24	576	625
10	48X48	2304	2401
11	96X96	9216	9409

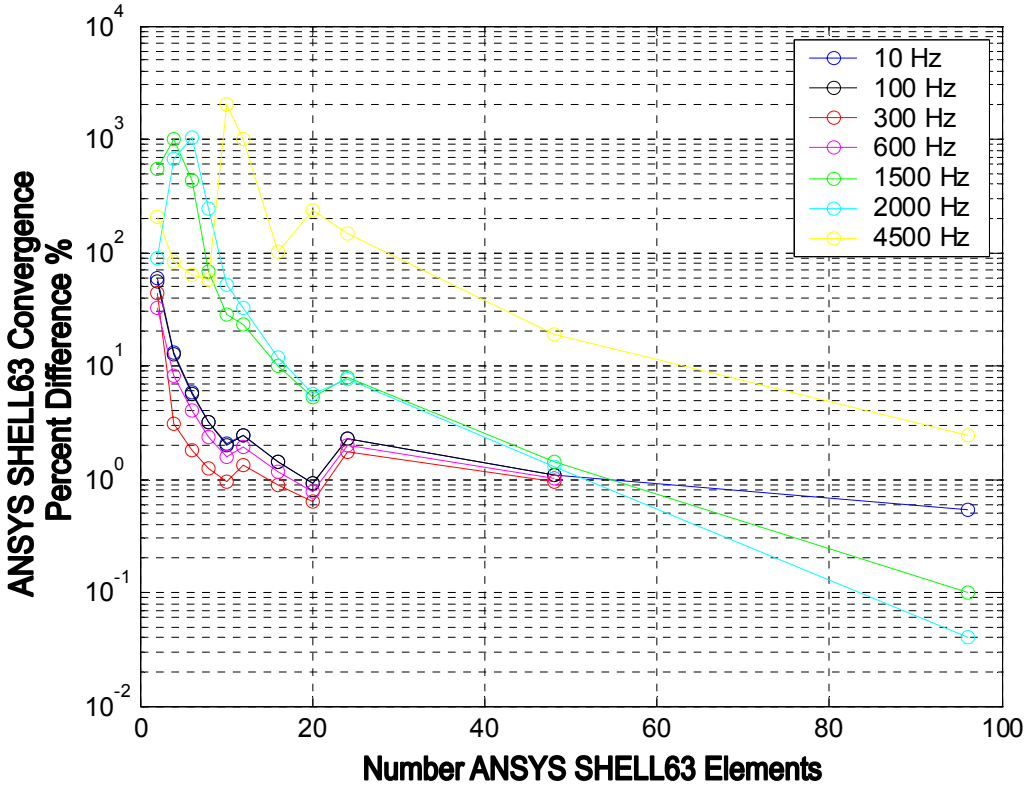

Figure 28. Convergence of the Displacement of the Center of Free Edge Using ANSYS Shell63 Mesh for Various Frequencies

The convergence technique used for the single spectral element model was to increase the number of Fourier terms and calculate the percent difference between the two solutions. Using odd Fourier terms 1 through 5 gives a percent difference below 2% for all frequencies except 4500 Hz, where using Fourier terms 1 through 13 gives a percent difference of less than 2%.

Figure 29 shows the percent difference for the frequencies under consideration and Fourier terms between 1 and 43.

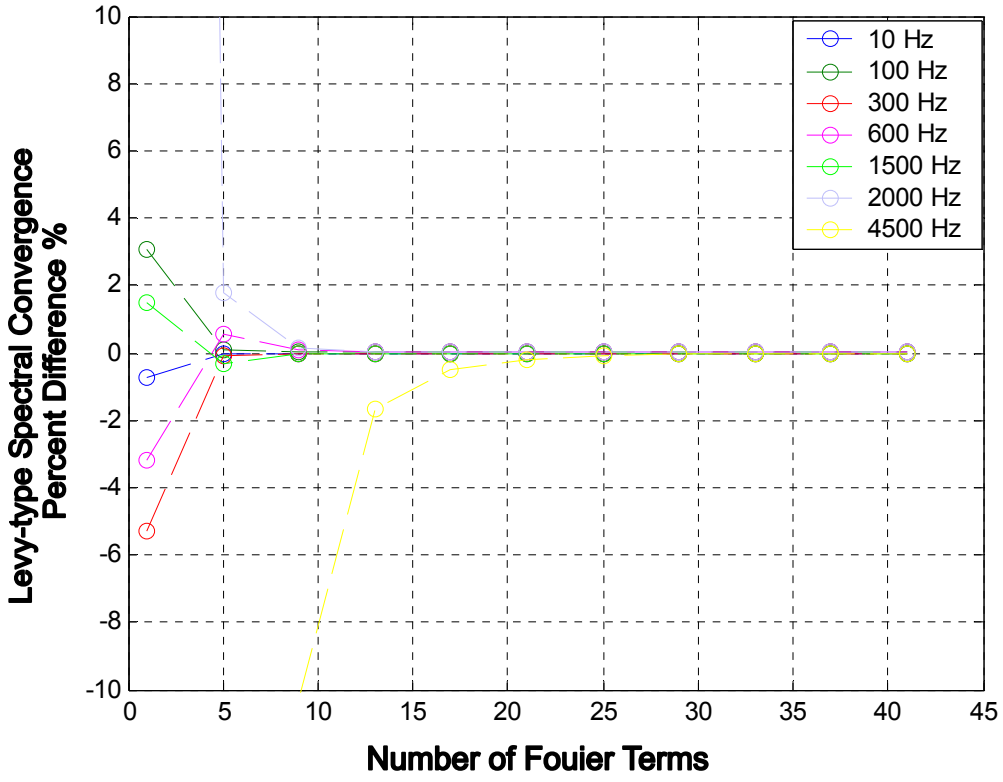

Figure 29. Convergence of the Displacement of the Center of Free Edge Using Single Levy-type Spectral Element

Figure 30 shows the response of the center of the free edge versus frequency for both the 24X24 ANSYS model and the spectral model using a single Fourier term. The two models agree very closely at mid-range frequencies, differing by 10% or less between 100 and 1500 *Hz*. The percent difference in this case was calculated as

$$Percent\ Difference = \frac{Spectral_{m=1} - ANSYS_{24X24}}{ANSYS_{24X24}} \times 100 \qquad (210)$$

The difference in the two solutions becomes larger as frequency increases. The percent difference for 10, 2000, and 4500 *Hz* is much larger, ranging from 1% to

1590%. Table 7 shows a summary of harmonic response results for the 24X24 ANSYS mesh and the *m=1* spectral element. See Appendix C for a summary of the convergence for both conventional and spectral single-point responses.

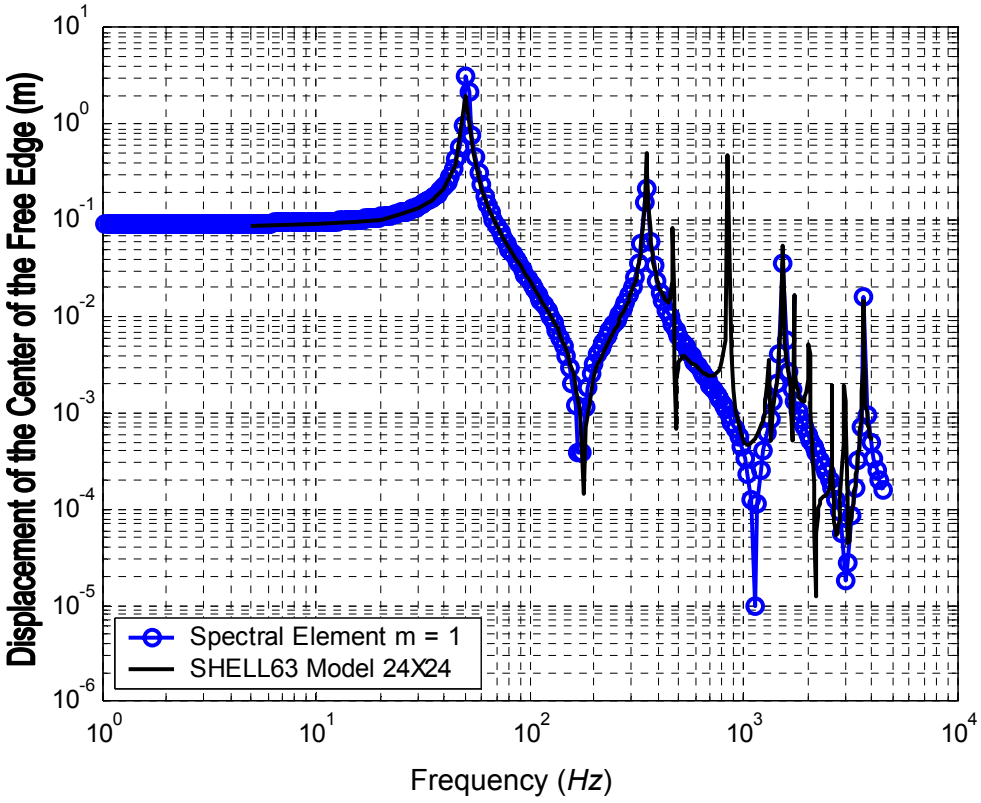

Figure 30. Response of Center of Free Edge vs. Frequency *m=1* Spectral and 24X24 SHELL63

Table 7. Comparison of Displacement of the Center of the Free Edge for 24X24 FEA Mesh and *m=1* Spectral Models

Frequency (*Hz*)	ANSYS 24X24	Spectral *m=1*	% Difference
10	9.14E-02	9.62E-02	5.25%
100	-2.33E-02	-2.35E-02	0.86%
300	1.78E-02	1.96E-02	10.11%
600	-3.07E-03	-3.30E-03	7.49%
1500	8.09E-03	7.30E-03	-9.77%
2000	-2.22E-03	-6.04E-04	-72.79%
4500	1.08E-05	-1.61E-04	-1590.74%

Figure 31 shows the response of the center of the free edge versus frequency for both the 24X24 ANSYS model and the spectral model using odd Fourier terms 1 to 11. The peaks above 600 *Hz* are now captured by the spectral model.

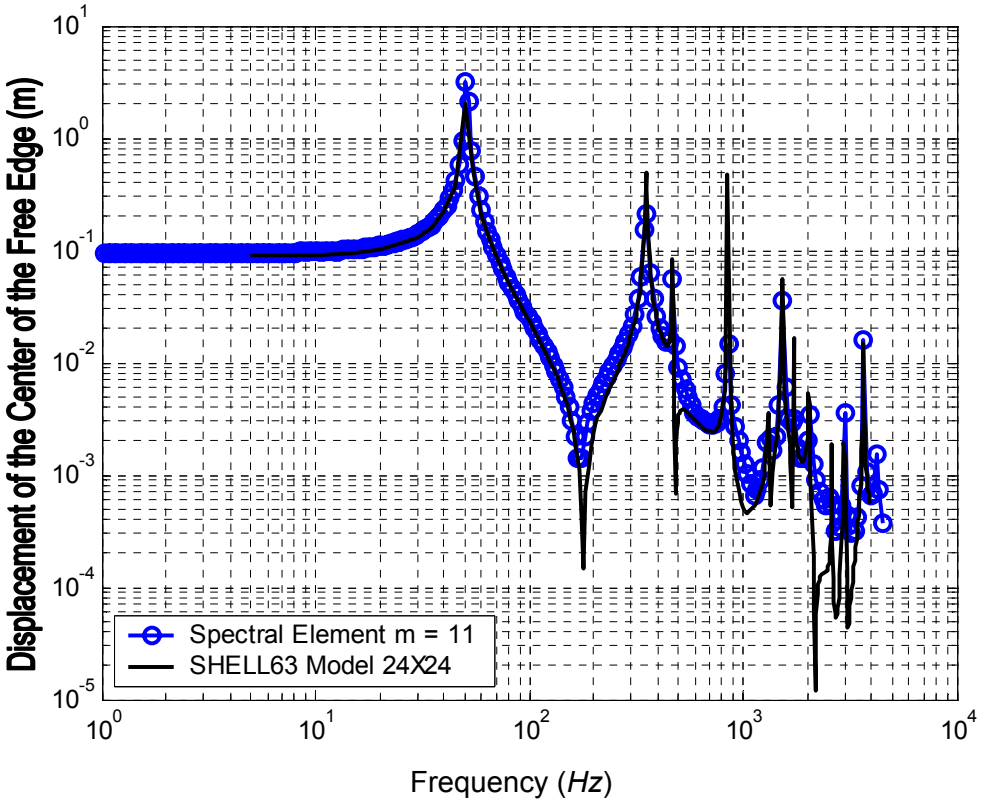

Figure 31. Response of Center of Free Edge vs. Frequency *m=11* Spectral and 24X24 SHELL63

Figure 32 shows the deformed shapes of the spectral model at 10, 100, 300, and 600 Hz using odd Fourier terms 1 through 11. Figure 33 shows the deformed shapes of the spectral model at 1500, 2000, 3000, and 4500 *Hz* using odd Fourier terms 1 through 11.

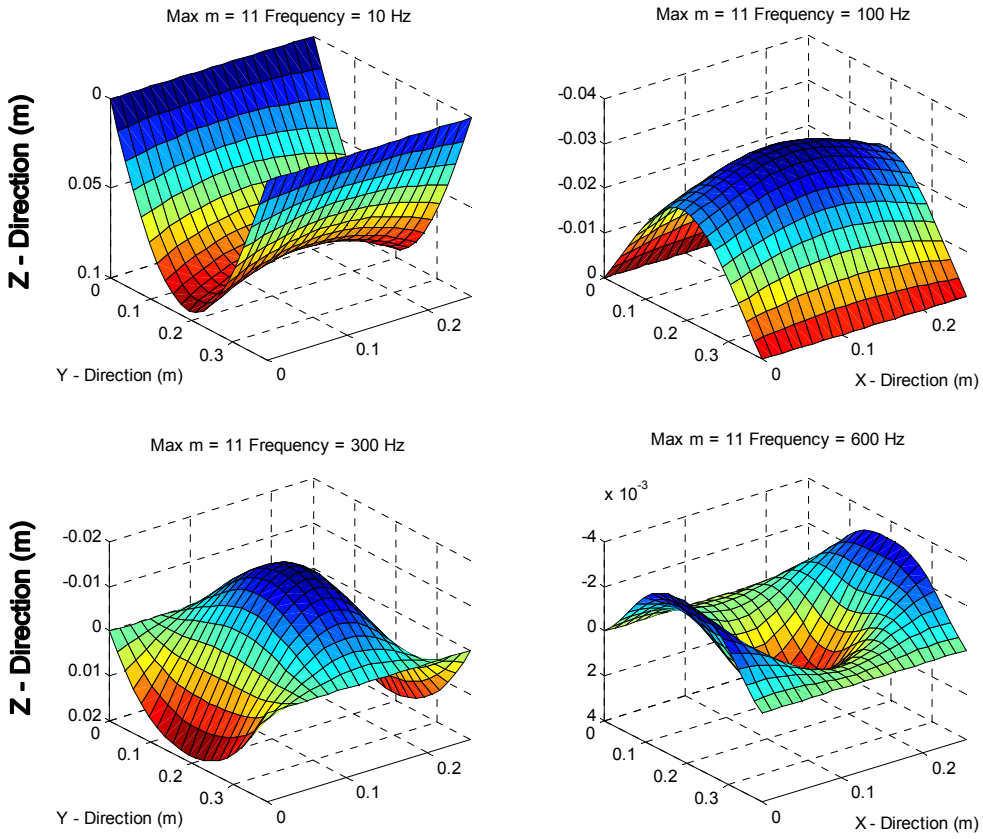

Figure 32. Deformed Shapes of Single Levy-type Spectral Model at 10, 100, 300, 600 *Hz, m=11*

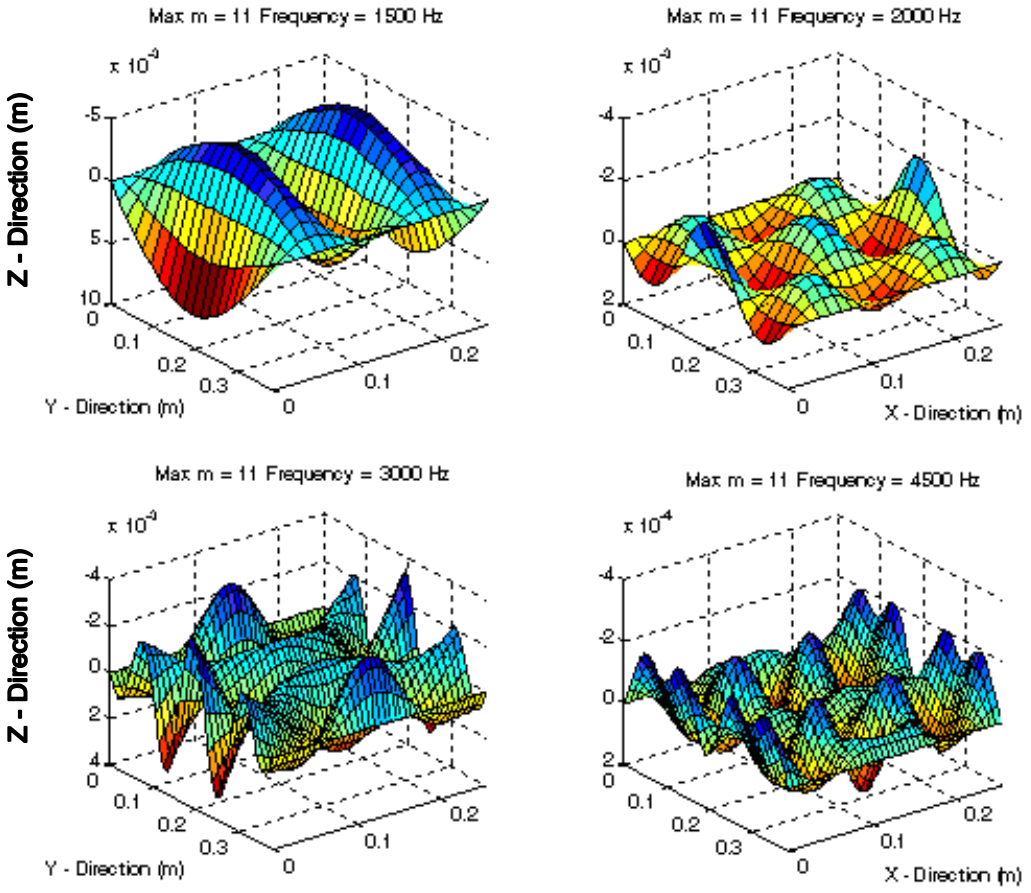

Figure 33. Deformed Shapes of Single Levy-type Spectral Model at 1500, 2000, 3000, 4500 *Hz, m=11*

As the numbers of ANSYS shell63 elements and Fourier terms are increased, the percent difference between the two solutions decreases for low and high frequency ranges. The percent difference in center free edge displacement decreases to near 1% for all frequencies tested except for the 600 *Hz* case were the percent difference is 4.43%. Table 8 shows the percent difference between the two solutions for a 96X96 ANSYS mesh and *m=11* spectral element. The percent difference was calculated in the same way as in Equation (210), only using the spectral response with *m=11* Fourier terms and a 96X96 ANSYS mesh.

Table 8. Comparison of Displacement of the Center of the Free Edge for 96X96 FEA Mesh and *m=11* Spectral Models

Frequency (*Hz*)	ANSYS 96X96	Spectral *m=11*	% Difference
10	9.45E-02	9.55E-02	1.06%
100	-2.40E-02	-2.43E-02	1.25%
300	1.83E-02	1.85E-02	1.09%
600	-3.16E-03	-3.30E-03	4.43%
1500	7.35E-03	7.40E-03	0.68%
2000	-2.02E-03	-2.00E-03	-0.99%
4500	3.22E-05	3.25E-05	0.86%

5.3.2. Multiple Point Response Comparison

Again the plate was modeled using SHELL63 plate elements in ANSYS. The harmonic response of the plate was obtained for meshes ranging from 2 elements per edge to 96 elements per edge and for forcing frequencies of 10, 100, 300, 600 Hz. Meshes of 12, 24, 48, and 96 elements per edge were used to show the convergence of the conventional solution with doubling the number of elements. A signal-to-noise type metric was used to measure the convergence of the transverse displacement with increasing mesh density. The convergence metric was defined as the magnitude of displacement of the original mesh $(Mesh_1)$ divided by the standard deviation of the difference between the doubled mesh $(Mesh_2)$ and the original mesh $(Mesh_1)$ displacements at each of the 25 sample locations shown in Figure 34.

$$Convergence\ Metric = \frac{Magnitude(Mesh_1)}{Std(Mesh_2 - Mesh_1)} \tag{211}$$

The displacement values used to compute the convergence metrics were sampled from 25 equally spaced nodes as shown in Figure 34.

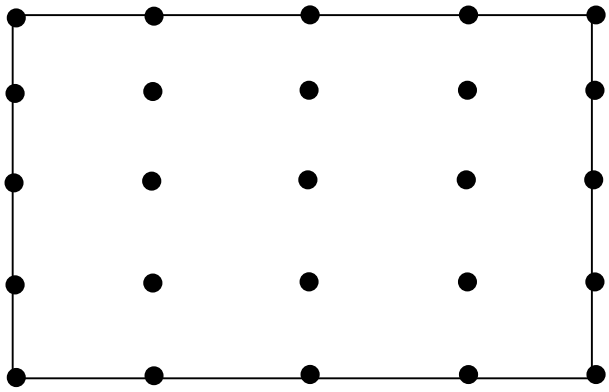

Figure 34. Layout of Nodes Used in the Multi-point Convergence Study

The values of the convergence metric versus the doubled mesh value are plotted in Figure 35 for the four test frequencies. The convergence metric for the conventional element model ranges from an order of magnitude of 1 to an order of magnitude of 2. This means that the difference between the two mesh solutions is 1 to 2 orders of magnitude below the maximum value of the displacement. Due to time and computational limitations, the maximum number of elements used was 96 elements per side. If the number of elements were continually doubled, the convergence metric curves should level out to some maximum level of precision. In the current limits of the analysis, the maximum level of precision for the conventional element is 2 orders of magnitude below the maximum displacement of the plate.

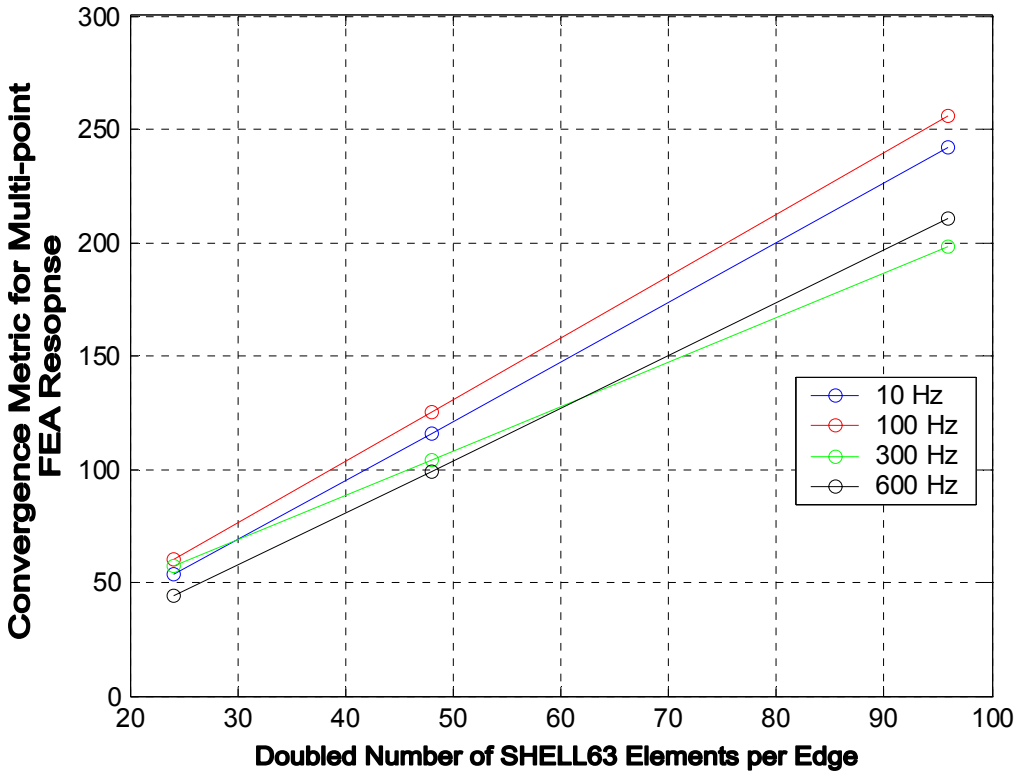

Figure 35. Conventional Element Convergence by Doubling Number of Elements per Edge

The multi-point Levy-type spectral element model used a single Levy-type plate element. The harmonic response was obtained using odd Fourier terms ranging from 1 to 45. The same convergence metric was used as in the conventional FEA convergence study only now; increasing the number of Fourier terms replaces increasing the number of elements per edge. The convergence metric for the spectral model is plotted versus the number of Fourier terms in Figure 36. The value of the convergence metric for the spectral solutions ranged from 10^1 to 10^8. This means that the difference in the spectral solutions between m-values ranged from 1 to 8 orders of magnitude below the maximum values of displacement.

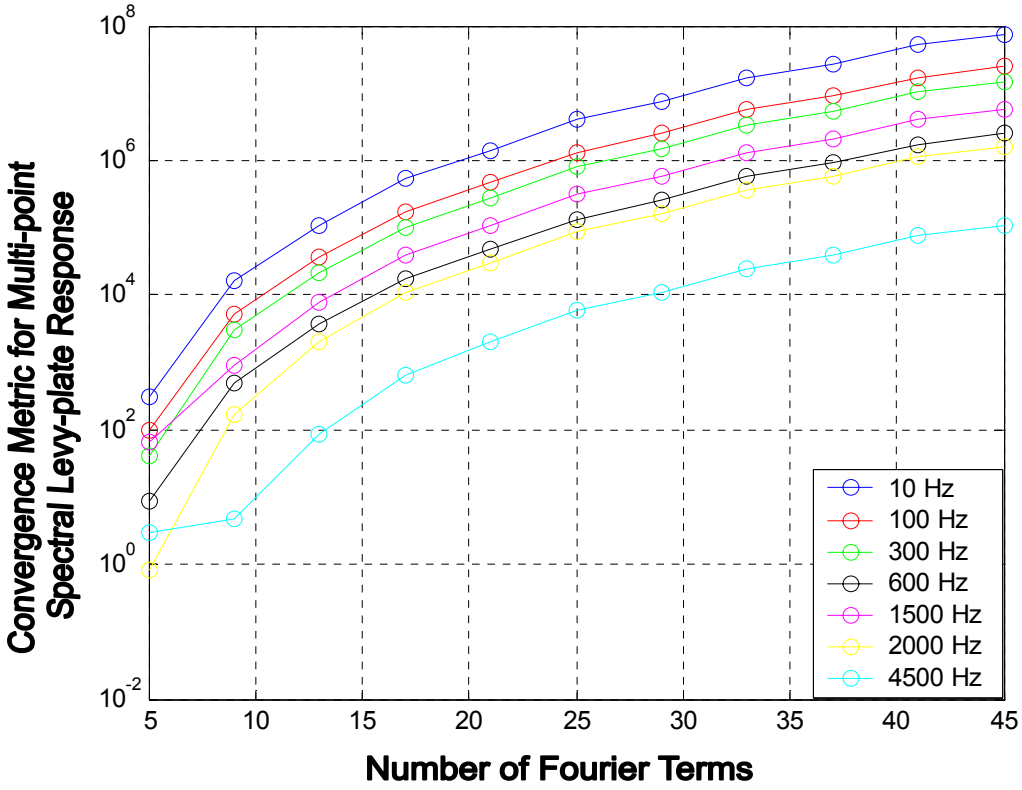

Figure 36. Levy-Type Spectral Element Convergence by Increasing Number of Fourier Terms

To compare the multi-point conventional and spectral solutions, 11 Fourier terms were used for the spectral solution and the FEA mesh was varied from 2X2 to 96X96. The relative error for frequencies of 10, 100, 300, and 600 *Hz* was defined as

$$Relative\ Error = \frac{Std\left(Spec_{m=11} - FEA\right)}{Max\left(FEA\right)} \times 100 \tag{212}$$

A plot of the relative error is shown in

Figure 37. The relative error between the two solutions decreases sharply with increasing number of conventional elements. The percent error is below 2% for conventional meshes with 24 elements per edge or more for all frequencies compared.

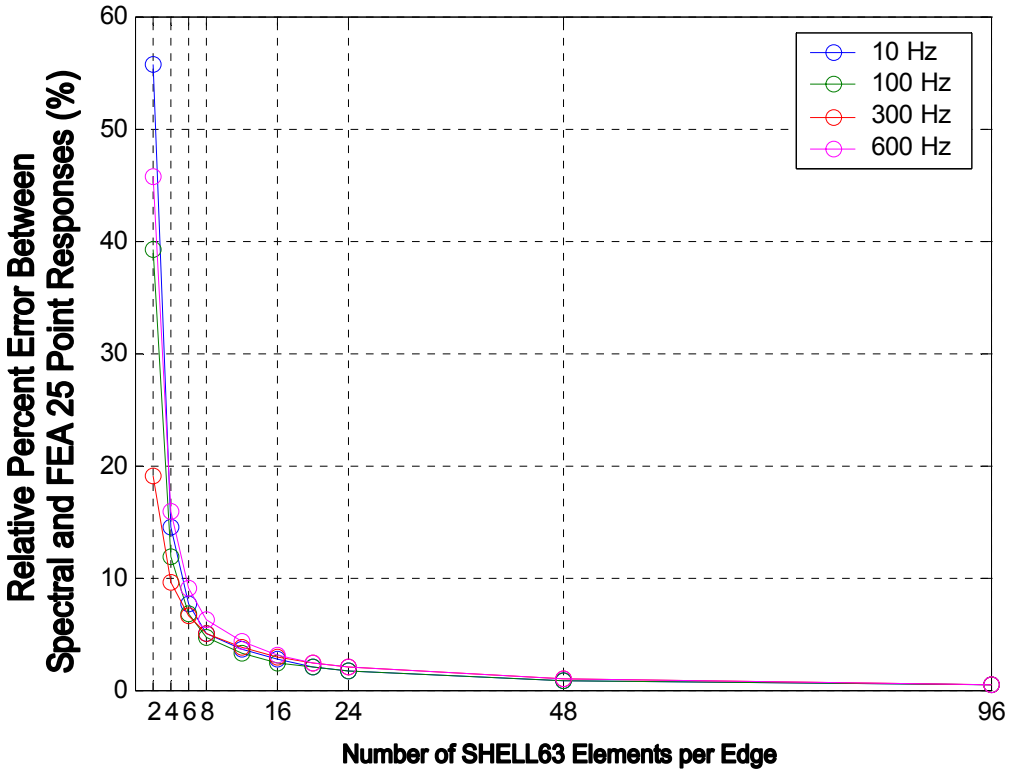

Figure 37. Relative Error of 25 Point Response Between Spectral *m=11* and FEA

5.4. Chapter Summary

The major difference in the formulations of the conventional and spectral plate elements is that the spectral element uses the eigenfunction of the governing PDE, in the form of a Fourier series, in the basis functions where, the conventional element uses polynomial functions.

Table 9 shows a side-by-side comparison of the formulation differences between the conventional and spectral plate elements.

Table 9. Formulation Differences Between Conventional and Spectral Levy-type Plate Elements

	Conventional Plate Element Governing Equation
Governing Equation	$$[\mathbf{m}]\{\ddot{\mathbf{d}}\}+[\mathbf{k}]\{\mathbf{d}\}=\{\mathbf{r}_{ext}\}$$
	Spectral Levy-typePlate Element Governing Equation
	$$D\left(\frac{\partial^4 w(x,y,t)}{\partial x^4}+2\frac{\partial^4 w(x,y,t)}{\partial x^2\partial y^2}+\frac{\partial^4 w(x,y,t)}{\partial y^4}\right)-P(x,y,t)+\mu h\frac{\partial^2 w(x,y,t)}{\partial t^2}=0$$
	Conventional Plate Element Basis Function
Basis Function	$$w(x,y,t)=(\overline{A}+\overline{B}x+\overline{C}y+\overline{D}x^2+\overline{E}xy+\overline{F}y^2+\overline{G}x^3\ldots+\overline{H}x^2y+\overline{I}xy^2+\overline{J}y^3+\overline{K}x^3y+\overline{L}xy^3)e^{\mathbf{i}\omega t}$$
	Spectral Levy-type Plate Element Basis Function
	$$w(x,y,t)=\sum_{m=1}^{\infty}f_m(x)\sin\left(\frac{m\pi y}{b}\right)e^{\mathbf{i}\omega t}$$
	Conventional Plate Element Dynamic Stiffness
Dynamic Stiffness	$$[\mathbf{K}_{Dyn}]=-\omega^2[\mathbf{m}]+[\mathbf{k}]$$
	Spectral Levy-type Plate Element Dynamic Stiffness
	$$[\mathbf{K}_{Dyn\ m}]=[\mathbf{F}_m][\mathbf{D}_m]^{-1}$$
	Conventional Plate Element Shape Functions
Shape Function	$$[\mathbf{N}]=\begin{bmatrix}\mathbf{N}_w\\ \mathbf{N}_{\theta_x}\\ \mathbf{N}_{\theta_y}\end{bmatrix}=\begin{bmatrix}1 & x & y & x^2 & xy & y^2 & x^3 & x^2y & xy^2 & y^3 & x^3y & xy^3\\ 0 & -1 & 0 & -2x & -y & 0 & -3x^2 & -2xy & -y^2 & 0 & -3x^2y & -y^3\\ 0 & 0 & 1 & 0 & x & 2y & 0 & x^2 & 2xy & 3y^2 & x^3 & 3xy^2\end{bmatrix}[\mathbf{A}]^{-1}$$
	Spectral Levy-type Plate Element Shape Functions
	$$[\mathbf{N}_m]=\begin{bmatrix}\mathbf{N}_{w\,m}\\ \mathbf{N}_{\theta_x m}\end{bmatrix}=sin\left(\frac{m\pi y}{b}\right)e^{\mathbf{i}\omega t}\begin{bmatrix}e^{p_1x} & e^{p_2x} & e^{p_3x} & e^{p_4x}\\ -p_1e^{p_1x} & -p_2e^{p_2x} & -p_3e^{p_3x} & -p_4e^{p_4x}\end{bmatrix}[\mathbf{D}_m]^{-1}$$

The use of a spatial Fourier series to represent the generalized forces, displacements, and applied loading is a major difference between the spectral Levy-type plate element and the spectral beam element. The spectral beam element did not require a spatial Fourier series to represent the displacements and loading because the

governing equation was separable and a solution that satisfied arbitrary boundary conditions was easily found in terms of end-condition values. The governing Kirchhoff plate PDE is, in general, not separable in space. The inseparability of the governing equation causes difficulties in obtaining a solution that will satisfy arbitrary boundary conditions. The special case of the Levy-type plate allows the separable Fourier series solution to satisfy the specific simply supported boundary conditions on two of the edges while, permitting arbitrary boundary conditions on the remaining two opposing edges.

Another difference between the spectral beam and Levy-type plate element is the plate uses edge Fourier series coefficients as DOF where, the beam uses points as DOF. The spectral plate requires the choice of the number of spatial Fourier terms to use in the analysis. The number of Fourier terms influences the accuracy of the representation of the forces and displacements and thus the solution.

The convergence of the plate modeled with a spectral element is faster than the plate modeled with conventional FEA elements on a number of DOF basis. The spectral element converged to a difference less than 3% over the frequencies of 10, 100, 300, 600, 1500, 2000, and 4500 *Hz* in *m=11* odd Fourier terms or less. Using 11 odd Fourier terms is equivalent to 24 DOF and required less than 1-minute computation time. The ANSYS models on the other hand required meshes of 10X10 to 192X192 to achieve the same precision based on percent difference. The ANSYS meshes are equivalent to 484 and 111,747 DOF for a 10X10 and 192X192 mesh respectively. The computation time required for the 10X10 ANSYS mesh was about 1-minute while the 192X192 was about 1 hour. The tremendous reduction in model size results in large savings in computer memory and solution time.

The single point comparison of the conventional and spectral plate differed slightly from the trends of the conventional and spectral beam comparison in section 4.3. The difference is mainly due to the choice of the number of Fourier terms to use in the solution. The percent difference at low frequency with a single Fourier term was larger than with the beam element, mid frequency differences were on the same level as in the straight beam example, and high frequency differences were larger than with the beam element. The percent difference between conventional and spectral beam elements was near 1% for the entire frequency range, out to the 10^{th} bending mode. The single-point percent difference between conventional and spectral plate methods was reduced to near 1% for frequencies out to 4500 *Hz* by using 11 Fourier terms.

The multiple point comparison of the conventional and spectral plate models showed that the spectral element converges very quickly. The spectral model had a convergence metric one to four orders of magnitude larger than the conventional model in frequency ranges between 10 and 600 *Hz*. The multi-point measure of the percent difference between the two solutions was below 2% for 48 elements per edge in the conventional model and 11 odd Fourier terms in the spectral model. The multiple point comparison is a better metric of the solution because it looks at the solution at 25 points over the plate opposed to the solution of just a single location. The multi-point comparison also considers the seriousness of the error by comparing it to the maximum deflection of the plate. The main purpose of the multi-point comparison is to investigate how the elements compared over the entire plate, not only at a single point.

Overall, the spectral Levy-type plate element performed well. Again, the main advantages of the spectral model were a reduced number of DOF, reduced computational memory, and reduced computation time. The spectral Levy-type plate element will yield the most benefit in models with relatively large spans of flat plates. The dynamics of the large spans can be easily modeled using only a few spectral

elements. Stresses and internal forces can also be computed very accurately due to the C^n continuity of the shape functions. Spectral elements will also function well in situations were edge loading must be used. The edge DOF of the Levy-type spectral element has the edge loading built-in, eliminating the need for additional nodes to get the load into the model.

6. Summary, Conclusions, and Recommendations

This chapter reviews the research objectives set forth in section 1.3, discusses the major conclusions resulting from the research, and suggests a logical path for future research. The conclusions drawn from this research result from the specific cases studied within each chapter.

6.1. Review of Objectives

6.1.1. Develop a Love Spectral Bar Element

A spectral bar element was developed based on Love's dynamic bar theory. The eigenfunction of the dynamic bar governing equation was incorporated into the representation of the displacement field and thus into the shape function of the element. The spectral bar element used two nodes with the axial displacement at each node as the DOF of the element. The dynamic stiffness relating the bar element DOF to the nodal loads was then formulated based on the displacement field. Chapter 3 gives the development of the governing equation, the displacement field, and the dynamic stiffness matrix. The bar element was used to develop the fundamental process of developing a spectral element. Chapter 3 shows that it is possible to incorporate the eigenfunction of the governing PDE into the shape function of a spectral element.

6.1.2. Develop Euler-Bernoulli and Timoshenko Spectral Beam Element

A two node spectral beam element was developed based on each Euler-Bernoulli and Timoshenko beam theories in sections 4.2 and 4.5 respectively. Each section contains the development of the governing equations, representation of the displacement fields, and formation of the dynamic stiffness matrices. The beam elements used the transverse displacement and rotation at each node as nodal DOF. For each beam element, the eigenfunctions of the governing PDE was incorporated

into the representation of the displacement field and thus into the shape functions of the element. A cantilever beam example problem was used to compare the performance of the Euler-Bernoulli spectral and conventional elements.

6.1.3. Develop a Spectral Beam Element of Arbitrary Orientation

The spectral beam elements formulated in sections 4.2 and 4.5 were extended to arbitrary orientation in the plane by superimposing the DOF of the spectral bar element onto the beam elements. The transformation matrix then accounted for the orientation of the element in the plane. A simply supported curved beam example problem was used to show the ability of the spectral element to represent the dynamics of a curved structure by refining the mesh to capture the geometry.

6.1.4. Develop a Spectral Levy-type Plate Element

A Levy-type spectral plate element was developed in section 5.2. Sections 5.2.1, 5.2.2, and 5.2.3 show the developments of the governing equations, representation of the displacement field, and the construction of the dynamic stiffness matrix for the element. The eigenfunctions for the dynamic Levy-type plate were incorporated into the representation of the displacement field and thus the element shape function. The representation of the displacement field ensured that the simply supported boundary conditions of the Levy-type plate were met. The element used the Fourier series coefficients of the transverse displacement and rotation of the two free plate edges as the 4 DOF for the element. A simply supported plate with uniform loads on the free edges was used as an example to show the performance of the spectral element compared to the conventional FEA element. The Levy-type spectral element results of Chapter 5 give insight into the fundamental process of developing a general spectral plate element.

6.2. Conclusions

6.2.1. Incorporating Eigenfunctions into Element Shape Functions

The work in this thesis shows that it is possible to formulate spectral elements by incorporating eigenfunctions into the representation of the displacement field and then into the shape functions of the spectral elements. Eigenfunctions were incorporated into bar, beam, and Levy-type plate elements. The spectral elements performed much better than conventional FEA elements on the simple dynamic problems studied because the spectral elements were based on the "exact" eigenfunctions of the governing equations and the geometry and loading was simple.

6.2.2. Performance of Spectral Elements

It was found that fewer spectral elements were required than conventional FEA elements to provide the same level of precision. A single spectral beam element was capable of capturing the dynamics of a straight cantilever beam "exactly". Up to 35 conventional beam elements were required to give the same level of precision as a single spectral beam for the modes out to the 13^{th} cantilever-bending mode at 15,000 *Hz*.

It was also shown that beam elements could be arranged in a mesh to capture the effect of curvature. A larger number of spectral elements were required to converge a curved geometry model than a straight geometry model because the spectral elements are based on straight beams. The curved geometry must be approximated by a number of straight elements. The number of straight elements required to represent a curve was found by increasing the number of straight elements until the solution met the convergence criteria. In the curved simply supported beam problem, 14 spectral beam elements were required to converge dynamic response. It required 30 conventional elements to achieve the same level of convergence out to the 9^{th} bending mode at frequencies up to 10,000 *Hz*. The up to 50% reduction in the

number of elements for a given level of precision results in savings in computation memory and solution time.

The Levy-type spectral plate performance was slightly different than the spectral beam element because of the choice of the number of Fourier terms to use in the solution. The Levy-type plate required up to 11 odd spatial Fourier terms, equivalent to 24 DOF, to achieve a displacement convergence near 1% out to the 7^{th} bending mode at frequencies up to 4500 *Hz*. The conventional FEA ANSYS SHELL63 plate element required from 484 to 111,747 DOF for the same level of convergence over the same frequency range.

Overall, spectral elements are well suited for dynamic analysis. The bar and beam elements are capable of "exactly" modeling the dynamics with relatively few elements to capture the curvature. The Levy-type plate element requires the additional step to choose the number of spatial Fourier terms to uses in the analysis. The edge loading and DOF of the Levy-type plate make it more difficult to fit the element into the traditional FEA framework. Edge loading enables the use of a reduced mesh, compared to conventional FEA, in situations where edge loading must be included in the model.

6.3. Future Work

6.3.1. General Spectral Plate Element

The Levy-type spectral plate element points the way to formulate a general plate element capable of representing arbitrary boundary conditions. Kulla [14 and 15] suggests a way to formulate a general spectral plate. The method would use edges as DOF just as with the Levy-type element discussed here. The general plate element would require a double spatial Fourier series representation, one in each the x and y-

directions. A large problem in the development of the general plate element is the solution to the dynamic governing equation. The general plate equation is not separable and no general form of the solution in commonly known.

It is suspected that the number of Fourier terms required to converge a general plate element would be larger than the number required to converge the Levy-type element. The larger number of Fourier terms would be due to the increase in the complexity of the boundary conditions of the generalized plate. The convergence rate of the Fourier series decreases with the increase in the number of discontinuities in the function being represented. More discontinuities can be expected in complex boundary conditions and thus, more Fourier terms required to converge the solution. Despite a possible larger number of Fourier terms required to converge a solution, the computational savings and increased precision would most likely be worth the effort to develop a general spectral plate element.

Another interesting area of study for spectral elements that use the Fourier series is the interplay between the number of Fourier terms used and the number of elements used in the mesh. A fewer number of Fourier terms may be required for a mesh with more elements. The interplay between mesh size and number of Fourier terms could was not studied because the Levy-type plate element does not lend itself well to meshing a region due to the two simply-supported edges.

6.3.2. Spectral Element User Interface

Spectral elements will only be used to analyze somewhat simple geometry and loading problems until a user interface is developed to handle more complex problems. Currently, the user must code a spectral element analysis. The level of coding experience limits the level of the problem that can be analyzed. The code structure for the Levy-type plate element must be able to handle edge DOF and a

varying number of Fourier terms based on the solution convergence. It would also be beneficial if the terms of the dynamic stiffness matrix could be analytically formulated. If dynamic stiffness matrix terms were known, time could be saved by not having to invert the $[\mathbf{D}]$ matrix for each element and summation index. Finally, traditional plotting routines would need to be extended to handle the summation of responses over a given number of Fourier terms. Until spectral elements are capable of being linked to a code structure that can handle a large or complicated problem, conventional finite elements will remain the formulation of choice.

7. References

[1] Arruda, J.R.F., Donadon, L.V., Nunes, R.F., "On the Modeling of Reinforced Plates in the mid-frequency Range." Proceedings of the ISMA. 2004. pages 1407-1416.

[2] Boyce and DiPrima. Elementary Differential Equations and Boundary Value Problems. Wiley, New York. 1997.

[3] Cook, Malkus, Plesha, and Witt. Concepts and Applications of Finite Element Analysis. Wiley, New York. 2002.

[4] Danial, A.N. and Doyle J. "Dynamic Analysis of Folded Plate Structures." Journal of Sound and Vibration. October 1996: pages 591-598.

[5] Doyle, James F. Wave Propagation in Structures. Springer, New York. 1997.

[6] Dym and Shames. Energy and Finite Element Methods in Structural Mechanics. Hemisphere, New York. 1985.

[7] Gorman, D.J. Free Vibration Analysis of Rectangular Plates. Elsevier, New York. 1982.

[8] Gorman, D.J. Vibration Analysis of Rectangular Plates by the Superposition Method. Singapore, River Edge, N.J. 1999.

[9] Haug, Choi, and Komkov. Design Sensitivity Analysis of Structural Systems. Mathematics in Science and Engineering Vol. 117. Academic Press, New York. 1986.

[10] Horr, A. and Schmmidt, L. "Dynamic Analysis of Large Shell Structures: Complex Damped Spectral Element Method." International Journal of Space Structures Vol 14 No. 4 1999: pages 241-254.

[11] Inman, Daniel J. Engineering Vibration. Prentice Hall, Englewood Cliffs, New Jersey. 1994.

[12] Kevorkien and Pascal. "An Accurate Method for free Vibration Analysis of Structures with Application to Plates." Journal of Sound and Vibration Vol 246. 2001: pages 795-814.

[13] Kreyszig. Advanced Engineering Mathematics. Wiley, New York. 1999.

[14] Kulla, P.H. "High Precision Finite Elements." Finite Element in Analysis and Design. Vol 26. 1997: pages 997-114.

[15] Kulla, P.H. "The Continuous Elements Method". Proc. Internat. Conf. Spacecraft Structures and Mechanical Testing. Nordwick, Netherlands. 1994.

[16] Larson, Hostetler, and Edwards. Calculus Early Transcendental Functions. D.C. Heath, Lexington, Massachusetts. 1995.

[17] Lee, U. and Lee, J. "Spectral-Element Method for Levy-Type Plates Subject to Dynamic Loads." Journal of Engineering Mechanics. February, 1999. pages 243-247.

[18] Mathematica. Version 5.0. Champaign, IL: Wolfram Research. 2002

[19] Rizzi, Stephen A. "A Spectral Analysis Approach to Wave Propagation in Layered Solids." Ph.D. Dissertation, Purdue University, August 1989.

[20] Timoshenko, Young, Weaver. Vibration Problems in Engineering. Wiley, New York. 1974.

[21] Timoshenko, Woinowsky-Krieger. Theory of Plates and Shells. McGraw Hill, New York. 1959.

[22] Thomson, William. Theory of Vibration with Application. Prentice Hall, Englewood Cliffs, New Jersey. 1988.

[23] Ventsel, Eduard and Krauthammer, Theodor. Thin Plates and Shells. Marcel Dekker, New York. 2001.

Appendix A Euler-Bernoulli Spectral Beam Dynamic Stiffness Matrix

$$\alpha = \sqrt[4]{\frac{\mu A \omega^2}{EI}}$$

$$\begin{bmatrix} -\frac{(1-i)\alpha^3(\sin[(2+2i)a\alpha]+\sinh[(2+2i)a\alpha])}{-2+2\cos[2a\alpha]\cosh[2a\alpha]} & -\frac{\alpha^2\sin[2a\alpha]\sinh[2a\alpha]}{-1+\cos[2a\alpha]\cosh[2a\alpha]} & \frac{\alpha^3(\sin[2a\alpha]+\sinh[2a\alpha])}{-1+\cos[2a\alpha]\cosh[2a\alpha]} & \frac{\alpha^2(\cos[2a\alpha]-\cosh[2a\alpha])}{-1+\cos[2a\alpha]\cosh[2a\alpha]} \\ \bullet & \frac{(1+i)\alpha(-\sin[(2+2i)a\alpha]+\sinh[(2+2i)a\alpha])}{-2+2\cos[2a\alpha]\cosh[2a\alpha]} & \frac{\alpha^2(-\cos[2a\alpha]+\cosh[2a\alpha])}{-1+\cos[2a\alpha]\cosh[2a\alpha]} & \frac{\alpha(\sin[2a\alpha]-\sinh[2a\alpha])}{-1+\cos[2a\alpha]\cosh[2a\alpha]} \\ \bullet & \bullet & -\frac{(1-i)\alpha^3(\sin[(2+2i)a\alpha]+\sinh[(2+2i)a\alpha])}{-2+2\cos[2a\alpha]\cosh[2a\alpha]} & \frac{\alpha^2\sin[2a\alpha]\sinh[2a\alpha]}{-1+\cos[2a\alpha]\cosh[2a\alpha]} \\ \bullet & \bullet & \bullet & \frac{(1+i)\alpha(-\sin[(2+2i)a\alpha]+\sinh[(2+2i)a\alpha])}{-2+2\cos[2a\alpha]\cosh[2a\alpha]} \end{bmatrix}$$

Appendix B Spectral Plate Element Code

```
%%%=============================================================================
function  [x,y,W_total]=Single_Freq_Analysis_Exp(w,m,M,N)
%%% M is number of plotting divisions in the Y-direction
%%% N is the number of plotting divisions in the X-direction
%%% m is the number of Fourier Terms used in the anlaysis
%%% w is the frequency of the Analysis in rad/sec

FRF_Include_Parameters; % General parameters needed for the Analysis
b=38.1e-2;       %meters plate length y-direction
a=25.4e-2;       %meters plate length x-direction
mm=1:2:m;

for m_count=1:length(mm)% Only odd m-values are needed for the constant load analysis

    p1(m_count)=sqrt(sqrt((rho*h*w^2)/D)+(mm(m_count)*pi/b)^2);
    p2(m_count)=sqrt(-sqrt((rho*h*w^2)/D)+(mm(m_count)*pi/b)^2);
    p3(m_count)=-sqrt(sqrt((rho*h*w^2)/D)+(mm(m_count)*pi/b)^2);
    p4(m_count)=-sqrt(-sqrt((rho*h*w^2)/D)+(mm(m_count)*pi/b)^2);

    load(1:4,m_count)=[4*P/(mm(m_count)*pi);0;4*P/(mm(m_count)*pi);0];
% Form the constant load fourier decomposition vector for each m-   value

    Disp(:,:,m_count)=[
        Exp_trans_disp(0,p1(m_count),p2(m_count),p3(m_count),p4(m_count),mm(m_count))
         -Exp_dw_dx(0,p1(m_count),p2(m_count),p3(m_count),p4(m_count),mm(m_count))
         Exp_trans_disp(a,p1(m_count),p2(m_count),p3(m_count),p4(m_count),mm(m_count))
         -Exp_dw_dx(a,p1(m_count),p2(m_count),p3(m_count),p4(m_count),mm(m_count))];

    Force(:,:,m_count)=[
        -Exp_shear(0,p1(m_count),p2(m_count),p3(m_count),p4(m_count),mm(m_count),b)
         -Exp_moment(0,p1(m_count),p2(m_count),p3(m_count),p4(m_count),mm(m_count),b)
         Exp_shear(a,p1(m_count),p2(m_count),p3(m_count),p4(m_count),mm(m_count),b)
         Exp_moment(a,p1(m_count),p2(m_count),p3(m_count),p4(m_count),mm(m_count),b)];

    Coeff(:,:,m_count)=inv(Disp(:,:,m_count));

    K_method(:,:,m_count)=Force(:,:,m_count)*Coeff(:,:,m_count);
%Form the Dynamic Stiffness

    d_method(:,m_count)=inv(K_method(:,:,m_count))*load(1:4,m_count);
%Calculate displacments

end
[x,y,W_total]=plot_def_shape_Exp(d_method,Coeff,w,mm,a,b,p1,p2,p3,p4,M,N);
%%%=============================================================================

function W=Exp_trans_disp(x,p1,p2,p3,p4,m)
FRF_Include_Parameters;
W=[exp(p1*x) exp(p2*x) exp(p3*x) exp(p4*x)];
%%%=============================================================================

function dw_dx=Exp_dw_dx(x,p1,p2,p3,p4,m)
%%% The derivative of the basis function with respect to x
FRF_Include_Parameters;
dw_dx=[ p1*exp(p1*x), p2*exp(p2*x), p3*exp(p3*x), p4*exp(p4*x)];
%%%=============================================================================

function Vxz=Exp_shear(x,p1,p2,p3,p4,m,b)
%%%Vxz= -D*(diff(W,x,3)+(2-v)*diff(diff(W,x),y,2))
FRF_Include_Parameters;

Vxz=[ -D*p1*exp(p1*x)*(p1^2*b^2-2*m^2*pi^2+m^2*pi^2*v)/b^2, -D*p2*exp(p2*x)*(p2^2*b^2-
2*m^2*pi^2+m^2*pi^2*v)/b^2, -D*p3*exp(p3*x)*(p3^2*b^2-2*m^2*pi^2+m^2*pi^2*v)/b^2, -
D*p4*exp(p4*x)*(p4^2*b^2-2*m^2*pi^2+m^2*pi^2*v)/b^2];
%%%=============================================================================
```

```
function Mxx=Exp_moment(x,p1,p2,p3,p4,m,b)
%%%   Mxx = -D*(diff(W,x,2)+v*diff(W,y,2))
FRF_Include_Parameters;

Mxx=[ D*exp(p1*x)*(-p1^2*b^2+v*m^2*pi^2)/b^2, D*exp(p2*x)*(-p2^2*b^2+v*m^2*pi^2)/b^2,
-D*exp(p3*x)*(p3^2*b^2-v*m^2*pi^2)/b^2, D*exp(p4*x)*(-p4^2*b^2+v*m^2*pi^2)/b^2];
%%%=============================================================================================

function [x,y,W_total]=plot_def_shape_Exp(d_method,Coeff,w,mm,a,b,p1,p2,p3,p4,M,N)
x=linspace(0,a,N+1);
y=linspace(0,b,M+1);

for m_count=1:length(mm)
    for x_count=1:length(x)
        for y_count=1:length(y)

W_method(y_count,x_count,m_count)=sin(mm(m_count)*pi*y(y_count)/b)*Exp_trans_disp(x(x_
count),p1(m_count),p2(m_count),p3(m_count),p4(m_count),mm(m_count))*Coeff(:,:,m_count)
*d_method(:,m_count);

end
end
end

W_total=sum(W_method,3);
W_Center_Edge=sum(W_total((length(y)+1)/2,1,:),3);
figure;
surf(x,y,real(W_total))
grid on;
xlabel('X - Direction (m)');
ylabel('Y - Direction (m)');
zlabel('Z - Direction (m)');
set(gca,'ZDir','reverse');
set(gca,'YDir','reverse');
% x_limits=get(gca,'xlim');
% axis([0 b 0 a]);
title1=['Deformed Shape Max m = '];
title2=num2str(max(mm));
title3=[' Frequency = '];
title4=num2str(w/(2*pi));
title5=[' Hz'];
title_total=[title1 title2 title3 title4 title5];
title(title_total);
%%%=============================================================================================
```

Appendix C Spectral and Conventional Plate Convergence

FEA ANALYSIS

10 Hz Uniform Edge Load that changes with number of Nodes

Size of FEA Mesh	Center Edge Displacment (m)	% Difference
2	4.36E-02	58.41%
4	6.91E-02	13.25%
6	7.82E-02	5.77%
8	8.27E-02	3.22%
10	8.54E-02	2.05%
12	8.71E-02	2.47%
16	8.93E-02	1.42%
20	9.06E-02	0.93%
24	9.14E-02	2.26%
48	9.35E-02	1.08%
96	9.45E-02	0.53%
192	9.50E-02	

100 Hz Uniform Edge Load that changes with number of Nodes

Size of FEA Mesh	Center Edge Displacment (m)	% Difference
2	-1.14E-02	55.85%
4	-1.77E-02	12.68%
6	-1.99E-02	5.63%
8	-2.11E-02	3.16%
10	-2.17E-02	2.02%
12	-2.22E-02	2.45%
16	-2.27E-02	1.41%
20	-2.30E-02	0.92%
24	-2.33E-02	2.25%
48	-2.38E-02	1.08%
96	-2.40E-02	
192		

300 Hz Uniform Edge Load that changes with number of Nodes

Size of FEA Mesh	Center Edge Displacment (m)	% Difference
2	2.87E-02	-43.73%
4	1.62E-02	3.11%
6	1.67E-02	1.79%
8	1.70E-02	1.26%
10	1.72E-02	0.94%
12	1.73E-02	1.33%
16	1.76E-02	0.89%
20	1.77E-02	0.63%
24	1.78E-02	1.75%
48	1.81E-02	0.95%
96	1.83E-02	
192		

600 Hz Uniform Edge Load that changes with number of Nodes

Size of FEA Mesh	Center Edge Displacment (m)	% Difference
2	-3.75E-03	-32.57%
4	-2.53E-03	8.05%
6	-2.73E-03	4.08%
8	-2.84E-03	2.38%
10	-2.91E-03	1.56%
12	-2.95E-03	1.94%
16	-3.01E-03	1.17%
20	-3.05E-03	0.78%
24	-3.07E-03	2.00%
48	-3.13E-03	1.02%
96	-3.16E-03	
192		

Spectral ANALYSIS

Number of m values	Center Edge Displacment (m)	% Difference
1	9.62E-02	-0.83%
3	9.54E-02	0.00%
5	9.54E-02	0.10%
7	9.55E-02	0.00%
9	9.55E-02	0.00%
11	9.55E-02	

Number of m values	Center Edge Displacment (m)	% Difference
1	-2.35E-02	3.65%
3	-2.44E-02	-0.41%
5	-2.43E-02	0.00%
7	-2.43E-02	0.00%
9	-2.43E-02	0.00%
11	-2.43E-02	

Number of m values	Center Edge Displacment (m)	% Difference
1	1.96E-02	-5.92%
3	1.84E-02	0.54%
5	1.85E-02	0.00%
7	1.85E-02	0.00%
9	1.85E-02	0.00%
11	1.85E-02	

Number of m values	Center Edge Displacment (m)	% Difference
1	-3.30E-03	0.00%
3	-3.30E-03	-3.03%
5	-3.20E-03	0.00%
7	-3.20E-03	0.00%
9	-3.20E-03	0.00%
11	-3.20E-03	

% Diff Spectral and FEA

Difference taken between 96 Element and m=11

	% Difference
96 & m=11 %diff =	1.09%
24 &m=1 %diff =	5.26%
96 & m=11 %diff =	1.11%
24 &m=1 %diff =	1.24%
96 & m=11 %diff =	1.00%
24 &m=1 %diff =	9.68%
96 & m=11 %diff =	1.18%
24 &m=1 %diff =	7.52%

1500 Hz Uniform Edge Load that changes with number of Nodes

Size of FEA Mesh	Center Edge Displacment (m)	% Difference
2	3.22E-04	-548.22%
4	-1.44E-03	1012.07%
6	-1.60E-02	-430.06%
8	5.29E-02	-67.23%
10	1.73E-02	-28.53%
12	1.24E-02	-23.37%
16	9.50E-03	-10.14%
20	8.53E-03	-5.24%
24	8.09E-03	-7.82%
48	7.45E-03	-1.44%
96	7.35E-03	-0.10%
192	7.34E-03	

Number of m values	Center Edge Displacment (m)	% Difference
1	7.30E-03	0.00%
3	7.30E-03	0.00%
5	7.30E-03	1.37%
7	7.40E-03	0.00%
9	7.40E-03	0.00%
11	7.40E-03	

96 & m=11 %diff = 0.72%
24 &m=1 %diff = -9.74%

2000 Hz Uniform Edge Load that changes with number of Nodes

Size of FEA Mesh	Center Edge Displacment (m)	% Difference
2	5.36E-04	-87.44%
4	6.72E-05	669.42%
6	5.17E-04	1027.17%
8	5.83E-03	-242.13%
10	-8.29E-03	-52.41%
12	-3.94E-03	-32.20%
16	-2.67E-03	-11.94%
20	-2.36E-03	-5.68%
24	-2.22E-03	-7.75%
48	-2.05E-03	-1.27%
96	-2.02E-03	-0.04%
192	-2.02E-03	

Number of m values	Center Edge Displacment (m)	% Difference
1	-6.04E-04	214.47%
3	-1.90E-03	5.26%
5	-2.00E-03	0.00%
7	-2.00E-03	0.00%
9	-2.00E-03	0.00%
11	-2.00E-03	

96 & m=11 %diff = -1.17%
24 &m=1 %diff = -72.80%

4500 Hz Uniform Edge Load that changes with number of Nodes

Size of FEA Mesh	Center Edge Displacment (m)	% Difference
2	-2.31E-04	205.71%
4	-7.05E-04	-84.32%
6	-1.11E-04	-62.59%
8	-4.14E-05	-58.38%
10	-1.72E-05	-2016.29%
12	3.30E-04	-1012.57%
16	-3.01E-03	-100.11%
20	3.22E-06	236.98%
24	1.08E-05	149.38%
48	2.70E-05	19.12%
96	3.22E-05	2.46%
192	3.30E-05	

Number of m values	Center Edge Displacment (m)	% Difference
1	-1.61E-04	-69.02%
3	-5.00E-05	-17.23%
5	-4.14E-05	-146.26%
7	1.91E-05	104.91%
9	3.92E-05	-17.18%
11	3.25E-05	

96 & m=11 %diff = 0.83%
24 &m=1 %diff = -1588%